2010

Characterization of a Novel Chromatinâ€Induced Mechanism that Couples Microtubule Disassembly and Nuclear Reâ€Formation

Eileen Madeleine Woo

CHARACTERIZATION OF A NOVEL CHROMATIN-INDUCED MECHANISM THAT COUPLES MICROTUBULE DISASSEMBLY AND NUCLEAR RE-FORMATION

A Thesis Presented to the Faculty of

The Rockefeller University

in Partial Fulfillment of the Requirements for

the degree of Doctor of Philosophy

by

Eileen Madeleine Woo

June 2010

CHARACTERIZATION OF A NOVEL CHROMATIN-INDUCED MECHANISM THAT COUPLES MICROTUBULE DISASSEMBLY AND NUCLEAR RE-FORMATION

Eileen M. Woo, Ph.D.

The Rockefeller University 2010

Upon completion of mitosis, the disassembly of spindle components and reassembly of nuclear structures occur simultaneously around chromatin. Previous studies have suggested that an important step in this process is the inactivation of the Aurora B kinase by the Triple A-ATPase Cdc48/p97, which physically extracts the protein from chromatin at anaphase. Aurora B is the catalytic subunit of the Chromosome Passenger Complex (CPC), which promotes microtubule polymerization and spindle formation from mitotic chromosomes. Removal of the CPC from chromosomes at anaphase is required for proper nuclear reassembly, but the molecular basis for this requirement remains unclear. On the whole, the orchestration of structural events at the end of mitosis is poorly understood.

Using *Xenopus* egg extracts, we endeavored to identify uncharacterized proteins that bind to purified mitotic chromosomes. In doing so we discovered Vespera, a protein which is functionally antagonistic to the CPC. We show that Vespera promotes microtubule depolymerization from chromosomes and is required on chromatin for proper nuclear formation. We initially identified Vespera as a protein that is specifically SUMOylated upon interaction with chromatin, a modification that is dependent on the SUMO E3 ligase, PIASy. Immunodepletion of Vespera from *Xenopus* egg extracts interferes with proper nuclear formation and nuclear transport, and rescue of this defect requires Vespera SUMOylation. Addition of excess amounts of Vespera to metaphase

extracts disassembles spindle microtubules, and this activity is also dependent on SUMOylation of Vespera and PIASy. Importantly, the Vespera depletion defect in nuclear formation can be rescued by nocodazole or by co-depletion of the CPC. These manipulations depolymerize microtubules, suggesting that the microtubule-depolymerizing activity of SUMO-Vespera is central to its role in ensuring proper nuclear formation. Our results suggest that microtubules must be actively depolymerized around chromosomes to permit proper nuclear reassembly, a process that is promoted by SUMOylated Vespera.

Ultimately, we would like to understand how various post-translational modifications on chromosomal proteins signal events through the cell cycle. Towards this end, we have developed a chemical method for the identification of phosphorylation using mass spectrometry, and have applied it to identify novel phosphorylation sites on Vespera as well as on members of the CPC. Furthermore, although phosphorylation has been shown to play a central role during mitosis, we hypothesized that the interplay between phosphorylation and other covalent modifications may also prove to be important in this context. Here, we observed that, in the absence of SUMOylated Vespera, protein phosphatase 1 does not fully accumulate on chromosomes and dephosphorylation of Aurora B substrates is delayed. The interaction between protein phosphatases and SUMO may represent an interesting general principal in crosstalk between covalent modifications, and provides intriguing opportunities for future studies.

Ἔσπερε, πάντα φέρων, ὅσα φαίνολις ἔσκέδας' αὔως,
φέρεις οἶν, φέρες αἶγα, φέρεις ἄπυ ματέρι παῖδα."

Vespera, which brings all things which the gleaming Aurora has scattered,
Brings the sheep, the goats, and the children back to their mother.

--Sappho 104a

ACKNOWLEDGMENTS

I am indebted to many people who have contributed to my graduate education over the past several years. Without some of them, I would never have completed this thesis, and without a few others, I would likely have completed it far sooner, but I am sincerely grateful to all of them for what they taught me.

First, I would like to thank my advisor, the inimitable Hironori Funabiki, a man who speaks softly and carries a very big scientific intellect. It does sometimes seem that Hiro comes from a different world, but I think it must be a much better world than ours, and at times his peculiar and inscrutable logic can yield astonishing insights. He is also a scientist of unparalleled integrity, and I am honored to have worked with him. I must also thank my second advisor, Brian Chait, who is a role model not just as a scientist, but as an entire person. Brian is an inventor, mass spectrometry pioneer, surfer, macro photographer, world traveler, family man, and all-around adventurer, and he approaches all these things with a blend of pragmatism and eternal optimism that I strive to emulate.

I would also like to thank the chair of my committee, David Allis, for his support and helpful guidance over the years. Thanks also to Howard Hang, a later addition to my committee. I extend a special thanks to Arshad Desai for traveling from San Diego to serve as the external examiner on my committee.

Additionally, many past and present members of the Chait, Funabiki, and Allis labs have provided enlightening discussions—thanks to Sung-Hee Ahn, Andrew Xiao, Yifang Liu, Judith Recht, Wolfgang Fischle, Holger Dormann, Elizabeth Goneska, Martine Cadene, Emmanuel Chang, Ileana Cristea, Jeff Degrasse, Jeroen Demmers, Erica Jacobs, Tijana Jovanovic, Jin Mi, Ji-Eun Kim, Kelly Molloy, Sunnie Myung, Zachary Quinkert, Matt Sekedat, Qingjin Wang, and Wenzhu Zhang for their help. I extend special thanks to Trixi Uberheide, Alan Tackett, and Julio Padovan for mass spectrometry training. I thank Andrew Krutchinsky for lending me his bench space in the Chait Lab, and later, for lending me the instruments in his own lab at UCSF. I thank David Fenyö for assistance with data analysis.

I am indebted to Boo Shan Tseng, Kate Zelenova, Cristina Ghenoiu, Jessica Rosenberg, Oliver Leismann, Alex Kelly, Srinath Sampath, Nina Soares, John Xue, and Christian Zierhut for egg extract, antibodies, advice, cake, and much more. Thank you, benchmate Adriana Garzon, for endless patience and generosity. Thanks to Alin Vonica for his help with Xenopus embryos, and for his heroic efforts to remedy my utter ignorance regarding basic principles of development. I am grateful to Yoshi Azuma, Mary Dasso, S. Mochida, Ben Kwok, and Dale Shumaker for reagents. Thanks to Lisa Fish for a fun and

productive collaboration—her rotation work produced the key that unlocked the whole Vespera project. Thanks, too, to Lisa Postow for initial direction of that project. In my time at Rockefeller I have had many advisors, and Lisa is the most significant one. In the sink-or-swim world of graduate school, she provided me a life raft, fishing pole, moral compass—there are not enough metaphors available to convey what I owe to her. Thanks also to Bobby for convincing Lisa to get that giant flatscreen television.

For extracurricular enrichment, I would like to thank the members of Camerata Notturna, a chamber orchestra that started as the Erewhon Trio and certainly ended up Somewhere. Thanks to Jac Huberman, Anne Jump, and Alice for tea and sympathy, and to Sean Collins and Aaron Goldberg for advice over, and about, coffee. Thanks to Hunter Fraser for great travels. Thanks to Hans Cutiongco for cheesy music, and many other things, cheesy and profound, outside the scope of this section.

This work was funded by a graduate fellowship from the Howard Hughes Medical Institute, The Rockefeller University, and grants from the National Institutes of Health. A special thanks to The Rockefeller University Graduate School and members of the Deans Office for an outstanding program.

Lastly, my family has provided endless support. My dad is the ultimate scholar, and I am grateful for his example. My brother Ray keeps me entertained and grounded with his opinions on everything from how to cook omelettes to proper powerpoint etiquette. I thank him in advance for not minding that I completely ignored his advice on how to write an austere, scholarly thesis acknowledgments section that will not embarrass me (or him) in years to come. Finally, I simply could not manage without my mom, who has been there for me at every step of the way. She is my secret weapon.

TABLE OF CONTENTS

Materials and Methods

LIST OF FIGURES

LIST OF ABBREVIATIONS

APC	-	Anaphase-promoting complex
BAF	-	Barrier to Autointegration Factor
BLM	-	Bloom helicase
Cdk	-	Cyclin-dependent kinase
CID	-	Collision-induced dissociation
CPC	-	Chromosome Passenger Complex
CSF	-	Cytostatic factor
Dppa	-	Developmental pluripotency-associated
dnUbc	-	Dominant-negative Ubc9
ECD	-	Electron capture dissociation
ETD	-	Electron transfer dissociation
EM	-	Electron microscopy
ER	-	Endoplasmic reticulum
ERAD	-	Endoplasmic reticulum associated degradation
GFP	-	Green fluorescent protein
HF	-	Hydrogen fluoride
H3T3ph	-	phospho-histone H3 (threonine 3)
H3S10ph	-	phospho-histone H3 (serine 10)
INM	-	Inner nuclear membrane
LEM	-	LAP2, emerin, MAN1
MCAK	-	Mitotic centromere-associated kinesin
MS	-	Mass spectrometry
MS/MS	-	Tandem mass spectrometry
MTOC	-	Microtubule-organizing Center

MT	-	Microtubule
NE	-	Nuclear envelope
NEBD	-	Nuclear envelope breakdown
NLS	-	Nuclear localization signal or sequence
NPC	-	Nuclear pore complex
NRK	-	Normal rat kidney
ONM	-	Outer nuclear membrane
PP1	-	Protein phosphatase 1
SAC	-	Spindle assembly checkpoint
SAP	-	SAF-A/B, Acinus and PIAS
SENP	-	Sentrin-specific protease
SIM	-	SUMO-interacting motif
SUMO	-	Small ubiquitin-like modifier
Ub	-	Ubiquitin
VRK	-	Vaccinia-related kinase

CHAPTER ONE:
GENERAL INTRODUCTION

To divide itself, a cell must perform an intricate choreography that ensures faithful partitioning of its genetic material, or DNA. In eukaryotic cells, DNA is loosely packaged by histones and other proteins into chromatin, which is enclosed by membranes to form the nucleus. In interphase, as the cell prepares for division, chromatin is replicated inside the nucleus. The challenge in the ensuing mitotic phase is to divide the replicated chromatin equally to generate two membrane-bound nuclei with identical genetic makeup. To achieve this with maximal accuracy, chromatin is condensed into tightly packed chromosomes, in which the two copies of replicated DNA form two resolved sister chromatids. The sister chromatids are connected at the centromere of the chromosome, which is also the site of assembly of the kinetochore, a proteinaceous structure that attaches to microtubules. This attachment allows sister chromatids to be tethered to opposite poles of the bipolar metaphase spindle. Once all the chromosomes are properly attached to microtubules and aligned in the middle of the bipolar spindle, the cell proceeds from metaphase to anaphase, segregating each set of sister chromatids to opposite poles. At the final stage of nuclear division, telophase, the chromosomes decondense back to chromatin, and two distinct nuclei can be observed. The end of mitosis is followed by division of the cytoplasm, known as cytokinesis, to complete division of the cell into two daughter cells.

Here, we begin by discussing the structural and signaling events of nuclear division in greater detail. We describe the process of mitosis from the perspective of the nuclear membrane and bipolar spindle, and provide

an overview of the covalent modifications that provide crucial signaling mechanisms in cell cycle progression. We also discuss events at the end of mitosis, and the transition back to interphase, which are of particular relevance to the findings we present. The Aurora B Chromosome Passenger Complex (CPC) is a central player in events throughout mitosis, and we will explore the molecular basis of its action. These discussions serve to introduce the results described in this thesis, which deal primarily with the discovery and characterization of Vespera, a protein that we found to be required for proper spindle disassembly and nuclear re-formation at the end of mitosis.

1.1 *The phases of mitosis*

The process of mitosis was discovered in the 19th century with the advent of the light microscope. At the time, scientists understood the theory of cell division, that new cells arise from the division of old cells, but they knew nothing of the inheritance of genetic material. The German anatomist Walther Flemming was the first to document the phases of mitosis, through beautifully detailed drawings he published in 1882 (Figure 1.1). He coined the term "chromatin," to describe the dark material he observed as it condensed, aligned, separated, and decondensed in cells. Thus, Fleming discovered the chromosome, without possessing an understanding of what these structures contained. Years later, scientists would begin to make the connection between the genetic theories put forth by Gregor Mendel in 1865, and the chromosomal structures observed under the microscope, to develop the chromosomal theory of inheritance (O'Connor and Miko, 2008).

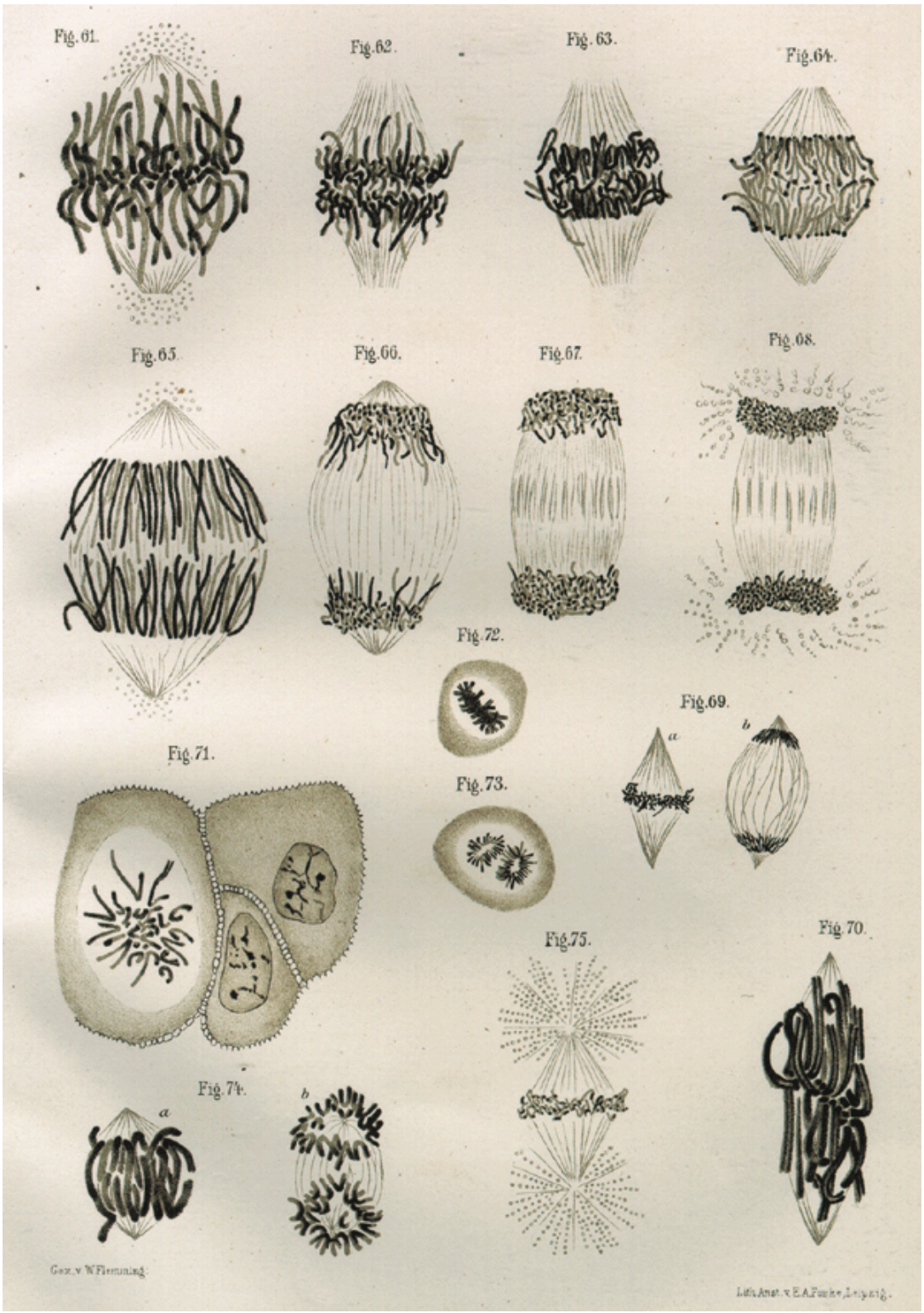

Figure 1.1. Early sketches of cell division, from *Zellsubstanz, Kern und Zelltheilung*, Walther Flemming, 1882.

We now understand that mitosis is the process by which cells divide their genetic material, and we divide this phase of the cell cycle into five parts termed prophase, prometaphase, metaphase, anaphase, and telophase. During interphase, which precedes mitosis, the genetic material of the cell exists in a diffuse structure known as chromatin, which is replicated during the portion of interphase known as S phase. Once the cell begins the process of mitosis, it enters prophase, which is characterized by condensation of chromatin into condensed chromosomes each containing two partially resolved, duplicated sister chromatids. The subsequent prometaphase is characterized in many higher eukaryotes by nuclear envelope breakdown and movement of chromosomes towards the plane of cell division. At metaphase, these chromosomes are attached to microtubule tethers and align to form a structure termed the bipolar spindle. Once all chromosomes are properly aligned at the center of the spindle (the metaphase plate), the spindle elongates, thereby pulling the two sister chromatids of each chromosome to opposite poles of the spindle. This phase, in which sister chromatids segregate to opposite sides of the cell, is termed anaphase. Finally, in telophase, the spindle disassembles, and segregated chromatids decondense, once again assuming the diffuse appearance of chromatin (Mitchison and Salmon, 2001).

The fidelity of mitosis relies on several crucial structural features. To ensure that each daughter cell receives equal genetic material, pairs of sister chromatids must travel together to the metaphase plate. Following replication, sister chromatids are attached by extensive catenation, or interwining, of their DNA, and "glue" proteins known as cohesins (Hopfner, 2003). Sister chromatids must be linked together thus, to ensure proper sorting of chromosomes, but subsequently, in order to achieve

proper segregation at anaphase, they must also be cleanly separated. As the cell progresses through prophase, motor proteins known as condensins act to wind chromatin into coiled structures, and topoisomerases decatenate the tangled DNA structures (Hirano, 2005). Through this process, sister chromatids are largely resolved, remaining attached mainly by connection in one region of the chromosome, known as the centromere. The centromere is also the site of assembly of the kinetochore, which makes essential contributions to the accuracy of mitosis because it serves as the site for determining proper attachment of microtubules. As chromosomes align on the metaphase plate, specialized proteins localized to the kinetochore monitor the attachment of microtubules to ensure that sister chromatids are attached to opposite poles. This proper configuration of microtubules is termed amphitelic attachment, in contrast to syntelic attachment, where both sister chromatids are attached to one pole, or merotelic attachment, where one sister is attached to both poles (Hauf and Watanabe, 2004).

1.2 *Regulation of mitosis*

To ensure the orderly progression of cell cycle events, the proteins that participate are tightly regulated by a complex network of post-translational modifications. Predominant among these is phosphorylation, a reversible covalent attachment of a phosphate group, which is attached and removed by kinases and phosphatases, respectively. The chief regulators of cell cycle progression are a group of Cyclin-dependent kinases (Cdks), which oscillate in activity through various phases of the cell cycle, dependent on the availability and association with different cyclin proteins. In organisms such as budding yeast and fission yeast, the entire cycle is controlled by the activity of Cdk1, while in multi-cellular eukaryotes there are two separate

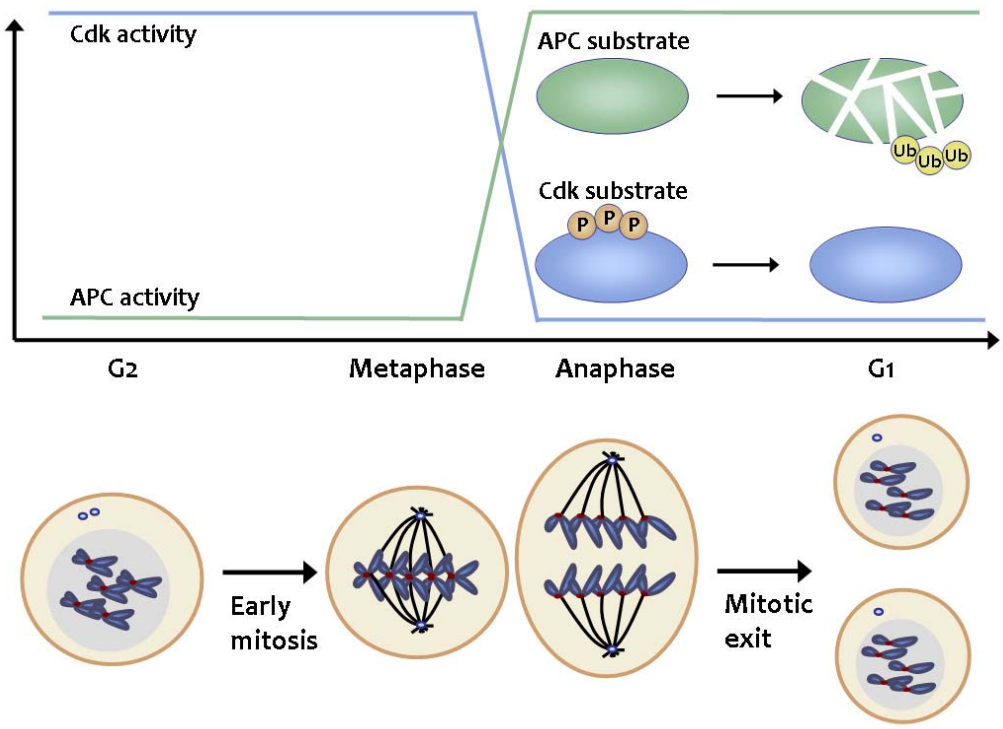

Figure 1.2. Control of late mitotic events. Adapted from (Sullivan and Morgan, 2007). Progression through mitosis is shown by the cells along the bottom of the figure (chromosomes in blue and spindle microtubules in black). The transition from metaphase to anaphase is triggered by an increase in the activity of the anaphase-promoting complex (APC) (green line; top of figure), a ubiquitin-protein ligase that promotes the assembly of chains of ubiquitin (Ub) on its substrates, thereby targeting them for destruction in the proteasome. The main APC targets are securin, the destruction of which leads to sister-chromatid separation, and cyclins, the destruction of which results in a drop in Cdk activity (blue line). Cdk inactivation allows phosphatases to dephosphorylate Cdk substrates during late mitosis.

Cdks that control S-phase and M-phase (Morgan, 1997). This Cdk activity is controlled, in turn, by regulated synthesis and proteolytic destruction of cyclins. In the *Xenopus* egg extract system (and other embryonic systems), high Cdk activity corresponds directly with M-phase, and its activity is largely determined by the availability of Cyclin B. This was shown to be the case by elegant experiments in which destruction of messenger RNA (mRNA) inhibited cell cycle progression, and addback of only cyclin B mRNA restored mitotic entry (Murray and Kirschner, 1989; Murray et al., 1989).

Exit from mitosis is driven by activity of the anaphase-promoting complex (APC) which targets M-phase cyclins and other mitotic substrates for destruction via the ubiquitin-proteasome system (Figure 1.2). The APC also targets the protein securin, releasing the enzyme separase, which cleaves cohesin proteins to promote sister chromatid separation. Following the inactivation of Cdk-cyclin by APC, ordered dephosphorylation of Cdk substrates by phosphatases orchestrates the completion of mitosis (Sullivan and Morgan, 2007).

1.3 *The Xenopus egg extract system for studying the cell cycle*

The early embryo of the African clawed frog *Xenopus laevis* is a system well-suited for cell cycle studies. *Xenopus* eggs are very large cells, with a diameter of 1.3 mm. They are arrested in metaphase of meiosis II, and upon fertilization, they begin a series of rapid, synchronous divisions. The egg contains sufficient stored components for twelve divisions, and therefore these early cycles proceed in the absence of gene transcription, providing an excellent system to study the events of interphase and mitosis in relative isolation from nuclear processes that are not directly related to cell division.

Furthermore, pioneering work of Lohka and Masui (Lohka and Masui, 1983), Lohka and Maller (Lohka and Maller, 1985) and later Murray and Kirschner (Murray, 1991; Murray et al., 1989) showed that many of the important functions of the *Xenopus* early embryo could be reconstituted in

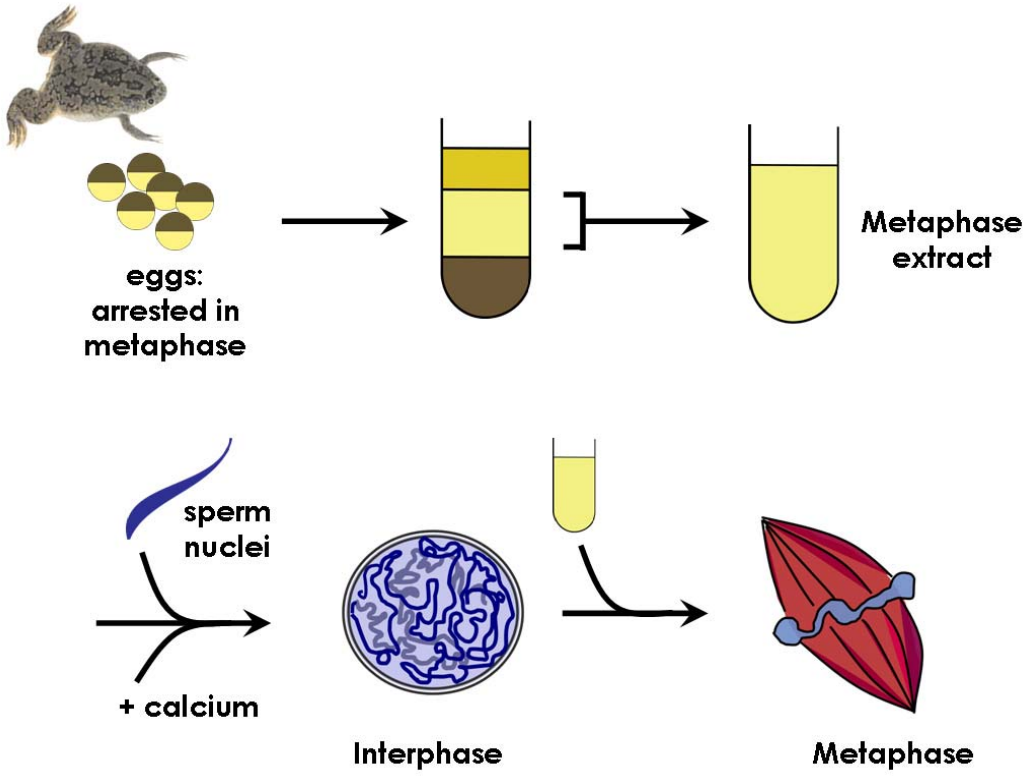

Figure 1.3. Preparation of *Xenopus* egg extract for cell cycle studies. Eggs laid by frogs are collected and subjected to a low speed spin to separate yolk, pigment, and cytoplasmic layers. Cytoplasm is extracted and utilized as metaphase-arrested (CSF) extract. Addition of sperm nuclei and calcium releases the metaphase arrest to allow interphase nuclear assembly of the sperm nuclei. After completion of interphase, more CSF extract can be added to induce metaphase and bipolar spindle formation.

vitro using cytoplasmic extracts of frog eggs. These functions include sperm nuclear remodeling, DNA synthesis, bipolar spindle formation, anaphase sister chromatid separation, and nuclear re-formation. The ability to study these processes in a test tube has provided many valuable opportunities to dissect their molecular mechanisms through biochemical manipulations. Components of the extract can be depleted using affinity methods, and exogenous components such as recombinant proteins, *in vitro*-translated materials, and small molecules can be added at will.

In a typical experiment, the egg extract is prepared by low-speed centrifugation of de-jellied eggs in buffer containing EGTA (Figure 1.3). This spin separates yolk, pigment, and cytoplasmic layers, from which the cytoplasmic extract can be isolated. In the absence of calcium, metaphase arrest is maintained in these extracts, but can be released by the addition of calcium to mimic fertilization signaling. Upon release from metaphase arrest, Cdk activity is downregulated in the extract, and interphase processes such as DNA replication and nuclear formation are induced. At the completion of interphase, the extract can continue cycling to metaphase, though it is customary to induce metaphase with the addition of more metaphase extracts that do not contain calcium.

1.4 *The nuclear envelope*

In eukaryotic cells, the nucleus is enclosed by the nuclear envelope, a structure that consists of a porous double membrane supported by a filamentous network known as the lamina (Figure 1.4). The two membranes are termed the inner nuclear membrane (INM) and outer nuclear membrane (ONM). Nuclear pore complexes (NPCs) embedded in the membrane control the flow of materials in and out of the nuclear

compartment. NPCs permit the free diffusion of small molecules and regulate the nucleocytoplasmic trafficking of larger molecules by providing docking sites for a large group of specialized transport molecules (Rout and Aitchison, 2000).

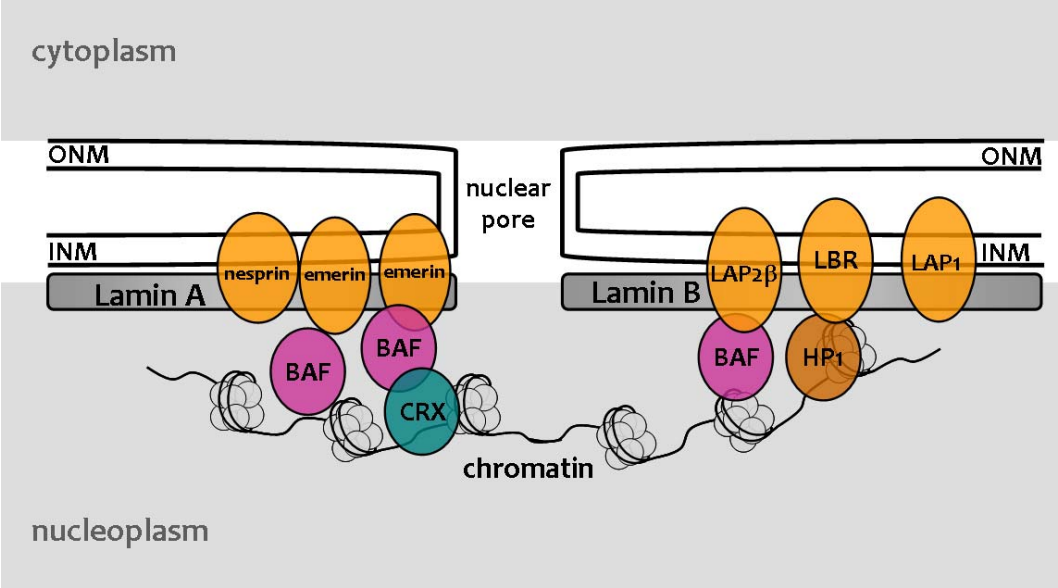

Figure 1.4. Schematic illustration of the NE. Adapted from (Hetzer et al., 2005). INM proteins are grouped into Lamin A- and Lamin B-binding proteins. Many INM proteins contact lamins, and bridge connections to chromatin via proteins like BAF.

The lamina consists of lamin proteins, intermediate filament-type proteins of two types. B-type lamins are expressed ubiquitously, while A/C-type lamins are present only in differentiated cells (Burke and Ellenberg, 2002). The lamin proteins that comprise the lamina interact with integral membrane proteins as well as chromatin components, thereby helping to organize intranuclear structure (Gant and Wilson, 1997). One key interaction in this arrangement appears to be that between chromatin-

binding factor BAF and emerin, which associates with lamina and inner nuclear membrane. Thus, chromatin can be tethered to the nuclear membrane in interphase. Lamin B receptor (LBR) protein and members of the LAP family of proteins also serve to link lamin and inner nuclear membrane.

1.5 *"Open" versus "Closed" Mitosis*

The nuclear envelope provides a useful barrier during interphase, but during mitosis, the cell must re-localize tubulin and mitotic regulatory factors to chromosomes to permit spindle assembly. The so-called "higher eukaryotes" including plants and animals achieve this through an open mitosis, in which the nuclear envelope breaks down and the spindle forms around chromosomes in cytoplasm. In contrast, many single-celled "lower eukaryotes" undergo a closed mitosis in which they retain the nuclear envelope during nuclear division. In budding yeast, the spindle forms between spindle pole bodies that are embedded in nuclear envelope (Sazer, 2005).

Open and closed mitoses present different challenges to the organisms that employ them. In open mitosis, cells must coordinate nuclear envelope breakdown and subsequent re-formation with the other events of mitosis. We discuss these processes in detail in sections below. In closed mitosis, cells must distinguish between the very different roles of their nuclei in interphase versus mitosis, in the context of maintaining the nuclear compartment. Budding yeast handle this situation by regulating the rate of import of mitotic regulatory factors through post-translational modifications (Hagting et al., 1999; Li et al., 1997)

It has become clear that rather than partitioning strictly between open or closed mitosis, many organisms employ intermediate mechanisms

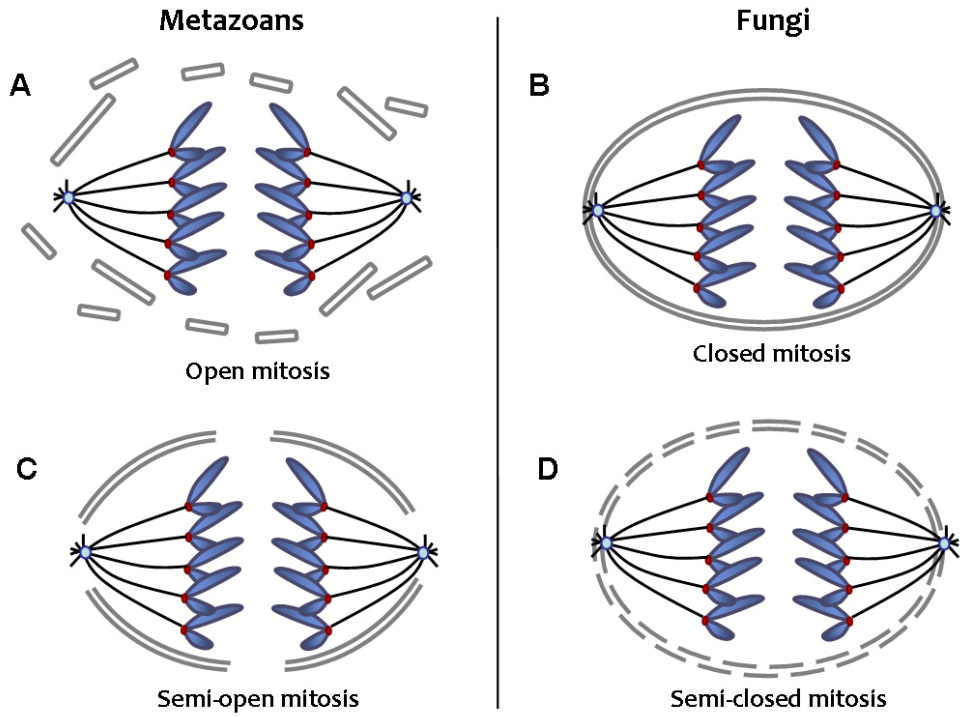

Figure 1.5. The terms 'open' and 'closed' mitosis designate extreme cases of the various ways in which cells handle the NE during mitosis. Adapted from (Guttinger et al., 2009). (a) In open mitosis, the NE is completely disassembled and removed from chromatin. (b) In closed mitosis, the NE stays intact. The establishment of a nuclear spindle requires nuclear uptake of tubulin. (c) In higher eukaryotes, semi-closed mitosis is accomplished by certain cell types, such as in *Caenorhabditis elegans* early embryos or during embryonic divisions in *Drosophila melanogaster*. The NE finally breaks down during anaphase. (d) Some lower eukaryotes, such as the filamentous fungus *Aspergillus nidulans*, also undergo semi-closed mitosis and partially disassemble their nuclear pore complexes to achieve the rapid influx of tubulin.

to effect the dramatic changes to the nucleus between interphase and mitosis (Figure 1.5). The nematode *C. elegans* displays a partially open mitosis in which the nuclear envelope disassembles very late, remaining intact except at spindle poles through early anaphase before fully disassembling in late anaphase (Lee et al., 2000). In the single-celled fungus *Aspergillus nidulans*, NPC structure changes dramatically in mitosis, allowing nuclear localization of Ran-GAP. This protein plays a central role in regulating nucleocytoplasmic transport, and its re-localization to the nucleus results in dramatic changes to that process, giving mitotic proteins access to chromosomes. Therefore, though *A. nidulans* undergoes closed mitosis with nuclear envelope intact, the mitotic reorganization of nuclear import makes it more closely resemble an open mitosis on the molecular level (De Souza et al., 2004; De Souza and Osmani, 2007). Clearly, a broad spectrum of processes have evolved for the division of the nuclear compartment, and there is much to be learned from studying the diversity of mechanisms.

1.6 *Nuclear envelope breakdown*

Two types of mechanisms have been reported to contribute to nuclear envelope breakdown (NEBD) at the start of open mitosis, but the details and relative contributions of each is not well understood. The first is phosphorylation of nuclear envelope components, likely controlled by Cdk activity, that results in their disassembly. Lamin proteins are phosphorylated during nuclear envelope breakdown (Ward and Kirschner, 1990), and mutation of some of these phosphorylation sites results in failure to disassemble the lamina in mitosis (Heald and McKeon, 1990)

Second, microtubules have been proposed to participate in active tearing of the nuclear envelope (Figure 1.6). This mechanism was proposed from visualization of the lamina by immunofluorescence of component proteins and electron microscopy. Earlier studies showed that invaginations formed that were occupied by microtubules. Though lamina disassembly occurs in the absence of microtubules (achieved by treatment with nocodazole, a microtubule-depolymerizing drug), it was reported

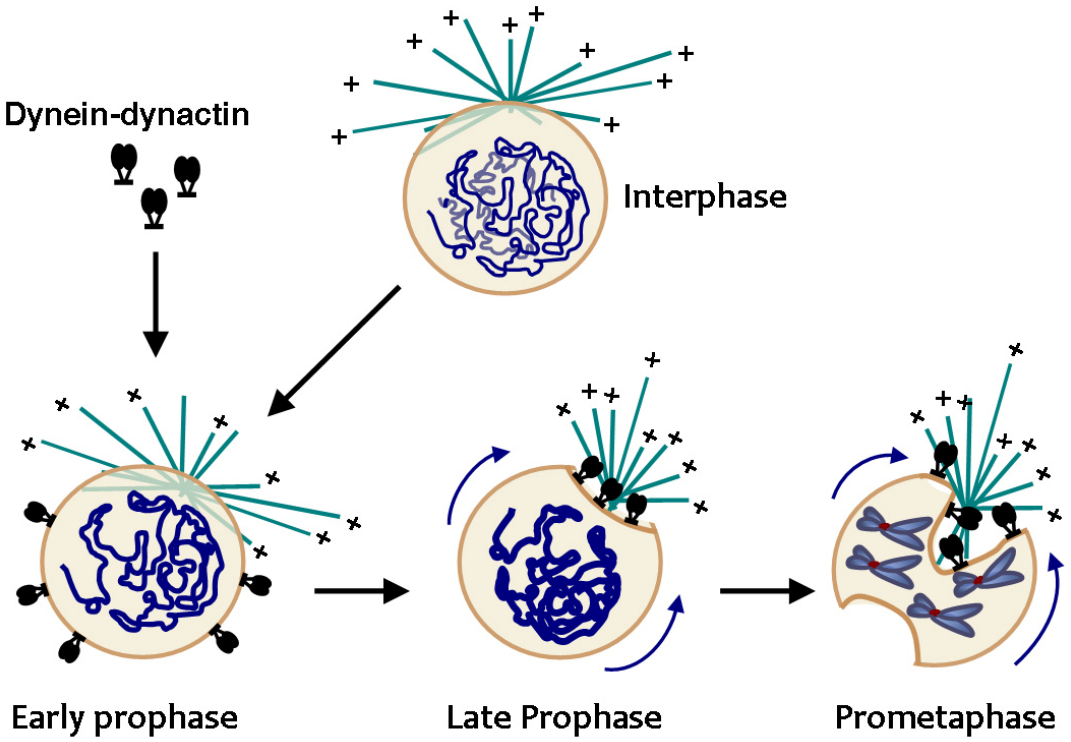

Figure 1.6. The role of dynein and MTs in nuclear membrane dynamics in early mitosis. Adapted from (Salina et al., 2002). NE-associated dynein has been proposed to interact with astral MTs, pulling NE components toward the centrosome, gradually forming a deep pocket or invagination. This results in disruption of the NE, potentially by causing the catastrophic expansion of nuclear membrane fenestrae created by NPC disassembly.

to be qualitatively different (Georgatos et al., 1997). More recently, higher resolution studies have confirmed the presence of asters containing dynein near the sites of lamina invaginations, and disruption of dynein and microtubules (again by nocodazole) has the effect of delaying NEBD in NRK cells (Salina et al., 2002). Interestingly, it appears that nuclear envelope pieces are actively removed from chromosomes in a microtubule-dependent manner, and transported towards centrosomes (Beaudouin et al., 2002).

1.7 *Nuclear re-formation*

In open mitosis, the disassembly of the nuclear envelope in prophase necessitates its reassembly in telophase. Live imaging of fluorescently-tagged nuclear envelope proteins has provided clues to the mechanism of nuclear re-formation. Some early studies focused on lamin B receptor, which was shown to be stable at interphase membranes, but mobile at the endoplasmic reticulum (ER) in metaphase (Ellenberg et al., 1997) At the end of mitosis, lamin B receptor is observed to coat decondensing chromosomes, but favors regions of lower microtubule density, away from areas of spindle attachment (Chaudhary and Courvalin, 1993; Gerlich et al., 2001). Subsequent localization studies of other nuclear envelope proteins confirmed this localization of lamin B receptor, and showed that LAP2B localizes all over chromosomes. In contrast, LAP2A, emerin, and BAF localize to an area termed the "core" region that is near the sites of microtubule attachment (Dechat et al., 2004). BAF (barrier-to-autointegration factor) is a DNA-binding protein and appears to play a critical role in the recruitment of nuclear membrane proteins to interphase

chromatin. Live imaging and electron microscopy studies showed that BAF localizes to the "core" region of anaphase chromosomes before other nuclear envelope components (Haraguchi et al., 2008), and BAF can recruit LEM domain-containing nuclear membrane proteins, like emerin (Haraguchi et al., 2001). BAF is mitotically phosphorylated by vaccinia-related kinase (VRK), causing it to dissociate from chromatin. This prevents nuclear envelope assembly during mitosis (Gorjanacz et al., 2007).

The mechanics of nuclear reassembly have been largely studied in *Xenopus* egg extracts, beginning in the mid-1980s when it was found that *Xenopus* eggs and their extracts would spontaneously assemble exogenous DNA into structures resembling nuclei (Forbes et al., 1983; Newmeyer et al., 1986). These structures recapitulate nuclear functions such as import and replication. Studies in *Xenopus* egg extracts have revealed stepwise assembly of nuclear membranes. Membrane components are targeted to chromosomes in late anaphase where they form sheets that envelope the chromatin, and finally expand by nuclear import (Hetzer et al., 2005) (Figure 1.7). This view has been refined to say that the nuclear envelope nucleates from intact tubules of mitotic endoplasmic reticulum (ER) which flatten to enclose the chromatin without fusion (Anderson and Hetzer, 2007). Recent studies have also identified cell cycle-regulated proteins that are involved in postmitotic nuclear assembly. TPX2 is a microtubule-associated protein (MAP) that is regulated by RanGTP and promotes spindle assembly in mitosis, but in interphase it relocalizes to chromatin where it recruits the inner nuclear membrane protein LAP2 to allow proper nuclear formation (O'Brien and Wiese, 2006). The AAA-ATPase Cdc48/p97 was identified in budding yeast as a protein required for completion of mitosis (Moir et al., 1982) and had been shown to play roles in assembly of

golgi and ER (Meyer, 2005; Uchiyama and Kondo, 2005). NE forms from ER. It was then shown that formation of a closed NE requires p97 in complex with

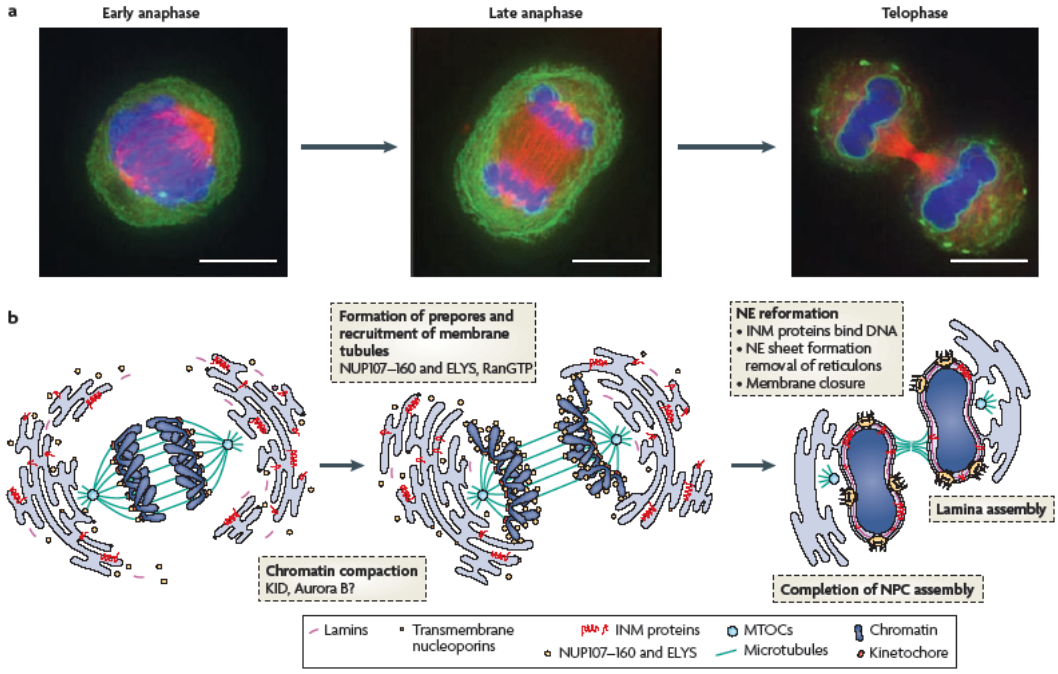

Figure 1.7. Nuclear envelope reassembly after mitosis. Reproduced from (Guttinger et al., 2009). (a) The images show HeLa cells with INM green (stained by GFP-LAP2β), DNA blue and microtubules red (stained by RFP-α-tubulin). Scale bars, 10 μm. (b) In anaphase, INM proteins are still dispersed in the tubular mitotic endoplasmic reticulum (ER). During late anaphase, ER membrane tubules start binding to the chromatin surface. During telophase, ER tubules are remodeled into flattened membrane sheets on the chromatin surface. Binding of INM proteins to DNA/chromatin supports the attachment of membrane sheets to chromatin. The first traces of lamins can be detected on chromatin at this stage. NPC formation is completed by the step-wise recruitment of further NPC constituents and the nuclear envelope (NE) is sealed.

Ufd1-Npl4 (Hetzer et al., 2001). It was thought that p97 acted by inducing nuclear membrane fusion, but it was later shown that N-ethylmaleimide sensitive factor (NSF) may be more important for that (Baur et al., 2007), and that fusion may in fact not be a primary mechanism for NE formation (Anderson and Hetzer, 2007).

1.8 *Spindle dynamics in mitosis*

Remodeling of the nuclear envelope at the start of mitosis generally serves to allow an influx of tubulin into the nucleus, activating microtubule polymerization from chromosomes to begin the process of bipolar spindle formation (Figure 1.8). In many cells with open mitosis, microtubule nucleation from centrosomes dominates over that from chromosomes, and in this case, breakdown of the nuclear envelope is necessary to give cytoplasmic centrosomes access to the chromosomes. In prophase, these centrosomes (which had duplicated in S phase) separate and mature, greatly enhancing their ability to nucleate microtubule polymerization (Khodjakov and Rieder, 1999). Centrosomes serve as the poles of the bipolar spindle, which forms as growing microtubules capture condensed chromosomes at their kinetochores. The dynamics of the growing microtubules are controlled by a variety of stabilizing and destabilizing proteins, and the microtubule array is organized by various motor proteins. Working in concert, the activities of these microtubule-binding proteins allow the self-assembly of a bipolar array of microtubules (Gadde and Heald, 2004; Kline-Smith and Walczak, 2004).

As the nuclear envelope is re-forming in telophase, the mitotic spindle is disassembled. Though it has not been demonstrated, this might occur via a shift in microtubule dynamics towards depolymerization from

kinetochores (Kirschner and Mitchison, 1986), as well as through the increased action of microtubule-destabilizing proteins such as Op18 and MCAK, or microtubule-severing proteins like katanin (Desai and Mitchison, 1997). Studies in yeast demonstrated that APC destruction of Ase1 is required for proper timing of spindle disassembly, and non-destructible mutant of Ase1 caused a delay in the process (Juang et al., 1997). Similar phenotypes were reported for mutants in Ipl1 and Sli15, yeast homologs of Aurora B kinase and its interacting protein, Incenp (Buvelot et al., 2003; Tanaka et al., 2002). Finally, nuclear envelope re-formation impedes access of tubulin to chromatin, reducing the ability of chromatin to nucleate microtubule polymerization.

As spindle microtubules capture kinetochores, chromosomes move towards the metaphase plate. Bi-oriented attachments, in which sister chromatids are attached to opposite spindle poles, are stabilized compared to mono-oriented attachments. A monitoring system known as the spindle assembly checkpoint (SAC) signals unattached kinetochores, and prevents the transition from metaphase to anaphase until all sister kinetochores are properly attached. One this happens, the cell proceeds to anaphase, with the spindle elongating and sister chromatids being pulled to opposite poles (Cheeseman and Desai, 2008).

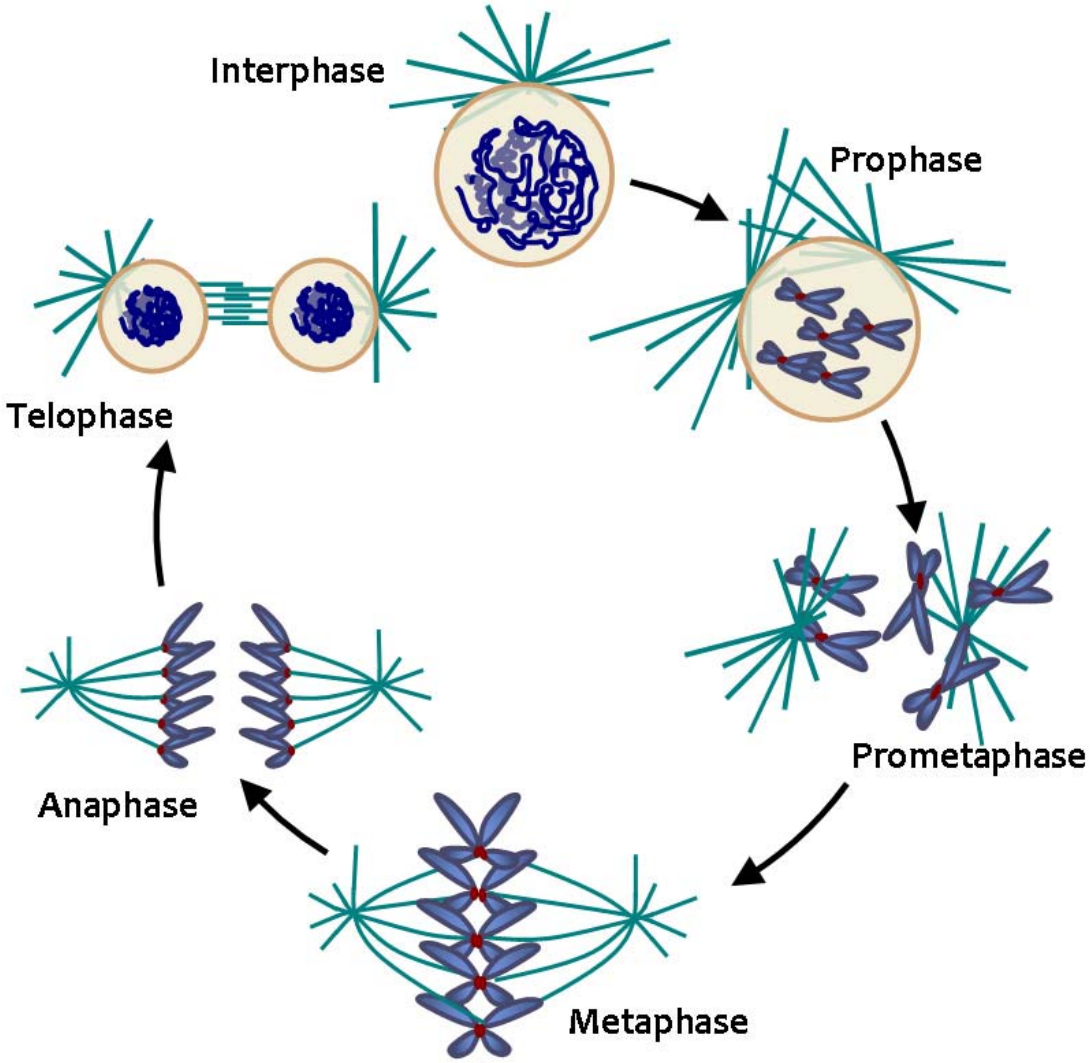

Figure 1.8. Chromosome-spindle interactions in the cell cycle. Adapted from (Cheeseman and Desai, 2008). During prophase, replicated interphase chromatin is condensed, while kinetochores assemble on the centromere regions of chromosomes. After nuclear envelope breakdown in prometaphase, kinetochores interact with spindle microtubules. By metaphase, all chromosomes are bi-oriented and aligned in the middle of the spindle. During anaphase, separated sister chromatids move away from each other to opposite spindle poles. Subsequently, during telophase, the chromatid masses decondense and the nuclear envelope reforms to generate the daughter nuclei.

1.9 *SUMOylation signaling*

This thesis concerns a protein that is specifically SUMOylated on chromatin, so here we describe this covalent modification in detail. The post-translational attachment of small ubiquitin-like modifier (SUMO) polypeptide was discovered in 1996 through investigations of the RanGAP protein, a critical factor for nucleocytoplasmic transport. The association of RanGAP with NPCs was found to depend on this post-translational modification (Matunis et al., 1996). The SUMO polypeptide is conserved throughout eukaryotes, and human SUMO-1 protein can rescue the yeast deletion (Takahashi et al., 1999). Also conserved is its conjugation system, which consists of a series of three enzymes, E1, E2, and E3 that hand off the modification in a cascade culminating in the substrate (Knipscheer et al., 2008) (Figure 1.9). SUMOylation is a reversible modification whose removal is catalyzed by a family of isopeptidases (Mukhopadhyay and Dasso, 2007). The E2 enzyme, Ubc9, is essential in budding yeast, and causes severe mitotic defects in fission yeast (al-Khodairy et al., 1995; Seufert et al., 1995). Mice lacking Ubc9 die at very early embryonic stages, due to inability of embryonic stem cells to proliferate. When cultured from inner cell mass, these stem cells exhibit abnormal cell growth, characterized by anaphase bridges and abnormal nuclear architecture (Nacerddine et al., 2005).

Multicellular eukaryotes contain three isoforms of SUMO termed SUMO-1, SUMO-2, and SUMO-3. SUMO-1 is 47% identical to SUMO-2, which is 97% identical to SUMO-3 (Geiss-Friedlander and Melchior, 2007). Due to their high degree of similarity, SUMO-2 and SUMO-3 are sometimes collectively referred to as SUMO-2/3. SUMO-1 knockout mice display no phenotype, and it appears that SUMO-2 can substitute for SUMO-1 in this situation (Zhang et al., 2008; Zhu et al., 2009). Though RanGAP is

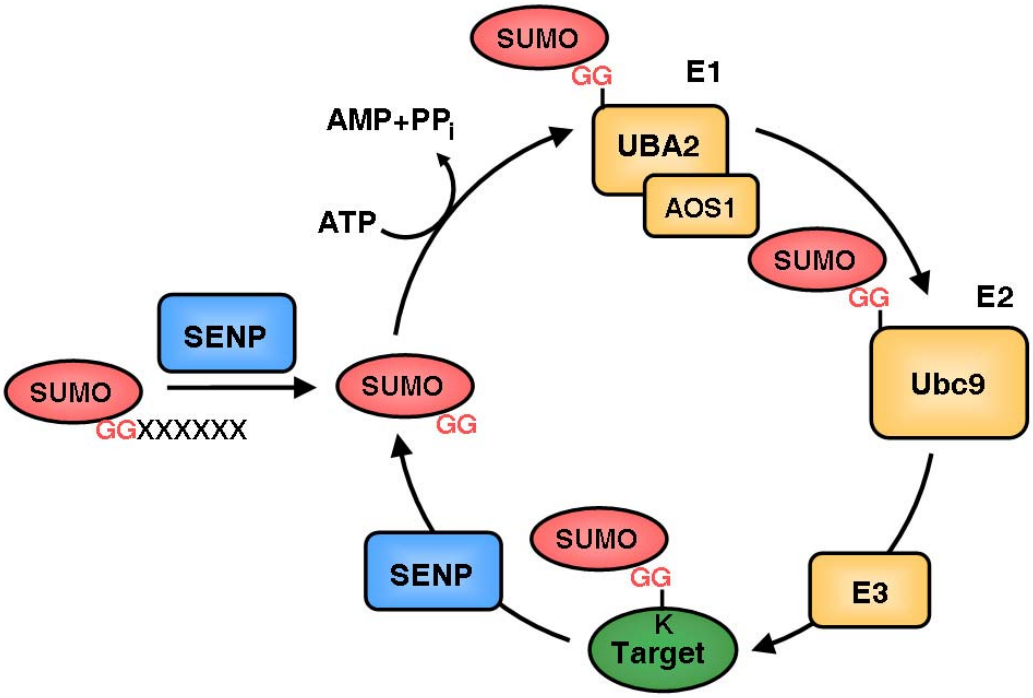

Figure 1.9. The mechanism of reversible SUMOylation. Adapted from (Geiss-Friedlander and Melchior, 2007). Before the first conjugation, nascent SUMO needs to be proteolytically processed to reveal its C-terminal Gly-Gly motif. This is accomplished by SUMO-specific isopeptidases (sentrin-specific proteases; SENPs). Mature SUMO is activated by the E1 heterodimer AOS1–BA2 in an ATP-dependent reaction, which results in a thioester bond between the C-terminal Gly residue and C173 in UBA2. SUMO is then transferred to the catalytic Cys residue of the E2 enzyme UBC9. Finally, an isopeptide bond is formed between the C-terminal Gly residue of SUMO and a Lys residue in the substrate. This step is usually aided by an E3 ligase. SUMOylated targets serve as substrates for SENPs, which ensures the reversible and dynamic nature of SUMOylation.

preferentially modified by SUMO-1 *in vivo* (Saitoh and Hinchey, 2000), it has been shown that there is no *in vitro* preference for attachment of SUMO-1 versus SUMO-2 on RanGAP, but that SUMO-1-RanGAP is stabilized compared to SUMO-2-RanGAP by association with Nup358, which protects it from isopeptidases (Zhu et al., 2009). Unlike Ran-GAP, the RecQ helicase BLM shows *in vitro* preference for modification by SUMO-2 over SUMO-1, and this selectivity is explained by preferential binding of SUMO-2 to BLM, compared to SUMO-1 (Zhu et al., 2008). Post-translation modification of SUMO and its conjugating enzymes could also help to explain paralog selectivity. Auto-SUMOylation of UBC9 was found to alter substrate specificity for certain targets (Knipscheer et al., 2008), and SUMO-1 is phosphorylated on a site that can potentially also be modified on SUMO-3, but is not present on SUMO-2 (Matic et al., 2008).

SUMOylation has been attributed to regulation of a diverse assortment of cellular processes, and seems to serve as an important signaling module in cells. Increasingly, SUMO-interacting proteins are being identified that contain SUMO-interaction motifs (SIMs). These motifs contain a hydrophobic core that may be flanked by acidic residues, though the complete consensus is not well understood (Hecker et al., 2006). A recent study has identified proteins that interact with SUMO in affinity purification, yeast two-hybrid screen, and yeast synthetic lethal screen (Makhnevych et al., 2009).

1.10 *Role of SUMOylation in the cell cycle*

Though many of the details remain unknown, many cell cycle-related proteins have been identified to interact with the SUMO pathway (Makhnevych et al., 2009). Among the best characterized of the mitotic

substrates is Topoisomerase II (Topo II), an enzyme involved in the decatenation of DNA loops in sister chromatid resolution at metaphase (Azuma et al., 2003). MS analysis of Topo II in *Xenopus* egg extracts identified it as a major SUMO substrate on metaphase chromosomes, and though addition of dominant-negative Ubc9 (dnUbc) did not affect decatenation activity, it resulted in chromosome segregation defects that could be attributed to problems with Topo II. A later study showed that PIASy is the SUMO E3 ligase required for Topo II SUMOylation, and that this is the predominant SUMO E3 ligase for substrates on metaphase chromosomes. Similar to dnUbc9, inhibition of PIASy by antibody addition resulted in chromosome segregation defects (Azuma et al., 2005). Contrary to the results in *Xenopus* egg extracts, a study in mouse demonstrated that RanBP2 is required for SUMOylation and proper localization of Topo II, with no apparent requirement for PIASy (Dawlaty et al., 2008). These organismal differences, or the interplay between these two different pathways of Topo II SUMOylation, remain unclear.

In addition to Topo II, the kinetochore-localized proteins Ndc10, Cep3, Ndc80, and Bir1 (Survivin in vertebrates) were found to be SUMOylated in budding yeast. This SUMOylation bears some relationship to microtubules, as these substrates were de-SUMOylated upon treatment of cells with nocodazole (Montpetit et al., 2006). In mammalian cells, the kinetochore protein CENP-E was found to be modified by SUMO-2/3, and overexpression of the SUMO isopeptidase SENP2 resulted in mislocalization of CENP-E. The same study reported that bubR1 and Nuf2 are also modified by SUMO2, but the functions of these modifications remain unknown (Zhang et al., 2008).

1.11 *The Aurora B Chromosome Passenger Complex*

Together with Incenp, Dasra (also known as Borealin), and Survivin, Aurora B forms a complex known as the Chromosome Passenger Complex (CPC). This complex derives its name from its pattern of localization during mitosis (Figure 1.10). Early in mitosis, the complex associates with chromatin. In metaphase, it localizes along chromosomes, with enrichment at inner centromeres. Upon entry into anaphase, the complex re-localizes from chromosomes to the spindle midzone, and it is present on the midbody structure between dividing cells in cytokinesis. The N-terminal portions of Incenp and Dasra/Borealin have been shown to associate with Survivin to form a three-helix bundle (Jeyaprakash et al., 2007) (Figure 1.11). It has also been shown that Dasra/Borealin promotes binding of Survivin to Incenp (Vader et al., 2006).

Aurora B kinase is the catalytic member of the complex, and it appears that the other members contribute to regulation of its activity. Dasra/Borealin and Survivin facilitate recruitment of Aurora B to chromosomal substrates, though the details of their function in the complex are not well understood. The interaction between Aurora B and Incenp is important for the activation of Aurora B kinase activity. It has been shown that phosphorylation of Incenp at three consecutive residues (the "TSS" motif) promotes its association with Aurora B, and that this association enhances the *in vitro* kinase activity of Aurora B (Bishop and Schumacher, 2002; Honda et al., 2003). Autophosphorylation of *Xenopus* Aurora B at Thr248 has also been shown to be an activating mark (Sessa et al., 2005). Finally, Aurora B is also activated by clustering, which could occur *in vivo* as the complex is recruited to chromatin (Kelly et al., 2007).

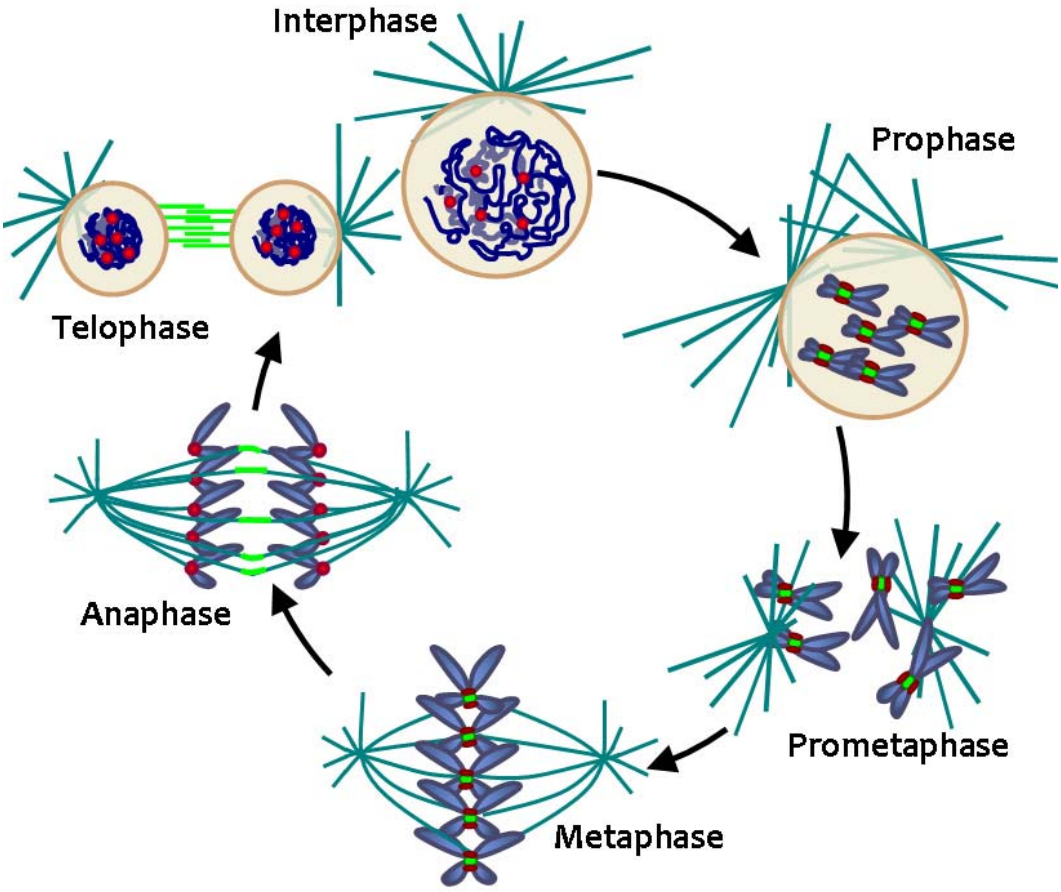

Figure 1.10. Chromosomal passenger complex localization during mitosis. Schematic representation of CPC localization (green) in mammalian cells during the main phases of mitosis, together with kinetochores (red), microtubules (teal) and DNA (blue). In prophase and prometaphase, CPC is found on chromosome arms and starts to accumulate at centromeres between kinetochores. In metaphase, chromosomes align on the spindle equator. In anaphase, Aurora-B leaves the chromosomes and relocates to the spindle midzone. In telophase, Aurora-B concentrates at the midbody between divided cells.

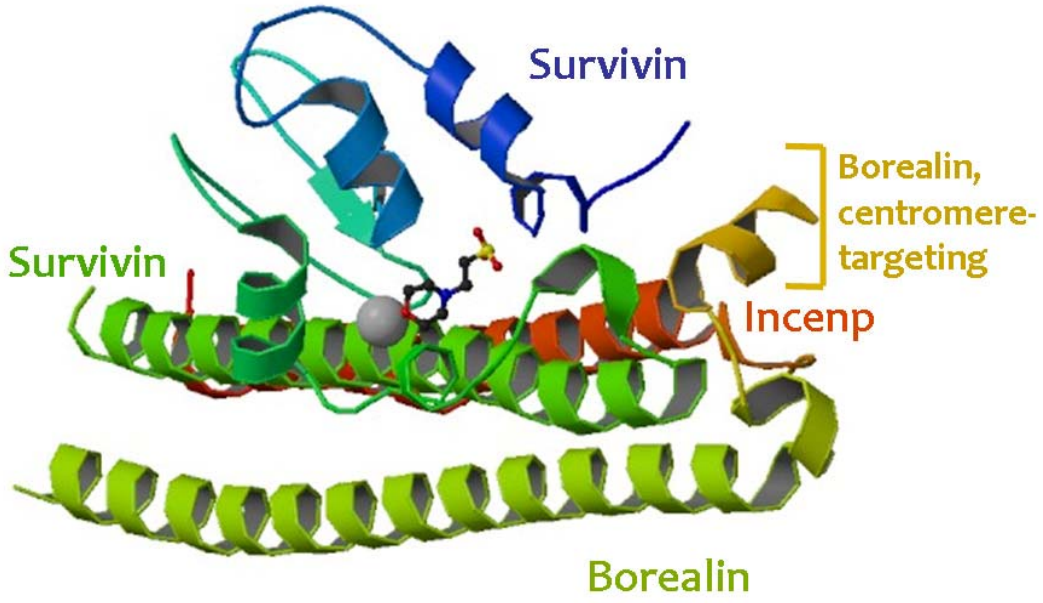

Figure 1.11. The Chromosome Passenger Complex Structure. Structure of a triple-helical complex of full-length Survivin with fragments of INCENP and Borealin/Dasra, adapted from (Jeyaprakash et al., 2007).

A number of important functions have been attributed to the CPC during mitosis. Depletion of the complex from *Xenopus* egg extracts using anti-Incenp antibodies results in loss of microtubule polymerization from chromosomes, and failure to form spindles. Therefore, the CPC is clearly required in this system for microtubule polymerization from chromosomes. Loss of CPC function in chromatin-induced microtubule assembly can be rescued by co-depletion of MCAK, a key microtubule-destabilizing protein (Sampath et al., 2004). MCAK negatively regulates microtubules by promoting catastrophe, or the transition from growth to shrinkage (Walczak et al., 2002; Walczak et al., 1996). The CPC is thought to promote

microtubule polymerization through inhibitory phosphorylation of MCAK by Aurora B. Additionally, Aurora B phosphorylates and negatively regulates Op18/stathmin, another catastrophe-promoting microtubule-destabilizing protein (Gadea and Ruderman, 2005). Therefore, two mechanisms by which the CPC promotes microtubule polymerization involve inhibition of microtubule-destabilizing proteins.

Budding yeast Aurora B is called Ipl1, and was shown to be required for release of spindle microtubules from kinetochores (Biggins and Murray, 2001; Biggins et al., 1999; Ruchaud et al., 2007; Tanaka et al., 2002). It was also known that Aurora B is required in a variety of organisms for proper chromosome bi-orientation, leading to the model that Aurora B detects and detaches improper kinetochore-microtubule attachments (Kelly and Funabiki, 2009). Proper attachment of sister chromatids to opposite spindle poles generates tension, and studies have suggested that the mechanism by which Aurora B recognizes improper attachments is the lack of this tension (Lampson et al., 2004; Liu et al., 2009). This leads to Aurora B activation of the spindle checkpoint (Pinsky et al., 2006).

One well-known mitotic substrate of Aurora B is histone H3 at Ser10 (H3S10ph). Phosphorylation of this site is a hallmark of mitosis, conserved from budding yeast to human, but the function of this modification is poorly understood. Mutation of the residue in the single-celled ciliate *Tetrahymena thermophila* resulted in loss of chromosome condensation and death due to failures in chromosomes segregation (Wei et al., 1999), but mutation of the corresponding residue in budding yeast results in no growth defects (Hsu et al., 2000). The roles of Aurora B and H3S10ph in mitosis and chromosome condensation remain mysterious.

Finally, studies in a variety of organisms have shown that the essential function of Aurora B and its associated proteins is in cytokinesis (Adams et al., 2001). Depletion of Aurora B from mammalian cells using siRNA results in the formation of multinucleate cells. The molecular details of Aurora B mechanism in cytokinesis are not well understood, but it appears that Aurora B phosphorylation of cytokinesis substrates including vimentin and CYK-4 are crucial for cytokinesis events such as cleavage furrow formation (Ruchaud et al., 2007).

1.12 *Aurora B at the completion of mitosis*

In addition to its many mitotic functions, Aurora B is emerging as an important player in the completion of mitosis. Yeast containing a mutant form of Ipl1, the yeast homolog of Aurora, were found to exhibit defects in mitotic spindle disassembly, resulting in a prolonged anaphase (Buvelot et al., 2003). A further role for aurora B complex in spindle disassembly comes from the observation that Cdc14 phosphatase targets Sli15 (the yeast homolog of Incenp), allowing it to relocalize to anaphase spindle microtubules (Pereira and Schiebel, 2003).

It has been known that the Triple A-ATPase Cdc48/p97 is critically important for events at the end of mitosis, and recently it was shown that the principal target of p97 in promoting nuclear assembly is Aurora B. p97 is a conserved, essential protein that plays roles in a variety of processes, including endoplasmic reticulum associated degradation (ERAD) of misfolded proteins (Ye et al., 2003), and activation of transcription factors NF-κB, SPT23, and MGA2 (Hoppe et al., 2000). Mutants in the yeast protein, Cdc48, lead to mitotic arrest (Moir et al., 1982), due to their inability to disassemble spindles and re-form nuclei and Golgi apparatus (Kondo et

al., 1997; Shorter and Warren, 1999). In *Xenopus*, it was shown that absence of p97 function inhibits spindle disassembly, though the mechanism remains unclear (Cao et al., 2003). Also in *Xenopus*, the formation of a closed nuclear envelope requires p97 (Hetzer et al., 2001). The mechanism of this requirement was revealed when it was found that p97 binds to ubiquitylated Aurora B and extracts it from chromatin, and that this process is necessary for proper nuclear formation (Ramadan et al., 2007).

One possible reason that Aurora B must be removed from chromatin at the end of mitosis is chromatin compaction. Studies of fluorescently-labeled chromosomes have shown that chromosomes are maximally compacted in anaphase, and that this compaction depends on Aurora B kinase activity (Mora-Bermudez et al., 2007). Cells that were treated with hesperadin, a chemical inhibitor of Aurora B, but not inhibitors of Cdk, showed loss of chromatid compaction. Therefore, Aurora B seems to play a role in chromosome compaction, which has itself been connected to nuclear assembly. Compaction mediated by the DNA-binding kinesin KID has been shown to be important for proper nuclear assembly—in the absence of KID, aberrant multiple small nuclei (multinucleate structures) form (Ohsugi et al., 2008).

Taken together, the results for p97 show that there is a link between the postmitotic processes of spindle disassembly and nuclear assembly, and that the removal of Aurora B from chromatin is central to this process, possibly through its chromosomal or spindle midzone substrates and a role for chromatin compaction. One thing that has been overlooked in this picture, however, is the role of microtubule depolymerization in nuclear formation. Aurora B complex has a well-characterized role in promoting microtubule polymerization from chromosomes (Kelly et al., 2007; Sampath

et al., 2004), and perhaps this activity presents a major obstacle to proper nuclear assembly. In the next section, we will briefly introduce the results of this thesis, which concern the identification of a chromatin-localized microtubule destabilizing activity that is required for proper nuclear re-formation.

1.13 *The role of Vespera in the completion of mitosis*

Using *Xenopus* egg extracts, we endeavored to identify uncharacterized proteins that bind to purified mitotic chromosomes. In doing so we discovered Vespera, a protein which is functionally antagonistic to the CPC. We chose the name "Vespera," after the Roman word for dusk, because this protein appears to oppose some functions of Aurora, which is the name for the Roman goddess of dawn. We show that Vespera promotes microtubule depolymerization from chromosomes and is required on chromatin for proper nuclear formation. We initially identified Vespera as a protein that is specifically SUMOylated upon interaction with chromatin, a modification that is dependent on the SUMO E3 ligase, PIASy. Immunodepletion of Vespera from *Xenopus* egg extracts interferes with proper nuclear formation and nuclear transport, and rescue of this defect requires Vespera SUMOylation. Addition of excess amounts of Vespera to metaphase extracts disassembles spindle microtubules, and this activity is also dependent on SUMOylation of Vespera and PIASy. Importantly, the Vespera depletion defect in nuclear formation can be rescued by nocodazole or by co-depletion of the CPC. These manipulations depolymerize microtubules, suggesting that the microtubule-depolymerizing activity of SUMO-Vespera is central to its role in ensuring proper nuclear formation.

Our results suggest that microtubules must be actively depolymerized around chromosomes to permit proper nuclear reassembly, a process that is promoted by SUMOylated Vespera.

CHAPTER TWO: IDENTIFICATION OF VESPERA AND CHARACTERIZATION OF ITS ROLE IN NUCLEAR FORMATION

2.1 *Introduction*

In an effort to better understand mitotic processes, we attempt to identify and characterize novel chromosome-binding proteins isolated from *Xenopus* egg extracts. Our approach relies on the ability to biochemically purify chromosomes from the extract. In a technique first described by Funabiki and Murray in 2000, biotin-dUTP is added to the extract and incorporated into replicating chromatin. After cycling to metaphase, the biotinylated chromosomes can then be pelleted out of the extract and purified on streptavidin-coated magnetic beads (Funabiki and Murray, 2000). This method was later adapted to perform a screen for chromosome-binding proteins (Figure 2.1.) that identified Dasra A as a new member of the CPC (Sampath et al., 2004).

As an alternative to the expression screening strategy, mass spectrometry (MS) can be used to identify proteins (Figure 2.2). This method is made possible by the increasing availability of genome and cDNA sequence data, which can translated in silico to generate protein sequence databases. A given protein sample is enzymatically digested by treatment with proteases, and the masses of the resulting peptides can be accurately measured by MS. These peptides can be further broken along peptide bonds using various gas phase chemical reactions, to generate ladders of fragments differing by discrete amino acids. The peptide and

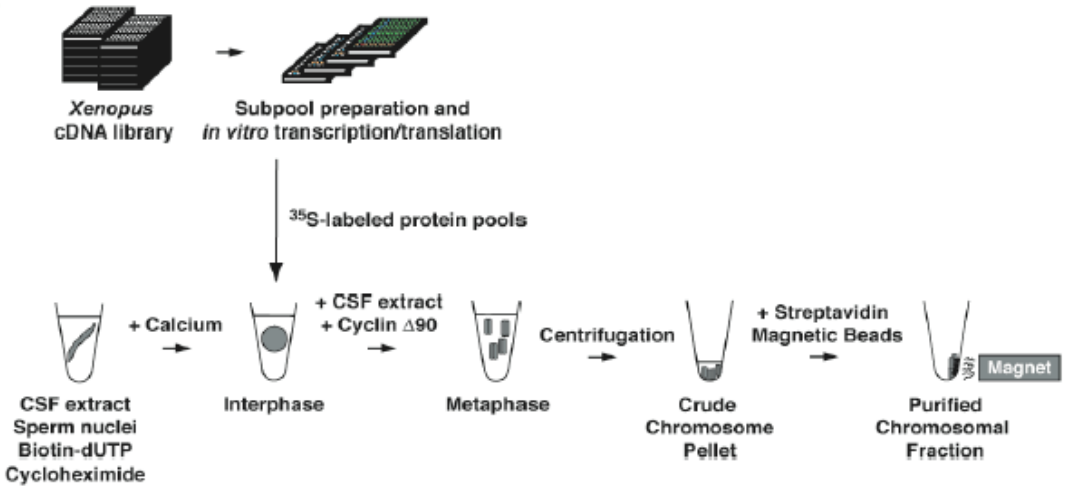

Figure 2.1. Schematic of the expression screening method used to screen an arrayed *Xenopus* egg cDNA library for mitotic chromosome-binding proteins. For complete method details, see (Sampath et al., 2004). Seven thousand bacterial colonies containing independent cDNA clones were robotically formatted into 96-well plates, and plasmid pools were prepared from columns, rows, and plates. These plasmid pools were added to a coupled transcription-translation system to produce labeled protein pools. These pools were then added to *Xenopus* egg extracts in interphase, while biotin-dUTP was incorporated into replicating chromatin. Following completion of interphase, extracts were cycled to metaphase as shown, and biotinylated chromosomes were purified using streptavidin-magnetic beads. Chromosome-associated proteins were analyzed by SDS-PAGE and autoradiography, and clones that showed strong binding to chromosomes were selected for further analysis.

fragment masses can then be compared to theoretical values for the entire protein sequence database, and an identification match can be determined. This approach to identify proteins using a combination of MS and database

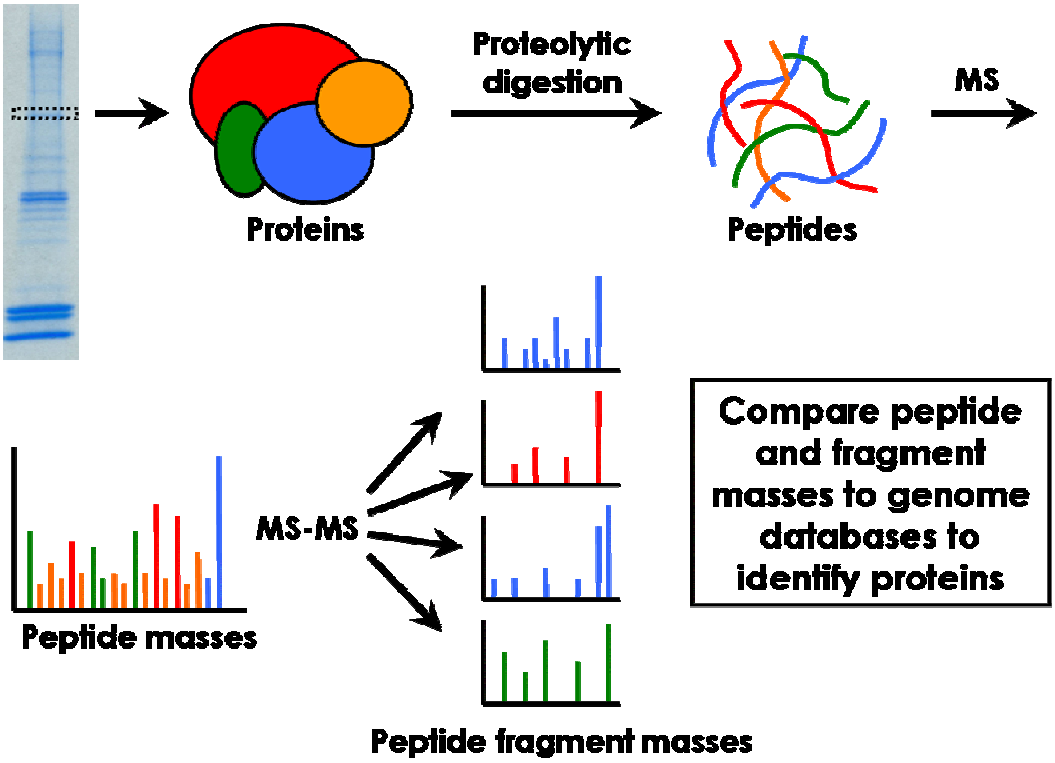

Figure 2.2. Schematic of procedure for identification of proteins by mass spectrometry (MS). Proteins are separated by SDS-PAGE, and gel slices are excised and subjected to proteolytic digestion. The resulting peptides are analyzed by MS to obtain their accurate masses, and by tandem MS (MS-MS) to determine fragment masses. Peptide and fragment masses are compared to theoretical values generated from genome sequence data to identify proteins.

searching has revolutionized biochemistry, allowing for the identification of proteins on a much faster and larger scale than was previously possible (Cronshaw et al., 2002; Mann et al., 2001; Pandey and Mann, 2000; Tackett et al., 2005).

We therefore devised a mass spectrometry (MS)-based proteomics approach for the identification of chromatin-binding proteins using *Xenopus* egg extracts (Figure 2.3). In order to study bulk chromatin contributions to large-scale structures in the cell cycle, we used DNA-coated magnetic beads, which are chromatinized in egg extracts and can support formation of interphase nuclei and mitotic spindles in the absence of centrosomes and centromeres (Anderson and Hetzer, 2007; Heald et al., 1996). DNA-beads were isolated from interphase or metaphase extracts, and the associated proteins were separated by SDS-PAGE and identified by MS (see Appendix I). Binding to DNA-beads was confirmed using 35S-labeled proteins translated *in vitro*.

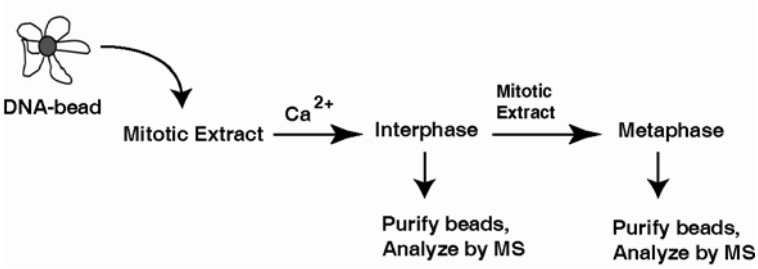

Figure 2.3. Method scheme for the identification of chromatin-bead-binding proteins. DNA-beads in interphase and metaphase *Xenopus* egg extracts were purified and analyzed by MS to identify associated proteins.

2.2 *Identification of Vespera, a Protein SUMOylated upon Binding Chromatin*

Following MS identification of DNA-beads-binding proteins, we singled out hypothetical protein MGC115729 for further study because it exhibited a prominent mobility shift (~10 kD) upon association with chromatin (Figure 2.4). In general, we want to understand chromatin-induced processes in the cell-cycle, and therefore a protein with chromatin-induced modification was of interest to us. An additional smaller mobility shift (~2 kD) is observed for *in vitro* translated protein (Figure 2.4), but not endogenous protein (see Figure 2.8), and is presumably due to use of an alternative translation initiation site. This protein, which we term Vespera, consists of 240 amino acids and contains an N-terminal SAP motif (after SAF-A/B, Acinus and PIAS) (Aravind and Koonin, 2000), which is a putative DNA-binding module.

We observed that the chromatin-dependent mobility shift of Vespera was consistent in size with posttranslational modification by ubiquitin or the small ubiquitin-related modifier SUMO. To identify the modification, we incubated 35S-labeled Vespera in CSF (cytostatic factor) extracts arrested at meiotic metaphase II, supplemented with a large excess amount of hexahistidine (6His)-tagged recombinant SUMO-1, SUMO-2, SUMO-3, or ubiquitin proteins. All three isoforms of

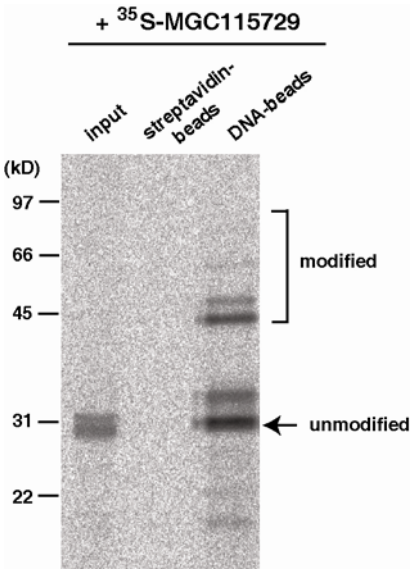

Figure 2.4 MGC115729 is modified on chromatin. ^{35}S-labeled, *in vitro*-translated MGC115729 (Vespera) was incubated for 40 min at 22°C with CSF (metaphase II-arrested) extract containing cycloheximide. DNA-beads or streptavidin-beads were then added to the extract for an additional 40 min, after which the beads were purified, and analyzed by SDS-PAGE and autoradiography. Arrow indicates unmodified protein, and bracket indicates chromatin-dependent modification. The double band is an artefact of *in vitro* translation in reticulocyte lysates**.**

SUMO, but not ubiquitin, were conjugated to Vespera, as evidenced by the additional mobility shift induced by attachment of the His tag (Figure 2.5A). Furthermore, this Vespera modification is dependent on the SUMO E3 ligase PIASy (Figure 2.5B). From this we conclude that the modification of Vespera on chromatin is PIASy-dependent conjugation of SUMO.

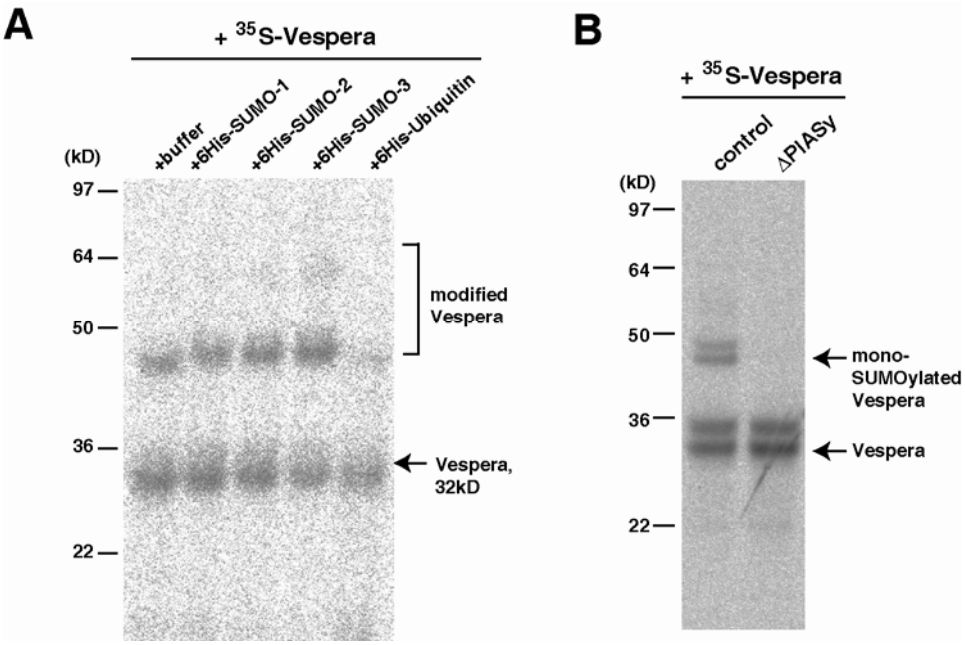

Figure 2.5. Characterization of Vespera SUMOylation. Chromatin-bound, ^{35}S-labeled Vespera was visualized as in Figure 2.4, (A) from extracts supplemented with 6His-SUMO-1, 6His-SUMO-2, 6His-SUMO-3, 6His-Ubiquitin, or buffer control, and (B) from extracts that were depleted with either control IgG-beads or anti-PIASy beads.

2.3 *SUMOylation Site Mapping of Vespera*

To determine the site of covalent SUMO attachment, we systematically mutated each of the thirteen lysine (K) residues in Vespera to arginine (R). 35S-labeled wild-type or mutant protein was incubated with DNA-beads in CSF extract, and the beads were collected and analyzed by SDS-PAGE and autoradiography. Most of the Vespera constructs were robustly SUMOylated on chromatin, with two exceptions (Figure 2.6). A K42R mutant was unable to bind to DNA, and a K230R mutant could bind DNA,

but was not SUMOylated. K42 corresponds to a highly conserved residue in the SAP domain that has been shown to make contacts with DNA (Suzuki et al., 2009), and appears to be strictly required for DNA binding. We therefore determined that K230 is required for SUMOylation, and is the apparent attachment site for SUMO chains. Since the SUMOylation site

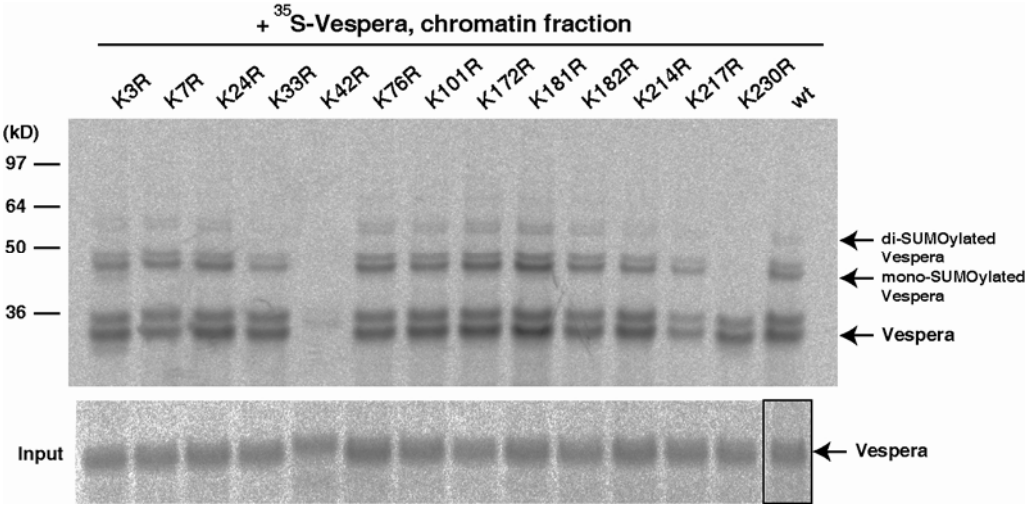

Figure 2.6. Mapping of Vespera SUMOylation site. Wild-type Vespera and thirteen Lys to Arg mutants were analyzed as in Figure 2.4. Top gel: Chromatin-bound Vespera proteins. Bottom gel: in put, *in vitro*-translated Vespera proteins. deficient K230R

mutant can bind DNA, SUMOylation is not required for targeting Vespera to chromosomes.

Finally, we asked if SUMOylation of Vespera is cell-cycle dependent. We prepared chromatin beads that were incubated in CSF extracts, or CSF extracts released with calcium. Vespera SUMOylation occurred in both cases (Figure 2.7), so we conclude that Vespera SUMOylation on chromatin beads is not cell-cycle dependent.

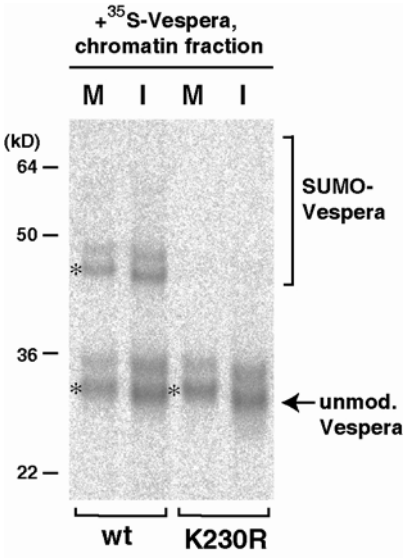

Figure 2.7 Vespera SUMOylation is not cell cycle-dependent. Wild-type or mutant Vespera was analyzed as in Figure 2.2. 35S-labeled Vespera was incubated with metaphase CSF extracts (M), or interphase extracts (I). Phosphorylated Vespera is marked with an asterisk (*).

2.4 *Vespera Is Required for Proper Interphase Nuclear Formation*

In order to study native Vespera, we raised polyclonal antibodies to the full-length recombinant protein. In Western blots of CSF extracts, these antibodies recognized one principal band corresponding to the molecular weight of Vespera, ~32 kD (Figure 2.8). Immunoprecipitation and MS analysis confirmed that these antibodies bind endogenous Vespera (Figure 2.9). Furthermore, native Vespera SUMOylation could be detected by Western blotting by adding high concentrations of DNA to egg extracts

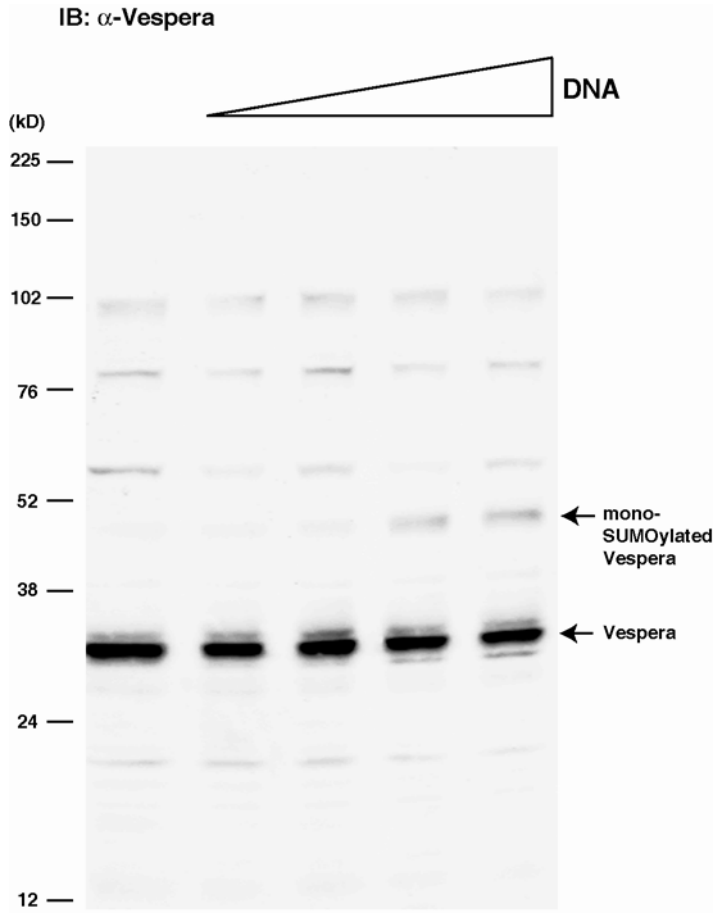

Figure 2.8. Detecting DNA-induced SUMOylation of endogenous Vespera. CSF extracts were incubated with increasing amounts of plasmid DNA (0, 20, 50, 100, 200 μg/ml) for one hour at 22°C. Total extract proteins are analyzed by Western blotting with anti-Vespera antibodies.

(Figure 2.8). Immunolocalization showed that Vespera binds throughout chromatin in interphase nuclei (Figure 2.10A) and all along chromosomes on metaphase spindles (Figures 2.10B and C).

List of Vespera peptides confirmed in Immunoprecipitated sample by MS/MS:

M(observed)	M(calculated)	ΔM	From-To	Peptide
800.492	800.487	0.005	35 - 42	LGLRGTGK
1668.762	1668.739	0.023	158 - 171	SVFQDNYPPMGQMR
1796.872	1796.834	0.038	158 - 172	SVFQDNYPPMGQMRK
1989.082	1989.09	-0.007	8 - 25	TPAPEPDLTPNSLQLLKR
2014.042	2014.033	0.009	197 - 214	RVDELLDQLATGQVDSQK

MS/MS data
for peptide [197-214]:

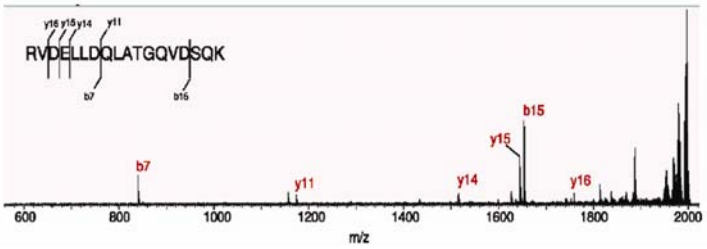

Figure 2.9. MS validation of anti-Vespera antibodies recognition of Vespera. CSF extracts were incubated with anti-Vespera beads for 30 min on ice. Beads were collected and washed, and the immunoprecipitated proteins were digested with trypsin (7h, 37°C). Tryptic peptides were collected using C18 resin and analyzed by MS and MS/MS. Listed in the table are the Vespera peptides confirmed by MS/MS, with MS/MS spectrum shown for one of these peptides.

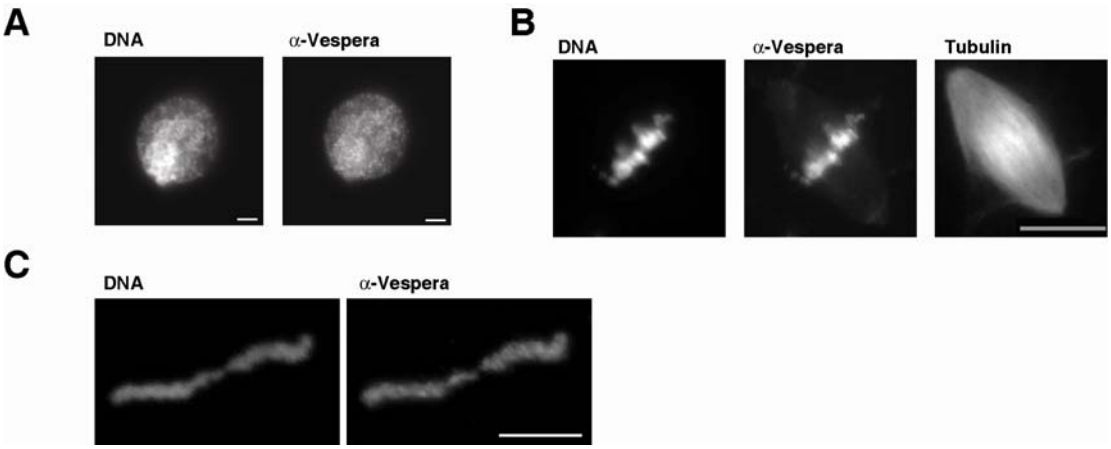

Figure 2.10. Immunofluorescence localization of Vespera. (A) Interphase localization of Vespera. Sperm nuclei were added to CSF extract, then cycled to interphase by addition of calcium for 80 min at 22°C. DNA was stained with Hoechst 33258, and Vespera was visualized by indirect immunofluorescence. Scale bar, 5 μm. (B) Immunolocalization of Vespera on metaphase spindles assembled on replicated chromosomes. Scale bar, 20 μm. (C) Immunolocalization of Vespera on an individual metaphase chromosome in diluted extracts. Scale bar, 10 μm.

We then sought to ascertain the function of Vespera and its modifications by immunodepletion of the native protein from CSF extracts and replacement with wild-type or mutant recombinant proteins (Figure 2.11).

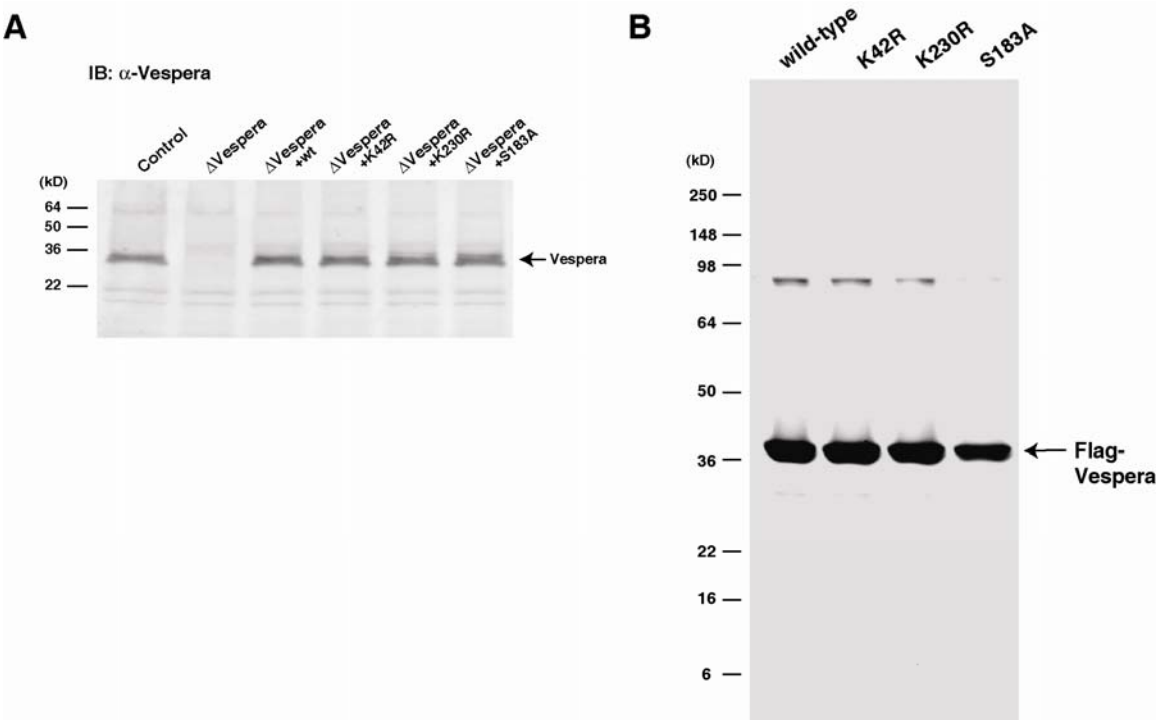

Figure 2.11. Immunodepletion and addback of Vespera. (A) CSF extracts containing cycloheximide were depleted with either control IgG-beads (lane 1) or anti-Vespera beads (lanes 2-6). In lanes 3-6, the indicated recombinant Vespera proteins were added to extracts following depletion. Total protein samples were collected and probed by Western blot using anti-Vespera antibodies. (B) Recombinant Flag-tagged wild-type and mutant Vespera proteins were analyzed by SDS-PAGE and Coomassie stain. See Materials and Methods for bacterial expression and purification methods.

Demembranated sperm nuclei were added to these extracts, followed immediately by addition of calcium, which mimics fertilization signaling to release extracts from metaphase to interphase. In mock-depleted interphase extracts, round nuclei formed around sperm chromatin within 30 min of

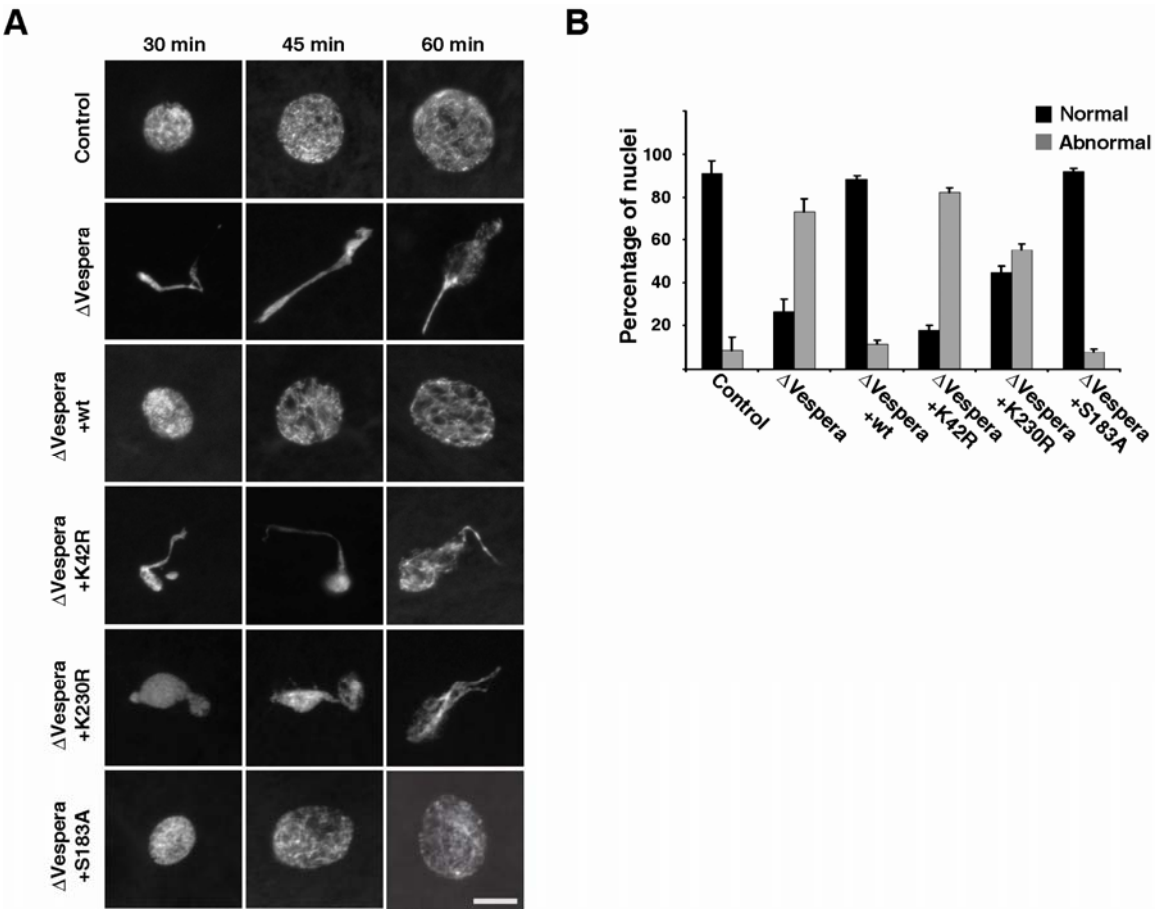

Figure 2.12. Timecourse analysis of nuclear formation. Sperm nuclei and calcium were added to depleted extracts shown in (A) at 22°C to induce assembly of nuclei. DNA was stained with Hoechst 33258. Scale bar, 10 μm (C) Quantitation of normal and abnormal nuclear formation in (B). Values shown are the mean and standard deviation from three independent experiments, with ~200 nuclei counted per sample per experiment.

sperm addition and decondensed further over time in a uniform manner. By contrast, sperm chromatin in Vespera-depleted (ΔVespera) extracts gave rise to deformed, pinched nuclei that swelled irregularly (Figure 2.12A).

This phenotype was rescued by adding wild-type or S183A (phosphorylation) mutant protein, but not K42R (DNA-binding) or K230R (SUMOylation) mutant proteins (Figures 2.12A and B). These results suggest that Vespera functions in interphase nuclear assembly, and that this role requires its DNA binding activity as well as its modification by SUMOylation. The defect is not due to impairment in release from metaphase arrest, as the metaphase-dependent phosphorylation of histone H3 at threonine 3 (H3T3ph) was properly removed upon induction of interphase in ΔVespera extracts (Figure 2.13A). Overall chromosomal SUMOylation did not appear to be affected in ΔVespera extracts (Figure 2.13B). Despite the morphological defects, the chromatin in ΔVespera extracts appears able to recruit nuclear membrane components (Figure 2.14C), as visualized by immunofluorescence staining of lamin B3 (Shumaker et al., 2008) and nucleoporins (Davis and Blobel, 1986).

Nuclear function, however, is defective, as deformed nuclei in ΔVespera extracts exhibit impaired import of green fluorescent protein (GFP) tagged with an SV40 nuclear localization signal (GFP-NLS, Figure 2.14). The defect we observe may encompass two activities of the extract: 1) sperm chromosome remodeling and 2) interphase nuclear assembly. The first is an egg-specific process whereby, upon fertilization, the highly compact sperm chromatin, devoid of histone H2A and H2B, is remodeled to a more relaxed structure containing nucleosomes (Wright, 1999). The second is a general process in open mitosis—nuclear envelope disassembly

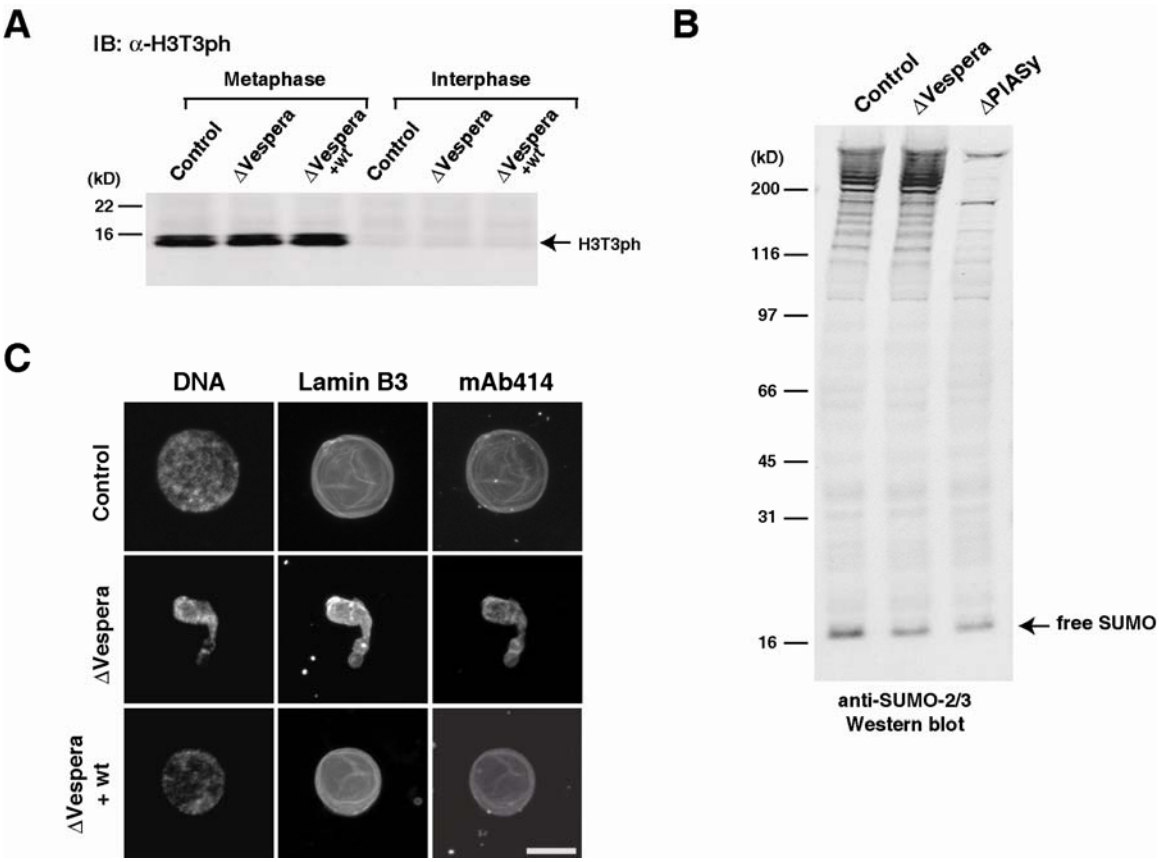

Figure 2.13. Characterization of Vespera Depletion. (A) Depleted extracts (Control, ΔVespera, and ΔVespera with wild-type addback) were probed by Western blot for anti-H3T3ph at 0 min and 20 min following the addition of calcium. (B) Vespera depletion does not affect global chromatin-induced SUMOylation. Plasmid DNA was added to control (IgG-depleted), Vespera-depleted, and PIASy-depleted extract, to a final concentration of 200 μg/ml. 0.5 ml of extract was analyzed by SDS-PAGE and Western blot using antibodies against SUMO-2/3. (C) Interphase nuclei were assembled for 60 min in the indicated extracts, and DNA was stained with Hoechst 33258, and Lamin B and nucleoporins were visualized by indirect immunofluorescence with anti-xLB3 and mAb414, respectively. Scale bar, 10μm.

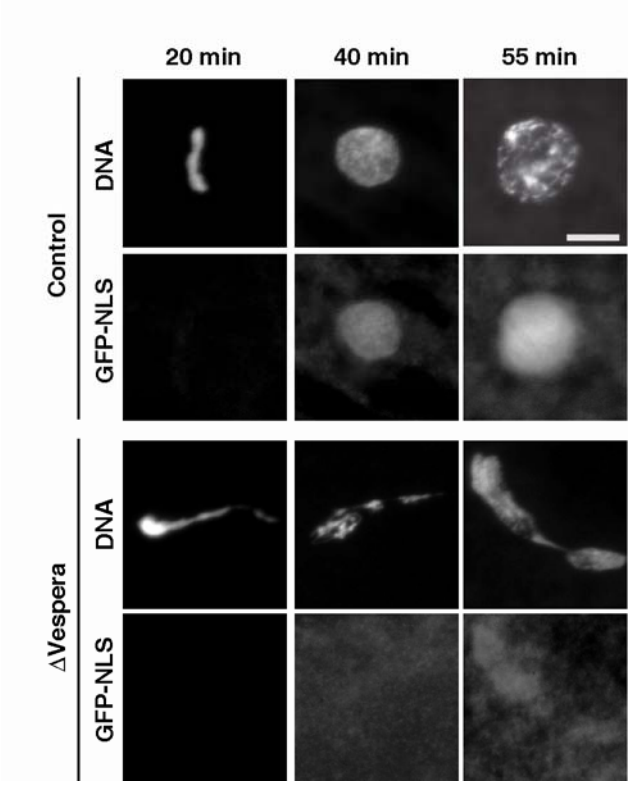

Figure 2.14. Nuclear Import is Impaired in ΔVespera Extracts. Nuclei were assembled in control and Vespera-depleted extracts containing GST-GFP-NLS, and visualized at the indicated timepoints. DNA was stained with Hoechst 33258. Scale bar, 10 μm.

in prophase must be followed by reassembly at the return to interphase. In addition, nuclear reassembly is important for sperm pronuclear formation at fertilization. To better understand the role of Vespera in these two processes, we decoupled them by preincubating compact sperm nuclei in CSF extracts for 45 minutes prior to addition of calcium. This allows time for sperm remodeling to occur prior to calcium-induced release from metaphase arrest. In this case, control and ΔVespera extracts both produced condensed, remodeled chromosomes from sperm, but ΔVespera extracts

remained deficient in interphase nuclear formation (Figure 2.15). Therefore, we conclude that Vespera is not required for sperm chromosome remodeling, but is required for nuclear re-formation.

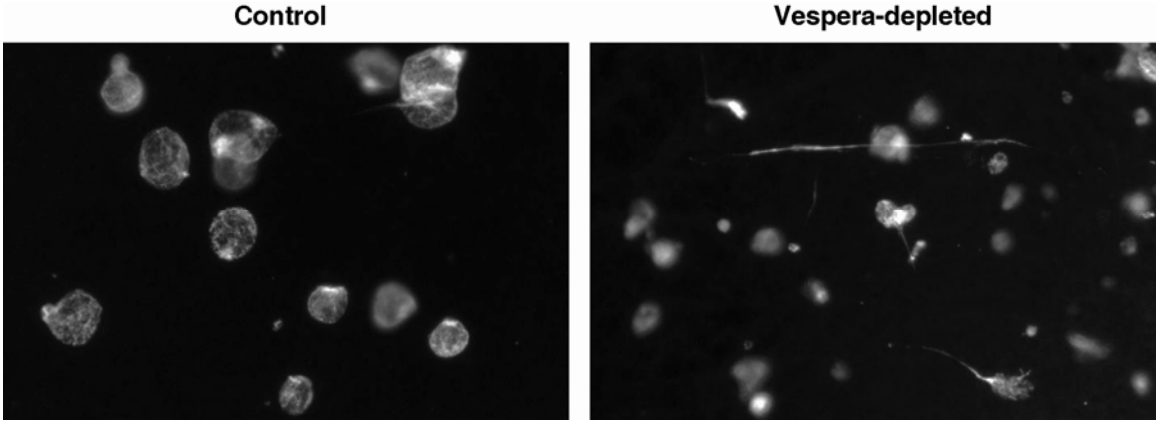

Figure 2.15. Vespera-depleted egg extracts exhibit defective nuclear assembly around remodeled sperm chromatin. CSF extracts were depleted with control IgG-beads or anti-Vespera beads, then incubated with sperm (2000/μl) for 45 min at 22°C. Calcium was then added to induce interphase, and DNA was visualized by Hoechst dye after 70 min.

2.5 *Excess Vespera Inhibits Metaphase Spindle Assembly*

As a further clue to Vespera function, we observed that excess Vespera protein disrupted bipolar spindle formation in metaphase extracts. We added 10-fold excess recombinant wild-type or mutant Vespera proteins to extracts (Figure 2.16A) and monitored spindle assembly on replicated sperm chromosomes. Interphase proceeded normally in all cases (data not shown), but 50 min after induction into metaphase, we found that extracts containing excess wild-type Vespera did not form spindles and exhibited

greatly reduced microtubule polymerization from chromosomes. Addition of mutant Vespera that is unable to bind DNA (K42R) or non-SUMOylatable Vespera (K230R) had no effect (Figures 2.16B and 2.16C). Note that non-SUMOylatable Vespera is still able to bind DNA (Figure 2.6) so these results do not reflect a nonspecific effect of excess proteins on DNA.

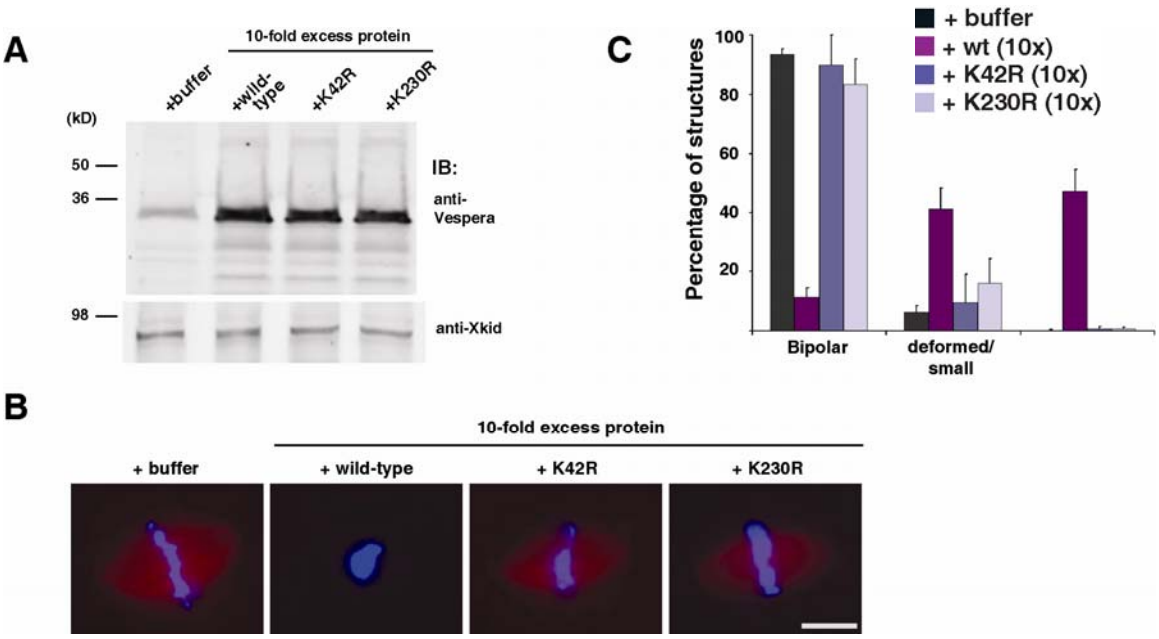

Figure 2.16. Effect of excess Vespera in control egg extracts. (A) CSF extracts were supplemented with excess (4.5 μM) wild-type or mutant Vespera, or buffer (control), as indicated. Total protein samples were collected and probed by Western blot using anti-Vespera or anti-Xkid antibodies (Funabiki and Murray, 2000). (B) Sperm nuclei were added to extracts shown in (A) and cycled through interphase to metaphase. Chromosomes were visualized with Hoechst 33258 (blue), and microtubules with rhodamine-tubulin (red). Scale bar, 10μm. (C) Quantitation of structures observed in (B). Values shown are the mean and standard deviation from three independent experiments, with >150 chromosomal structures counted per sample per experiment.

Having seen that nonSUMOylatable Vespera is unable to disrupt spindle formation, we next asked if the spindle-disruption activity of Vespera indeed acts through its SUMOylation. We repeated the excess Vespera addition experiment, this time in PIASy-depleted extracts where Vespera SUMOylation is inhibited (Figure 2.17A). Unexpectedly, without addition of Vespera, bipolar spindles form but their size was smaller in the absence of PIASy (Figure 2.17B, top)—there seems to be a PIASy target that promotes microtubule assembly. As predicted, however, excess wild-type Vespera protein was unable to disrupt spindle assembly in PIASy-depleted

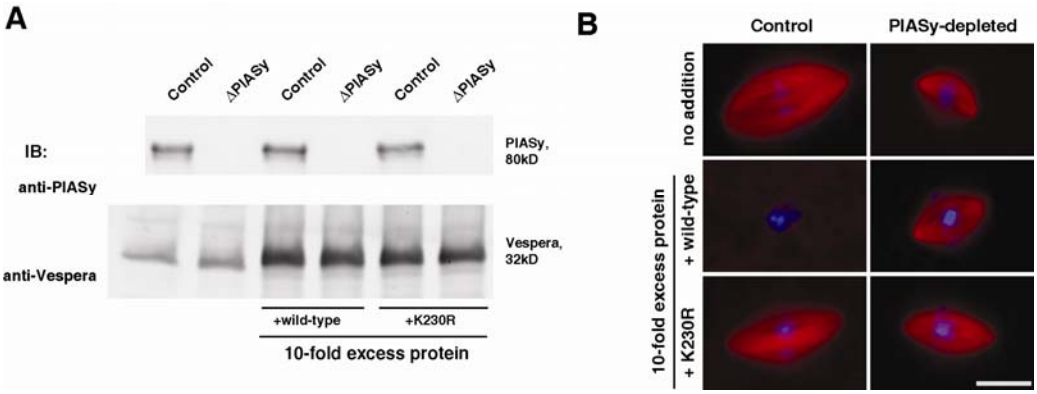

Figure 2.17. Effect of excess Vespera in ΔPIASy extracts. (A) CSF extracts were depleted with control IgG-beads or anti-PIASy beads, then supplemented with excess wild-type or mutant Vespera, or buffer, as indicated. Total protein samples were probed by Western blot using anti-PIASy or anti-Vespera antibodies. (B) Sperm nuclei were added to extracts shown in (A) and cycled through interphase to metaphase. Representative structures are shown, with DNA visualized by Hoechst 33258 (blue) and microtubules by rhodamine-tubulin (red). Scale bar, 10 μm.

extracts (Figure 2.17B). Therefore, we conclude that the mechanism by which excess Vespera disrupts spindle formation requires its SUMOylation.

2.6 *Vespera-Depletion Stimulates Microtubule Assembly in Metaphase Extracts*

The negative effect of excess Vespera on spindle formation suggested a role in microtubule destabilization. To examine if endogenous Vespera executes this function, we monitored aster formation in control and ΔVespera extracts. We visualized asters growing from sperm centrosomes 12 min after sperm addition to CSF extracts at 20°C, and found that Vespera-depleted aster microtubules were more dense than control asters (Figure 2.18A and 2.18B). This suggests that microtubule polymerization is increased in ΔVespera extracts, compared to control. Consistent with the requirement of sperm chromosomes for Vespera activation in this process, Vespera SUMOylation can be observed within 10 min after adding sperm nuclei (Figure 2.18C). We conclude that chromatin-bound, SUMOylated Vespera has a destabilizing effect on metaphase microtubules.

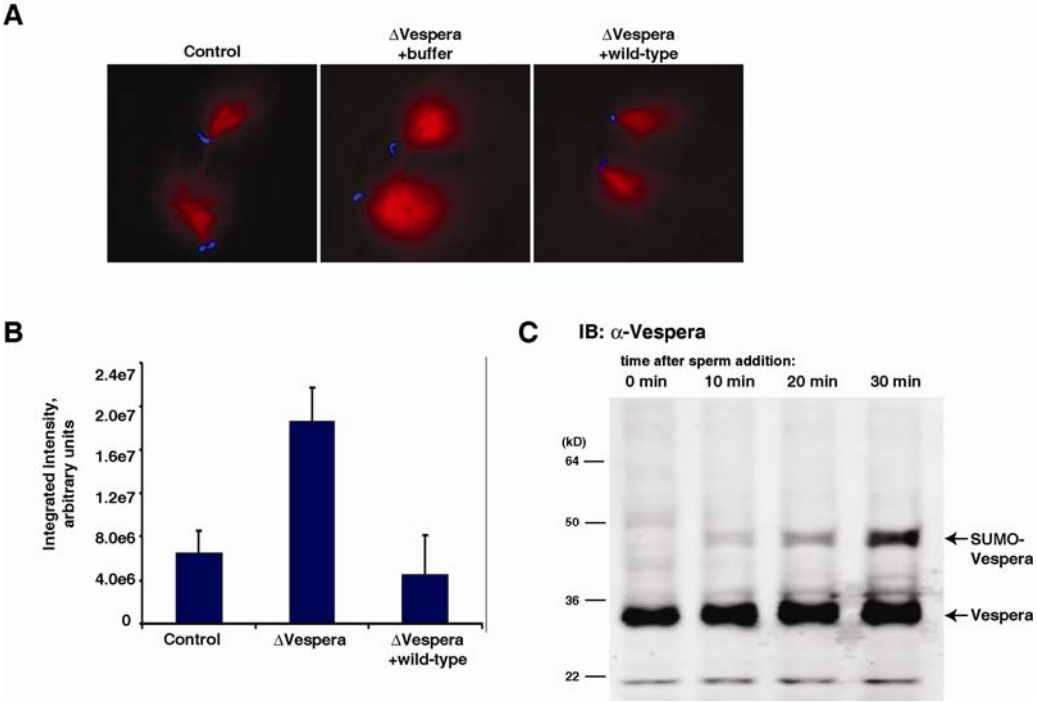

Figure 2.18. Microtubule polymerization from sperm centrosomes is increased in Vespera-depleted egg extracts. (A) Sperm aster visualization. Extracts containing cycloheximide were depleted with control IgG-beads or anti-Vespera beads. Vespera-depleted extracts were supplemented with buffer or wild-type Vespera, as indicated. Sperm nuclei (500/μl) and calcium were added to the extracts and incubated for 12 min at 20°C. DNA was stained with Hoechst dye and microtubules were visualized by rhodamine-tubulin. (B) Quantitation of integrated rhodamine-tubulin fluorescence intensity from samples in (A). Values represent mean and standard deviation for 50 asters per sample. For each aster, a background measurement from a region of equal dimensions was subtracted from the intensity value. (C) Timecourse analysis of Vespera SUMOylation. Sperm nuclei (10,000/μl) were added to CSF extract, and total protein samples were analyzed at the indicated timepoints by western blot using anti-Vespera antibodies.

2.7 *Nocodazole Bypasses the Requirement for Vespera in Nuclear Formation*

Having seen that Vespera exhibits microtubule-destabilizing effects, and that it is required for proper nuclear assembly, we asked if these two phenotypes might be related. We hypothesized that reduced microtubule disassembly activity might be the cause of deformed nuclei in ΔVespera extracts. To test this hypothesis, we examined if a microtubule-destabilizing drug, nocodazole, can rescue the deficiency of functional nuclear formation in ΔVespera extracts. ΔVespera CSF extracts containing sperm nuclei were released into interphase in the presence or absence of nocodazole. As described above, Vespera depletion resulted in deformed interphase nuclei. Addition of nocodazole, however, was able to restore the deformed nuclei to a round, normal shape in ΔVespera extracts (Figures 2.19A and 2.19B). This suggested that the interphase Vespera-depletion phenotype may indeed be caused by reduced microtubule depolymerization activity.

We sought to determine if this apparent rescue of interphase morphology reflects restoration of functional nuclei by examining nuclear import. When sperm nuclei were added to control extracts at 18°C, enrichment of GFP-NLS inside nuclei was visible after 30 min, and nocodazole addition did not impair the nuclear accumulation of GFP-NLS. Chromatin became condensed at a later time point (60 min) in the presence

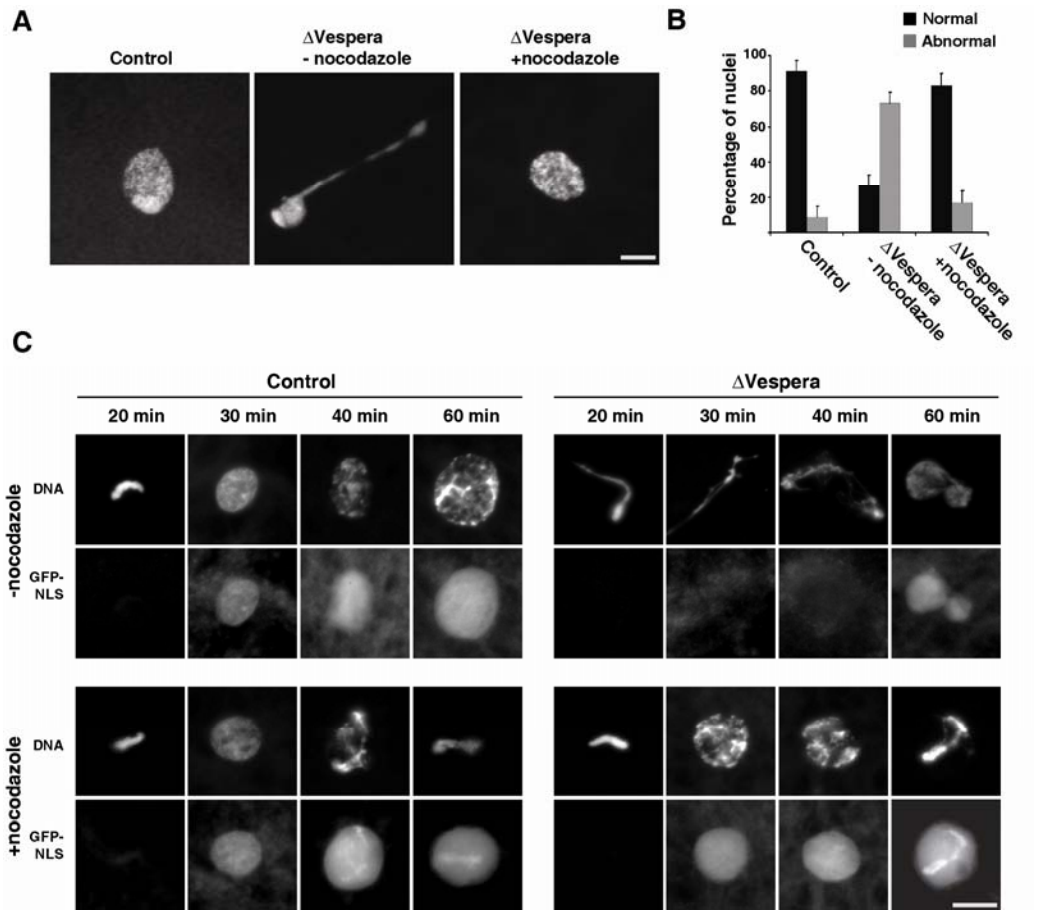

Figure 2.19. Nocodazole can bypass the requirement of Vespera in nuclear formation. (A) Sperm nuclei were assembled for 60 min at 22°C in control extracts, or ΔVespera extracts with or without 5 μg/ml nocodazole. DNA was stained with Hoechst 33258. Scale bar, 10 μm. (B) Quantitation of structures observed in (A). Values shown are the mean and standard deviation from three independent experiments, with >200 nuclei counted per sample per experiment. (C) Timecourse analysis of nuclear import in control and Vespera-depleted extracts, with or without nocodazole. Nuclei were assembled in the indicated extracts, with chromatin visualized by Hoechst 33258, and nuclear import monitored by GFP-NLS.

of nocodazole, but nuclei retained proper size and shape. For ΔVespera extracts, the nuclear morphological defect correlated with impaired import, and only some regions of the nuclei showed accumulation of fluorescence after 60 min. Strikingly, nocodazole addition was able to completely rescue this import defect (Figure 2.19C). It appears that Vespera is required to ensure both the uniformly round shape of nuclei and their proper function as a cellular compartment through microtubule destabilization.

2.8 *Discussion*

In conclusion, we identified a new chromatin-binding protein, Vespera, that is required for proper nuclear re-formation. Vespera displays microtubule destabilizing activity, and we therefore postulate that, at the end of mitosis, microtubules must be disassembled around chromosomes to permit nuclear envelope re-formation. Vespera also represents a novel chromatin-localized microtubule destabilizing activity. Further evidence that the essential requirement of Vespera in nuclear re-formation is based in its negative effect on microtubules comes from our observation that the microtubule-depolymerizing drug nocodazole can rescue the nuclear defect associated with Vespera depletion.

How could microtubules interfere with nuclear assembly? Nuclear envelope formation is mediated by proteins that bridge chromatin and components of the lamina or nuclear membrane (Guttinger et al., 2009). It is thought that lamin B receptor (LBR) and other DNA-binding proteins contribute to this process. Early observations of nuclear formation in HeLa cells noted that binding of LBR to chromosomes appeared to favor regions of lower microtubule density (Chaudhary and Courvalin, 1993). More recently, electron microscopy studies have demonstrated that continuous

stretches of new membrane are interrupted by gaps occupied by anaphase microtubules contacting chromosomes (Haraguchi et al., 2008). These observations suggest that the interaction between spindle microtubules and chromosomes may physically obstruct nuclear membrane attachment, or be otherwise refractory to the assembly of nuclear membrane components around chromatin. Since microtubules are known to play a mechanical role in nuclear envelope breakdown at the start of mitosis, they may correspondingly interfere with timely and efficient nuclear envelope assembly at the end of mitosis.

CHAPTER THREE: VESPERA IS FUNCTIONALLY ANTAGONISTIC TO AURORA B

3.1 *Introduction*

Our results from Chapter Two indicate that Vespera has a positive effect on interphase nuclear assembly, and a negative effect on metaphase microtubule polymerization. We noted that the opposite functions have been attributed to the Aurora B kinase, a member of the CPC (Figure 3.1). Excess Aurora B has been shown to disrupt interphase nucleus formation (Ramadan et al., 2007). Depletion of the Aurora B complex has been shown to be required for metaphase spindle assembly in *Xenopus* egg extracts (Sampath et al., 2004). Recall that excess Vespera results in failure to form metaphase spindles, while depletion of Vespera disrupts the formation of interphase nuclei.

Several pieces of evidence hint that the CPC plays a central role in the events at the end of mitosis. It has been previously shown that metaphase chromosomes activate the Aurora B pathway (while phosphatases suppress it in the cytoplasm), and that this local activation promotes microtubule assembly from chromosomes through the inactivation of the microtubule depolymerizing factors MCAK and Op18 (Gadea and Ruderman, 2005; Kelly et al., 2007; Sampath et al., 2004). The CPC associates with chromosomes in metaphase, but relocalizes to the spindle midzone in anaphase (Ruchaud et al., 2007). Aurora B removal from chromosomes is effected by the AAA-ATPase Cdc48/p97, an event that was found to be critical for proper nuclear formation (Ramadan et al., 2007). This discovery helped to explain previous observations that Cdc48/p97 is required to form a closed nuclear envelope (Hetzer et al., 2001).

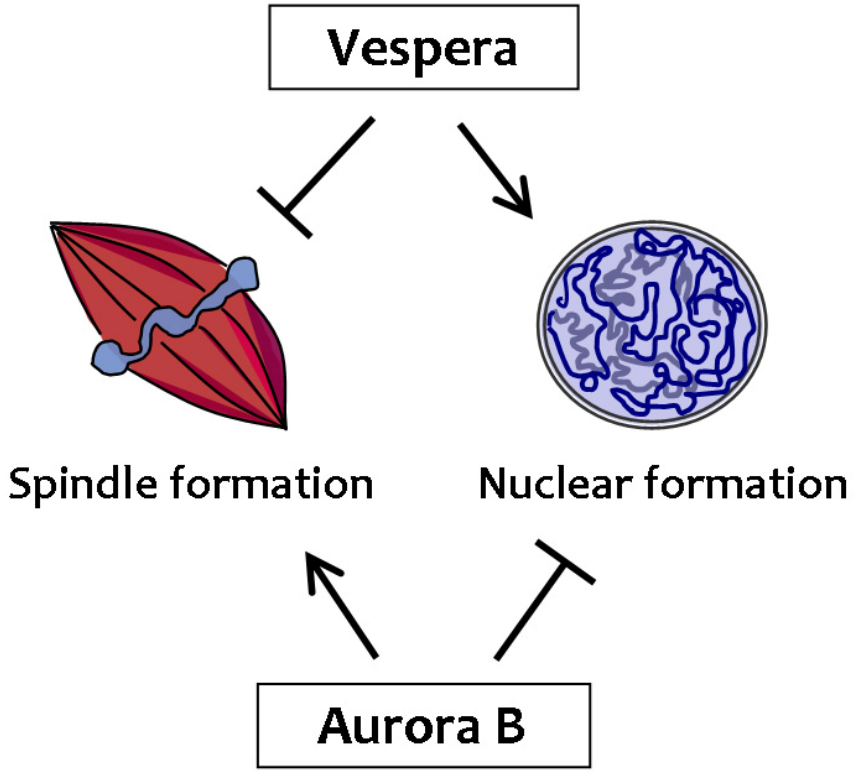

Figure 3.1. Vespera and Aurora B exhibit antagonistic functions. In Chapter Two we provided evidence that Vespera inhibits spindle formation and promotes nuclear formation. The opposite functions have previously been attributed to Aurora B.

In this chapter, we describe our observations that co-depletion of Vespera and Aurora B can complement one another. Furthermore, full chromosomal enrichment of protein phosphatase 1 (PP1), which antagonizes Aurora B, requires SUMOylated Vespera, and dephosphorylation of Aurora B substrates is attenuated in the absence of Vespera.

3.2 *Vespera and Aurora B Co-Depletion Can Suppress the Defects of Individual Depletions*

We asked if Vespera and Aurora B deficiencies can complement one another. While immunodepletion of the CPC results in failure to polymerize microtubules from metaphase chromosomes (Sampath et al., 2004), bipolar spindles can form in ΔVespera extracts, although some exhibit chromosome alignment defects that may be attributable to deformed nuclei in the preceding interphase (Figure 3.2A, see Figure 2.12A). When we examined extracts that had been co-depleted of Vespera and the CPC, we observed partial rescue of the CPC-depletion phenotype. Microtubule polymerization was largely restored, and though bipolar spindles did not form, many groups of chromosomes formed half-spindles (Figure 3.2A and 3.2B). We speculate that the rescue of CPC depletion by Vespera co-depletion may require residual amounts of Aurora B in the extract that are insufficient to fully restore spindle formation.

We also asked the converse question, and investigated whether co-depletion of CPC could rescue the Vespera defect in interphase. This was indeed the case, as co-depletion of Incenp restored normal, round shape in ΔVespera extracts (Figures 3.2C and 3.2D). It appears that, directly or indirectly, Vespera and Aurora B functionally oppose one another, and co-depletion of one can rescue the defects of individual depletion of the other.

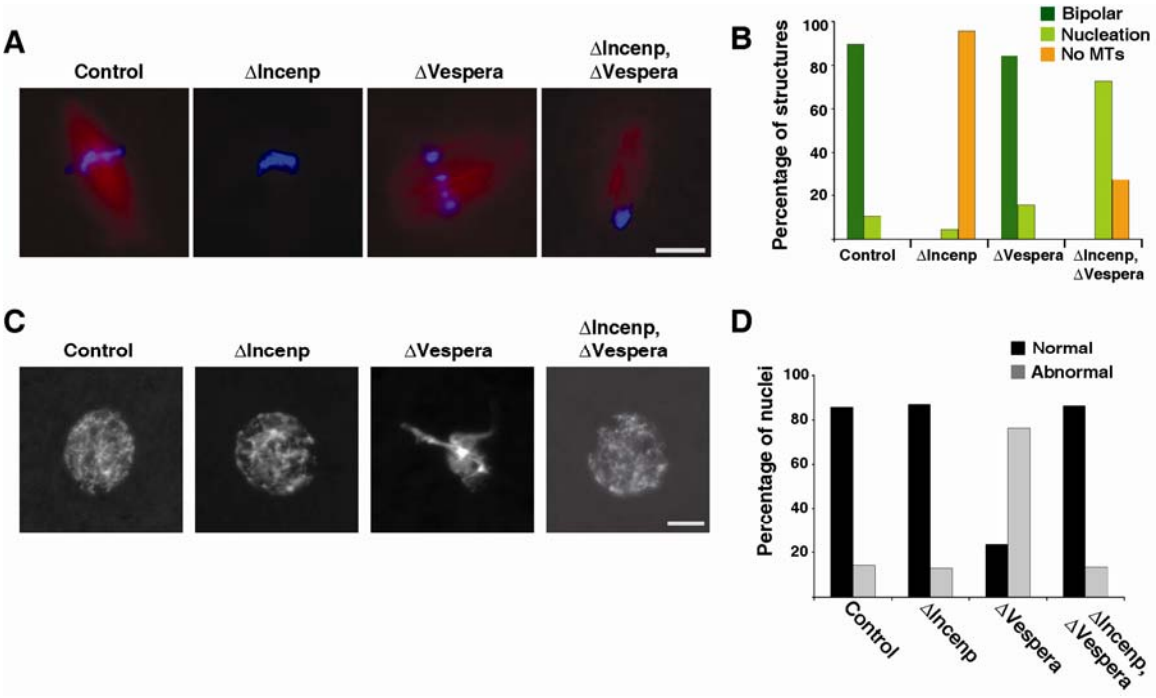

Figure 3.2. Vespera and Aurora B co-depletion can suppress the defects of individual depletions (A) CSF extracts containing cycloheximide were depleted with control IgG-beads, anti-Incenp beads, anti-Vespera beads, or both anti-Incenp and anti-Vespera beads. Sperm nuclei were added to these extracts and cycled through interphase to metaphase. DNA was visualized with Hoechst 33258 (blue), and microtubules with rhodamine-tubulin (red). Scale bar, 10μm. (B) Quantitation of structures observed in (A). Values shown are the mean from two independent experiments, with ~200 chromosomal structures counted per sample per experiment. (C) Sperm nuclei were assembled in extracts as in (A), and DNA was stained with Hoechst 33258. Scale bar, 10 μm. (D) Quantitation of structures observed in (C). Values shown are the mean from two independent experiments, with ~200 nuclei counted per sample per experiment.

3.3 *Vespera Reduces the Level of Aurora B-Mediated Phosphorylation*

To better understand the opposing relationship between Vespera and Aurora B, we examined the phosphorylation status of Aurora B substrates in the presence and absence of Vespera. Histone H3 serine 10 (H3S10) is a well-established Aurora B substrate, and its phosphorylation can be detected by immunofluorescence using phospho-specific antibodies (Hsu et al., 2000).

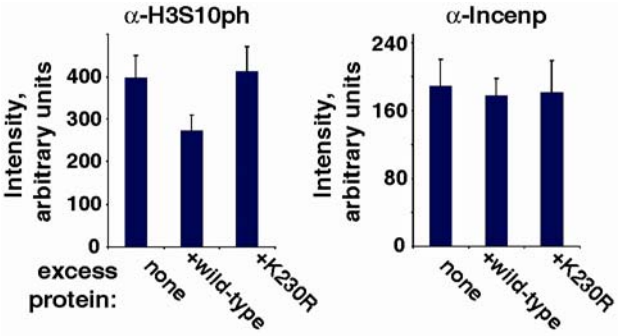

Figure 3.3. Effect of excess Vespera on chromosomal H3S10 phosphorylation. Metaphase replicated chromosomes in the presence or absence of excess (4.5 μM) Vespera recombinant proteins were treated with nocodazole (to equalize the chromosomal mass), and H3S10ph and Incenp were visualized by immunofluorescence. Average and standard deviation of intensities of 40 chromosomal clusters per sample are shown.

First, we tested the effect of 10-fold excess recombinant Vespera proteins in H3S10 phosphorylation (H3S10ph). Consistent with the hypothesis that Vespera antagonizes Aurora B-dependent phosphorylation (via dephosphorylation), excess wild-type Vespera, but not SUMOylation

deficient K230R mutant protein, effectively reduced H3S10ph-epitopes (Figure 3.3). By contrast, the amount of Incenp was not affected by excess Vespera.

Next, we monitored H3S10ph during the course of nuclear re-formation. Sperm nuclei were added to CSF extracts, and calcium was added immediately to promote release from metaphase arrest to interphase. As sperm nuclei contain histone H3, slight H3S10ph was transiently observed at 15 min after addition of calcium (Figure 3.4). At this point, a higher level of H3S10 phosphorylation was observed in ΔVespera extracts than in control extracts. Even though dephosphorylation is completed at 30 min in both extracts, chromosomes are not properly organized in ΔVespera extracts, suggesting that timely inactivation of the Aurora B pathway is critical for proper nuclear re-formation. Since the level of chromosome-associated Incenp was not affected by Vespera, Vespera does not appear to act by controlling chromosomal recruitment of the CPC.

A similar result was observed when sperm nuclei were pre-incubated with CSF extracts for 45 min before the calcium addition (Figure 3.5A). In this experiment, H3S10 is well phosphorylated in both extracts during the pre-incubation in metaphase, but dephosphorylation of H3S10 and chromosome decondensation were delayed in ΔVespera extracts upon release to interphase. Similar results were obtained by monitoring phosphorylation of another Aurora B substrate, Op18 (Figure 3.5B). These results strongly suggest that Vespera is required for timely inactivation of the Aurora B pathway at the exit from M phase.

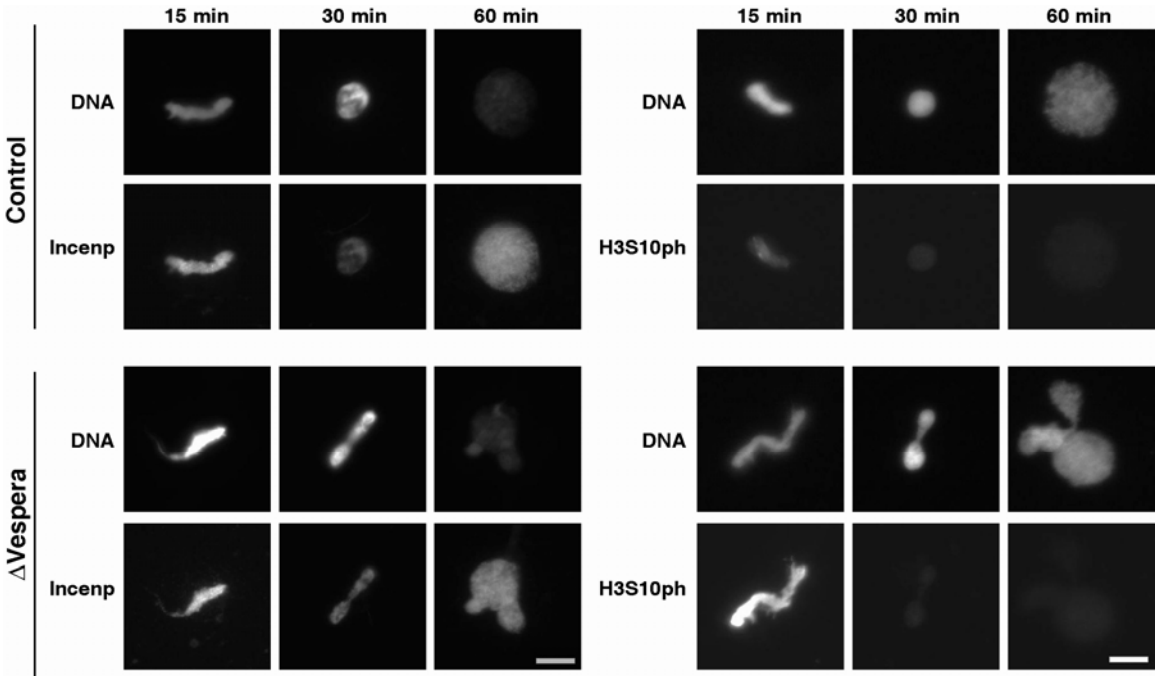

Figure 3.4. Effect of excess Vespera on chromosomal H3S10 phosphorylation. Metaphase replicated chromosomes in the presence or absence of excess (4.5 μM) Vespera recombinant proteins were treated with nocodazole (to equalize the chromosomal mass), and H3S10ph and Incenp were visualized by immuno-fluorescence. Average and standard deviation of intensities of 40 chromosomal clusters per sample are shown. (D) Monitoring H3S10 dephosphorylation on chromosomes upon interphase induction. Sperm nuclei (200/μl) were added to control or ΔVespera CSF extracts, along with calcium. At the indicated timepoints, DNA was stained with Hoechst 33258, and H3S10ph was visualized by indirect immunofluorescence. Scale bar, 10 μm.

3.4 *SUMOylated Vespera Promotes Recruitment of PP1 to Chromosomes*

A recent study of global SUMO-interacting proteins in budding yeast showed that the protein phosphatase 1 (PP1), Glc7, binds to the yeast homolog of SUMO, Smt3p (Makhnevych et al., 2009). It has been well established that PP1 dephosphorylates Aurora B substrates and antagonizes essential functions of Aurora B (Emanuele et al., 2008; Francisco et al., 1994; Hsu et al., 2000). Because Glc7/PP1 is highly conserved between species, we hypothesized that the interaction between PP1 and SUMO might be conserved in *Xenopus*, and that SUMOylated Vespera might oppose Aurora B function via PP1 recruitment to chromosomes.

To test this hypothesis, we purified metaphase chromosomes and monitored the amount of associating PP1. While chromosomal levels of Incenp, which is required for chromosome-targeting and activation of Aurora B, were unchanged, we saw that PP1 binding to chromosomes was reduced in ΔVespera extracts (Figure 3.6A). This reduced binding did not reflect an overall reduction in PP1, as depletion of Vespera did not affect cytoplasmic levels of PP1 (Figure 3.6B). Wild-type Vespera, but not DNA-binding deficient mutant (K42R) or SUMOylation deficient mutant (K230R), were able to rescue reduction of chromosome-associated PP1 in ΔVespera extracts. As confirmed by anti-Vespera antibodies, we observed that higher levels of PP1 binding to chromosomes correlated with Vespera SUMOylation (Figure 3.6A).

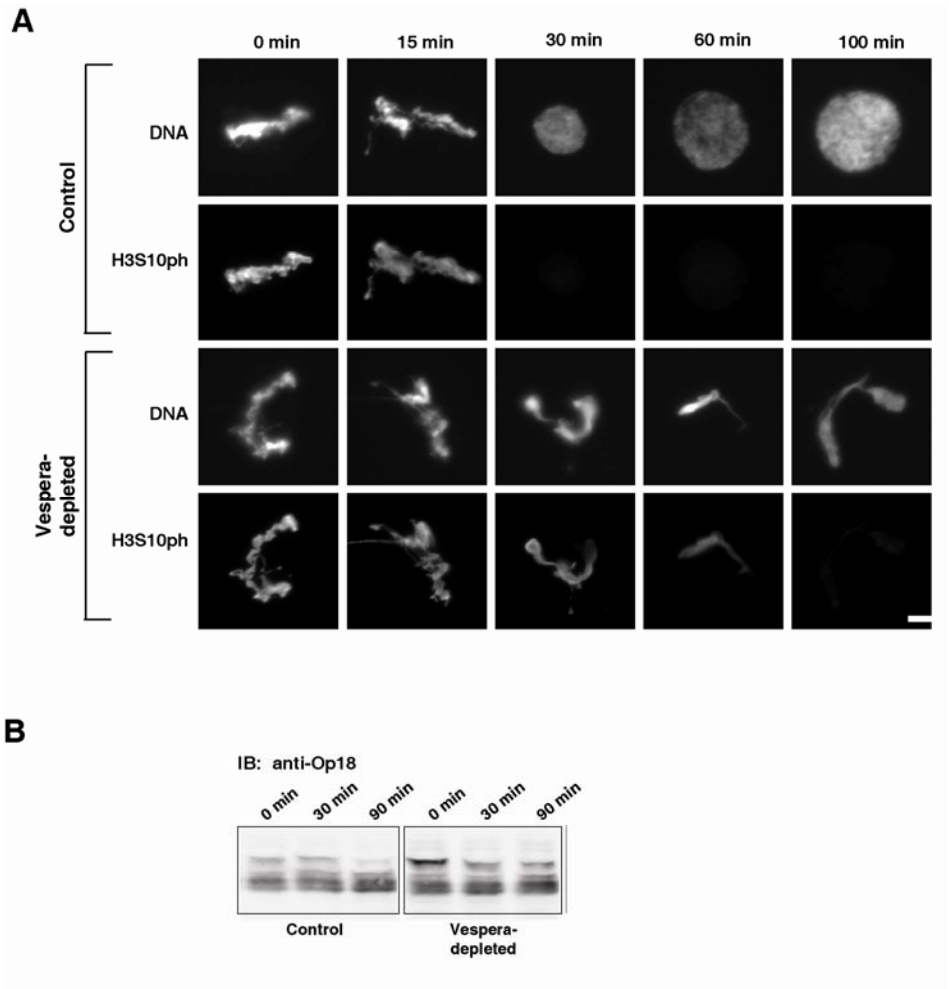

Figure 3.5. Aurora B Substrate dephosphorylation is impaired in ΔVespera extracts. (A) Monitoring dephosphorylation of H3S10ph upon interphase induction. Sperm nuclei (200/μl) were added to control or ΔVespera CSF extracts and pre-incubated for 45 min at 22°C. Calcium was then added and, at the indicated timepoints, chromosomal structures were fixed and spun down on coverslips. H3S10ph was visualized by indirect immunofluorescence. Scale bar, 10μm. (B) Monitoring Op18 dephosphorylation upon interphase induction. Sperm nuclei (10000/μl) were added to control or ΔVespera CSF extracts and pre-incubated for 45 min at 22°C before adding calcium and analyzing by Western blot.

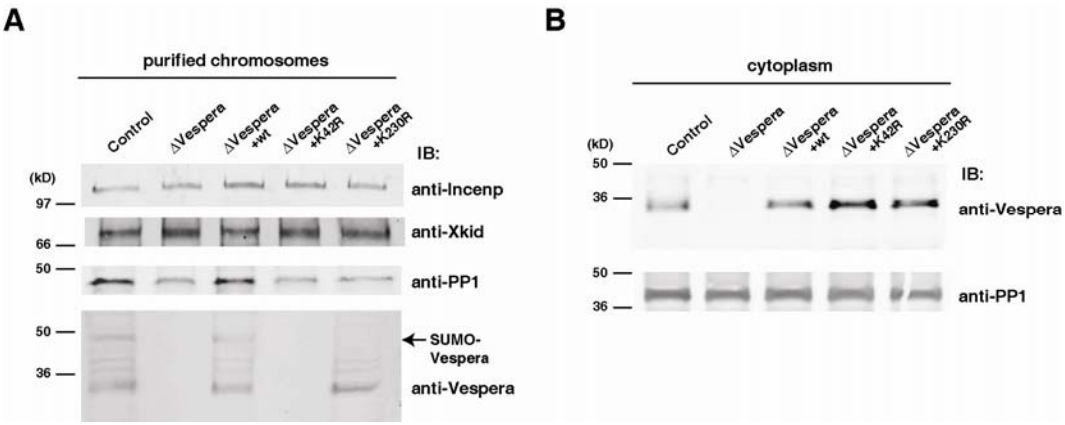

Figure 3.6. Vespera depletion affects PP1 association with chromosomes. (A) Western blot analysis of purified chromosomes. Replicated metaphase chromosomes assembled in control or ΔVespera extracts, in the presence or absence of recombinant Vespera proteins were purified, and probed by Western blot with the indicated antibodies. (B) Total protein from extracts in (A) was analyzed by western blot using anti-Vespera and anti-PP1α antibodies.

3.5 *Discussion*

In summary, we noted that the phenotypes we discovered for Vespera (described in Chapter Two) are opposite from those that have been previously attributed to Aurora B. Based on this, we asked if co-depletion of Aurora B complex (CPC) could rescue depletion of Vespera. We demonstrated that it could, that co-depletion of Aurora rescued the nuclear formation defect of Vespera depletion. The converse was also

true, that co-depletion of Vespera can rescue the spindle formation defect CPC depletion. Aurora B is locally activated on chromosomes, allowing it to promote spindle formation through inhibition of the microtubule destabilizers MCAK and Op18 (Andrews et al., 2004; Gadea and Ruderman, 2005; Lan et al., 2004; Ohi et al., 2003). Vespera is also locally activated on chromosomes, as it appears to require chromatin-dependent SUMOylation for its activity. Therefore, Aurora B and Vespera represent two opposing functions that are both spatially restricted to chromosome regions. We speculate that local activation of Aurora B requires a corresponding localized de-activation pathway to efficiently execute the transition from metaphase-to-anaphase. At that point, Aurora B is re-localized from chromosomes to the spindle midzone. Thus, in anaphase, Aurora B no longer phosphorylates substrates to promote microtubule polymerization around chromosomes.

At the end of mitosis, Aurora B is removed from chromosomes, and its substrates are dephosphorylated by cytoplasmic phosphatases. We postulate that, in addition to this mechanism for inactivation of Aurora B, Vespera represents an active pathway to reverse the effects of Aurora B, allowing for rapid inactivation of its function on chromosomes at anaphase. Our results show that, in the absence of Vespera, Aurora B substrates are aberrantly retained on chromosomes upon release from metaphase, indicating that Vespera is required for timely inactivation of Aurora B on chromosomes. A very similar failure to dephosphorylate Aurora B substrates in a timely fashion has been reported in the absence of proper p97/Cdc48 activity, which causes Aurora B itself to be improperly retained on chromosomes. Importantly,

this scenario also resulted in failure to properly form interphase nuclei, just as we observed for Vespera depletion.

We have demonstrated that, in order to oppose Aurora B function, Vespera must be SUMOylated on chromatin. Vespera does not appear to have any enzymatic function (or conserved enzyme domains), and we hypothesize that it serves a signaling function via its SUMOylation. We would like to know to what pathway Vespera signals in order to functionally oppose Aurora B. One intriguing possibility is the protein phosphatase PP1, which has been shown in various contexts to dephosphorylate Aurora B substrates. PP1 was shown to interact biochemically with the SUMO polypeptide in yeast, and since both PP1 and SUMO are well conserved, it is possible that this interaction is present in higher eukaryotes. We demonstrated that full recruitment of PP1 to chromosomes requires Vespera and its SUMOylation, providing an attractive model for the functional opposition of Vespera and Aurora. It remains to be established if this interaction is direct or indirect, and further investigations will demonstrate if Vespera indeed opposes Aurora B by recruitment of PP1 phosphatase.

Finally, in order to further understand the interplay between kinase and phosphatases in signaling events in mitosis, we would like tools for the detailed characterization of phosphorylation sites on proteins. In the following chapters, we will discuss a new mass spectrometric method for the identification of phosphorylation, and our application of this method to the CPC and Vespera.

CHAPTER FOUR: A NEW METHOD FOR IDENTIFICATION OF PHOSPHORYLATION USING MASS SPECTROMETRY

4.1 *Introduction*

Protein phosphorylation plays a central role in the regulation of many cellular processes. In recent years, mass spectrometry (MS) has become a method of choice for the analysis of protein phosphorylation (McLachlin and Chait, 2001; Ptacek and Snyder, 2006; Reinders and Sickmann, 2005). Although advances in instrumentation and software have made it possible to perform large-scale studies of phosphoproteomes (Li et al., 2007; Olsen et al., 2006), the comprehensive analysis of phosphorylation in single proteins remains challenging.

Detection of phosphorylation has been difficult due to the relative suppression of phosphopeptide MS signals compared to their unphosphorylated counterparts. Thus, even when the unmodified peptide can be observed as a strong peak in the spectrum, comparable amounts of the unmodified peptide are often obscured by the background (Kang et al., 1997; Zhou et al., 2000). Because of this difficulty, several approaches to study phosphorylation involve removal of the phosphate group. For example, enzymatic treatment with phosphatase has been employed to dephosphorylate proteins, resulting in an enhanced signal (Hirschberg et al., 2004; Ishihama et al., 2007; Larsen et al., 2001; Liao et al., 1994; Marcantonio et al., 2007; Torres et al., 2005; Zhang et al., 1998), but this method has been shown to be subject to enzyme preferences (Hunter and Games, 1994; Zeller and Konig, 2004). Alternatively, the phosphate group has been converted to moieties that enhance detection, including affinity

tags (Oda et al., 2001) or lysine analogs that are recognized and cleaved by trypsin (Knight et al., 2003; Rusnak et al., 2004).

Tandem MS (MS-MS) is frequently employed to confirm and map phosphorylation sites, but here too the phosphate group is often removed. Phosphate groups on amino acids are particularly unstable to collision-induced dissociation (CID), and are preferentially lost from the peptide as the elements of phosphoric acid. This loss of 98 Da provides a useful phosphopeptide, and many studies have taken advantage of this property to identify phosphorylation (Carr et al., 2005). For example, a neutral loss scan can be performed to identify any species that displays this signature loss, but this approach suffers from reduction in sensitivity arising from the need to scan the entire m/z range of interest (Krutchinsky, 2007). This so-called "scanning disadvantage" can be partially overcome by targeting either only discernable peaks in the spectrum (Casado-Vela et al., 2007) or by performing MS-MS on a hypothetical subset of m/z values (Chang et al., 2004). A major drawback of the former approach is its inability to analyze species that are obscured by the background. Although the hypothesis-driven approach overcomes this difficulty, it is costly in terms of time and sample.

In an effort to overcome some of the difficulties described above, we have revisited the dephosphorylation approach, employing a chemical dephosphorylation strategy. Hydrogen fluoride has been shown to rapidly dephosphorylate phosphopeptides in solution (Kuyama et al., 2003), and we have adapted this technique for use in-gel and on whole proteins. This chemical dephosphorylation results in enrichment of those unmodified peptides that correspond to previously phosphorylated peptides. Quantitative comparison of the signal-to-noise ratios of peaks in the treated

versus untreated samples are used to identify phosphopeptides. The ability to completely dephosphorylate proteins irrespective of amino acid sequence and the improved signal-to-noise ratio (S/N) of the resulting dephosphorylated peptides permit us to capture a mass spectrometric phosphorylation "fingerprint" of a given protein. We have applied this technique to characterize the phosphorylation of Aurora A, a centrosome-associated kinase whose auto-phosphorylation has been previously studied in detail (Haydon et al., 2003; Littlepage and Ruderman, 2002; Littlepage et al., 2002).

4.2 *In-gel chemical dephosphorylation of peptides and proteins*

As a test of our method for in-gel chemical dephosphorylation, 1 μg aliquots of three synthetic histone tail phosphopeptides (phosphorylated respectively on serine, threonine, or tyrosine) were immobilized in a polyacrylamide gel by electrophoresis and fixed with methanol-acetic acid. The precipitated peptides could be visualized directly in the gel, and were cut out as 2mm slices. The gel slices were dehydrated and treated with 70% HF-pyridine for one hour on ice, resulting in complete dephosphorylation of the phosphoserine-, phosphothreonine-, and phosphotyrosine-containing peptides, respectively (Figure 4.1). MS analysis of the reaction products revealed that the phosphopeptides were quantitatively converted to the unmodified backbone peptides with no detectable side products.

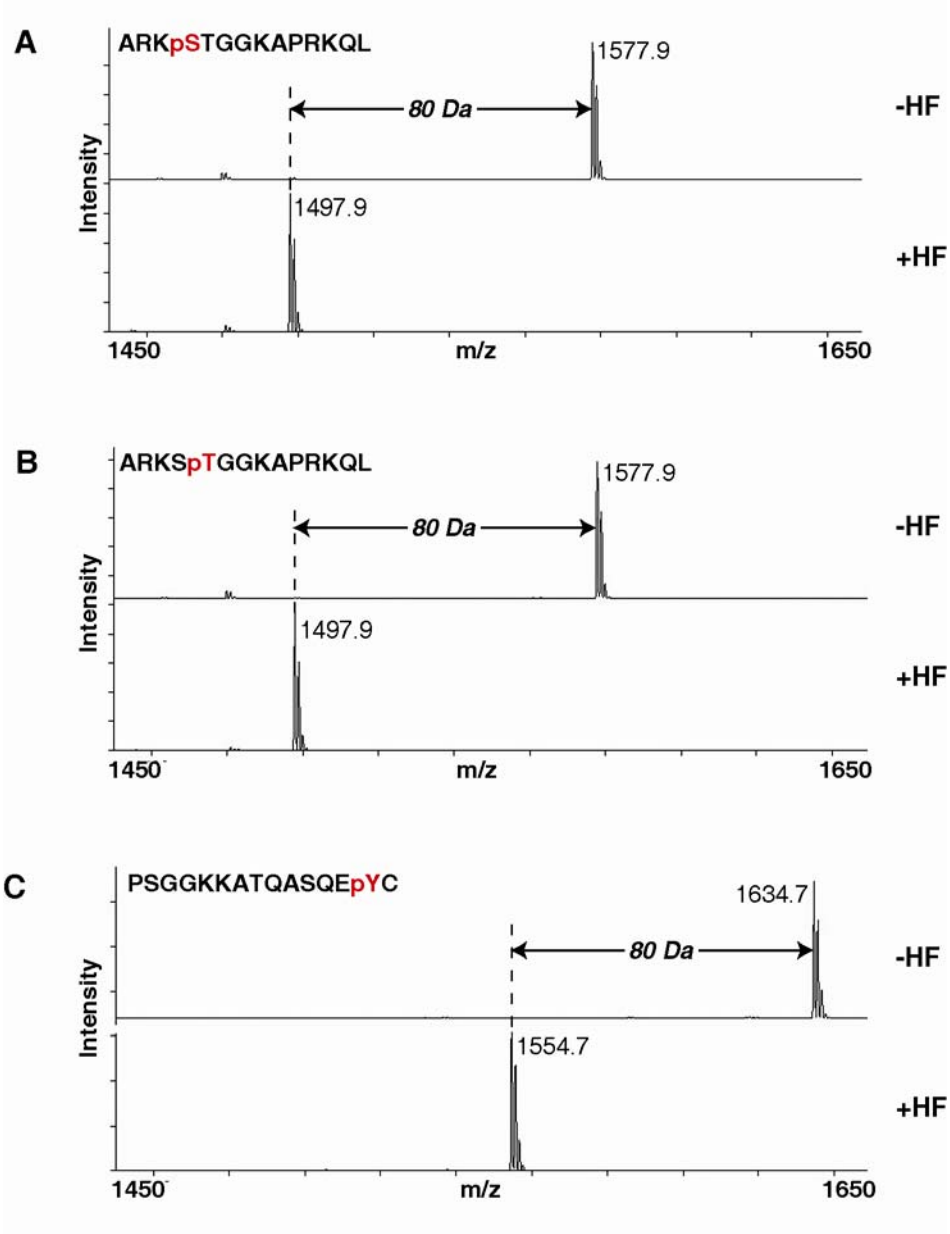

Fig. 4.1. In-gel dephosphorylation of peptides. Polyacrylamide gel slices containing peptides were dehydrated and incubated with 70% HF-pyridine for one hour on ice: (A) ARKpSTGG-KAPRKQL, (B) ARKSpTGGKAPRKQL, (C) PSGGKATQASQE-pYC. Each spectrum shows before treatment (-HF) and after (+HF).

Previously, this chemistry had been applied to peptides (Kuyama et al., 2003). Here, we tested its ability to dephosphorylate whole proteins using the model phosphoprotein ovalbumin. The protein was denatured by boiling in SDS sample buffer, purified by SDS-PAGE, and visualized by Coomassie staining. Gel slices were excised and destained, then dehydrated and treated with HF as before. The gel slices were then washed in 0.5M ammonium bicarbonate to bring the pH to ~8 prior to trypsin digestion. Tryptic peptides were collected and analyzed by MALDI-MS, which demonstrated that the HF-treated protein had been efficiently

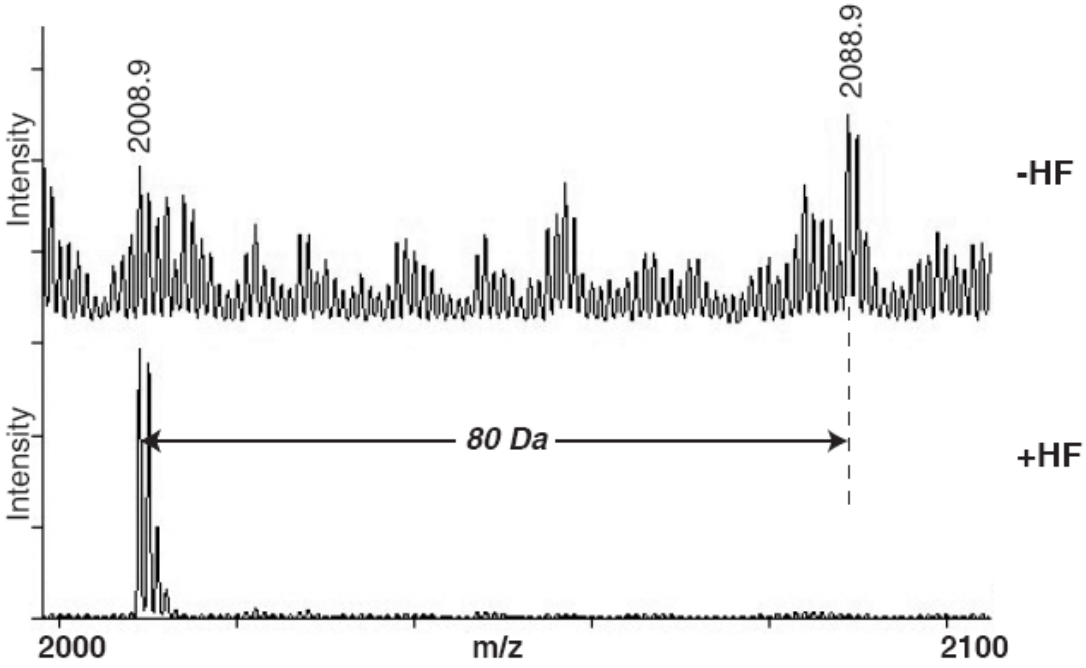

Fig. 4.2. In-gel dephosphorylation of protein. 5μg of ovalbumin were purified by SDS-PAGE, and gel slices containing the whole protein were either not treated (-HF) or treated (+HF) with 70% HF-pyridine for one hour on ice. The phosphopeptide EVVGpSAEAGVDAASVSEEFR (m/z = 2088.9) was dephosphorylated to yield the unmodified peptide (m/z = 2008.9).

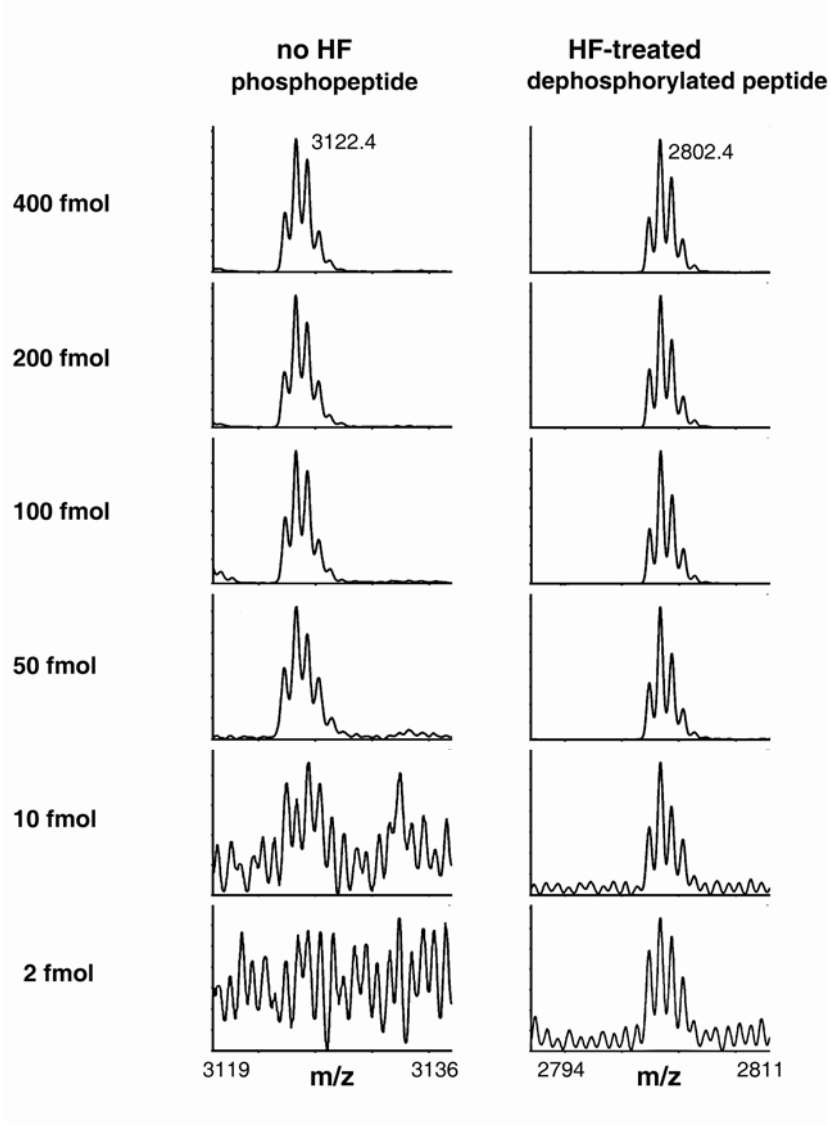

Figure 4.3. Sensitivity of HF dephosphorylation for detecting phosphorylation. Varying amounts of β-casein were either untreated or treated with HF. The peak corresponding to the singly protonated phosphopeptide, RELEELNVPGEIVEpSLpSpSp-SEESITR (m/z = 3122.4) is shown for the untreated samples, and the unmodified peak (m/z = 2802.4) is shown for the treated samples.

dephosphorylated (Figure 4.2). From these experiments, we conclude that HF-pyridine can efficiently dephosphorylate peptides, as well as whole proteins, in gel. We observed that the signal-to-noise ratio (S/N) for the dephosphorylated peak was significantly greater than the sum of the S/Ns of the unmodified and phosphorylated peaks prior to HF treatment. Dephosphorylated peptides should therefore be detectable down to lower levels than the corresponding phosphorylated peptides.

To test this hypothesis, we analyzed varying amounts (400 fmol to 2 fmol) of the model phosphoprotein casein, comparing HF-treated and untreated samples. Casein is quadruply phosphorylated on its N-terminal tryptic peptide, and we observed, as before, that HF treatment efficiently dephosphorylated the protein to yield the unmodified tryptic peptide (Figure 4.3). The dephosphorylated peptide peak was readily discernable at 2 fmol, while the phosphopeptide peak did not rise significantly above the background at 10 fmol. Thus, dephosphorylated peptide peaks are detected with considerably enhanced S/N compared with their phosphorylated counterparts.

4.3 *Identification of Phosphorylation by Phosphopeptide Fingerprinting*

We sought to take advantage of this enhancement of dephosphorylated peptide signals upon HF treatment in order to efficiently identify phosphopeptides. A schematic diagram of the method is depicted in Figure 4.4. As a test case, we examined tryptic peptides of ovalbumin, including four phosphopeptides corresponding to two known phosphorylation sites. We calculated the S/Ns for all ovalbumin peaks before and after HF treatment, and found a striking division of the peaks into two populations (Figure 4.5). The formerly phosphorylated peptides showed an increase in

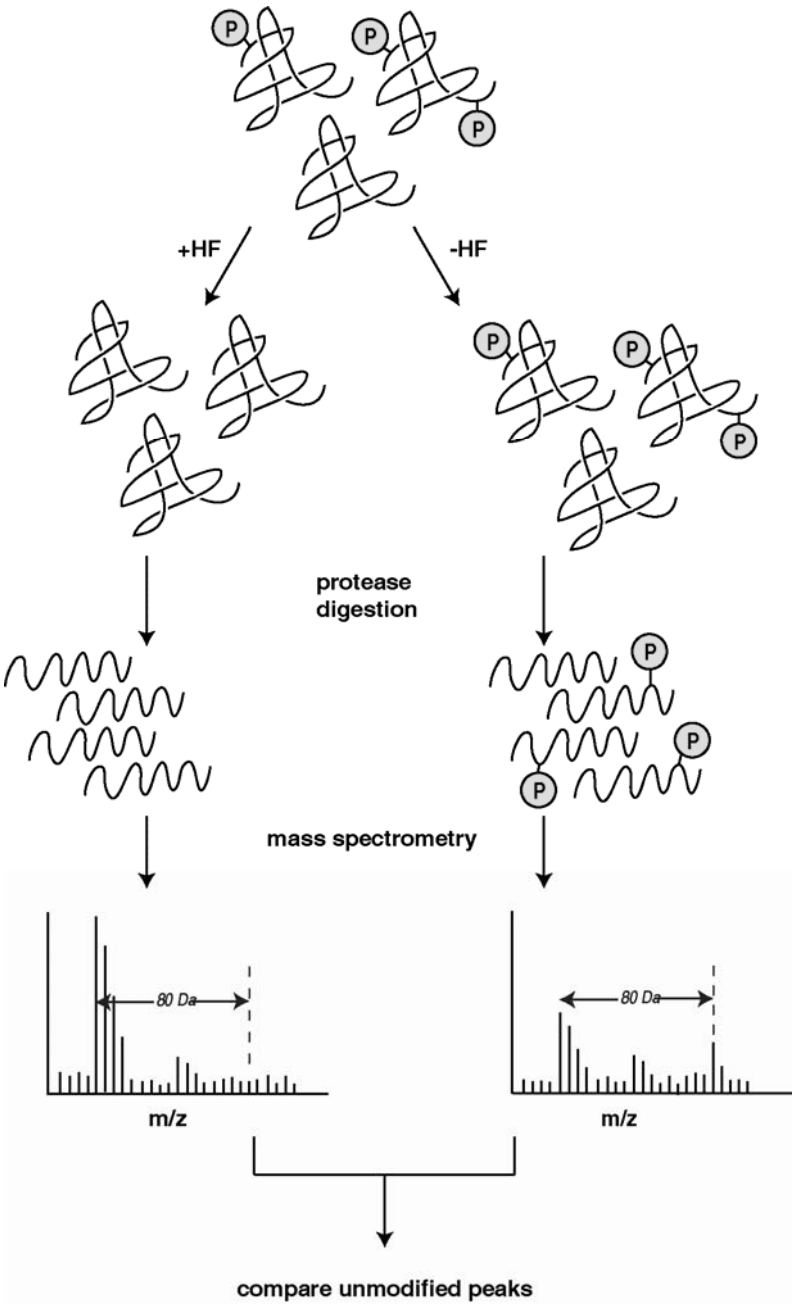

Figure 4.4. Strategy for the identification of phosphorylation using phospho-peptide fingerprinting.

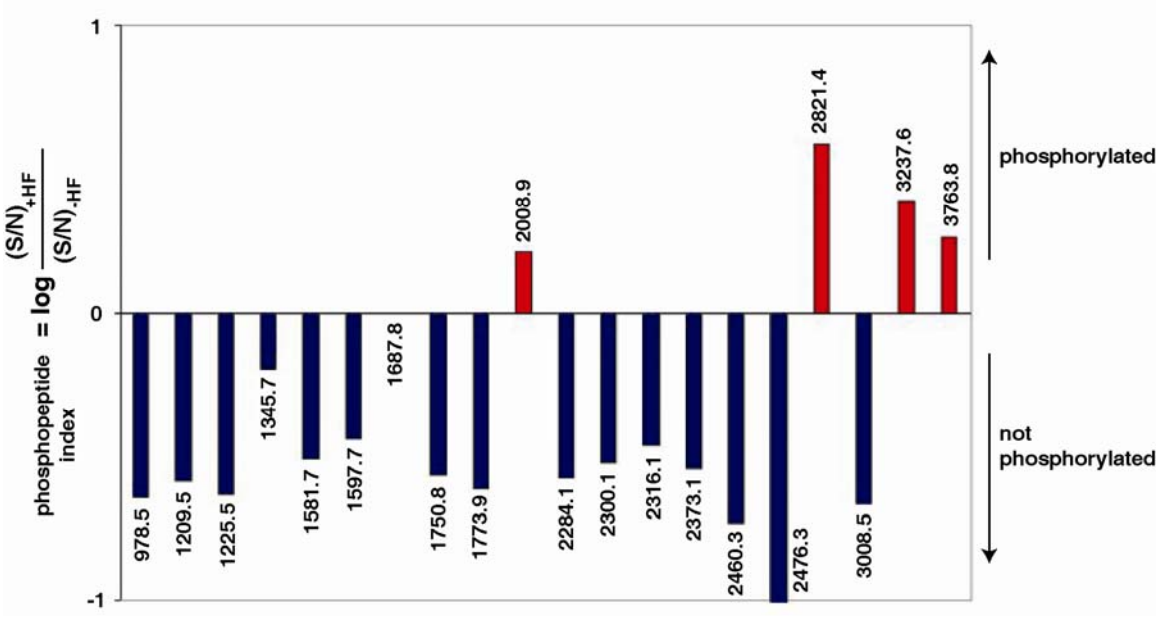

Figure 4.5. The observed increase in S/N of unmodified peptides upon HF treatment provides a "MS phosphopeptide fingerprint", indicating the likelihood that a given peptide is phosphorylated. The S/N was calculated for peaks corresponding to unmodified peptides from ovalbumin in HF-treated and untreated samples. The log of the ratio of S/Ns is plotted for each peptide to yield the "phosphopeptide index". Positive values were found to represent previously phosphorylated peptides, while negative values represented unphosphorylated peptides.

signal-to-noise, while unmodified peptides showed a decrease, upon HF treatment. Positive values for the phosphopeptide index were found to correspond to phosphorylated peptides, and negative values to unphosphorylated peptides. Visual examination of the spectra confirmed that peaks corresponding to dephosphorylated phosphopeptides showed an increase in S/N upon HF treatment (Figure 4.6A), while unmodified peaks showed a decrease in S/N (see, for example, Figure 4.6B).

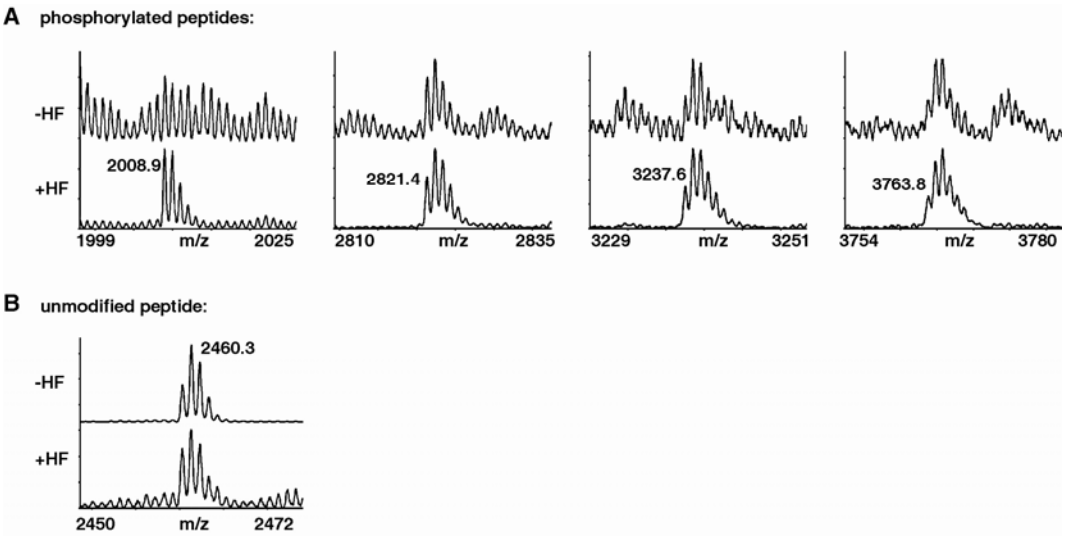

Figure 4.6. Signal-to-noise changes upon HF treatment. (A) Peaks corresponding to dephosphorylated versions of four phosphopeptides increased in S/N upon HF treatment. The four phospho-peptides are EVVGpSAEAGVDAASVSEEFR (singly protonated unmodified m/z = 2008.9), DKLPGFGDpSIEAQ-CGTSVNVHSSLR (unmodified m/z = 2821.4), EVVGpSAEAGVDA-ASVSEEFRADHPFLFCIK (unmodified m/z = 3237.6), and ISQAV-HAAHAEINEAGREVVGpSAEAGVDAASVSEEF (unmodified m/z = 3763.8). (B) Unmodified peptide peaks showed a decrease in S/N with HF. The example shown here is NVLQPSSVDSQTAM-VLVNAIVFK (m/z = 2460.3).

4.4 *Identification of In vitro Autophosphorylation Sites on Aurora A Kinase*

We tested our approach on the recombinant *Xenopus laevis* phosphoprotein, Aurora A kinase. Subsequent to *in vitro* autophosphorylation in the presence of ATP, SDS-PAGE analysis showed an additional mobility shift for Aurora A (Figure 4.7A). The shifted band was excised from the gel and split into four samples, which were digested with trypsin or Glu-C and either treated or not treated with HF. These four samples were then analyzed by single-stage mass spectrometry, and a phosphopeptide index was calculated for each unmodified Aurora A peak (Figure 4.7B). The phosphopeptide indexes generally correlated well with phosphorylation, as gauged by the S/N of the peak for neutral loss of phosphoric acid (98 Da) in MS-MS. Thus, of the ten peptides with a positive phosphopeptide index, nine were verified as phosphorylated by clear detection of the 98 Da signature loss (i.e., with a S/N>2). The phosphorylation modifications on these nine phosphopeptides were mapped by tandem MS, yielding eight phosphorylation sites that all agreed with previous characterizations of Aurora A phosphorylation (Haydon et al., 2003; Littlepage and Ruderman, 2002; Littlepage et al., 2002). None of the peptides with a negative phosphopeptide index was found to be phosphorylated.

A

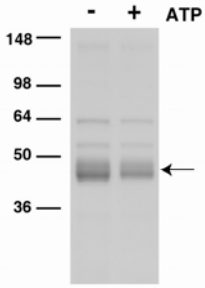

B

residues	peptide sequence	phosphopeptide index	S/N -H_3PO_4	phosphorylation site
[49-58]	ILGPSNVPQR	0.47	149	Ser-53
[344-352]	TYRRISKVE	0.09	104	Ser-349
[293-311]	RTTLCGTLDYLPPEMIEGR[a]	0.07	37	Thr-295
[113-129]	KKGSTDQGKTSAVPKEE	0.11	34	S116, T122
[348-364]	ISKVEFQYPPYVSEEAR	0.13	23	Ser-349
[149-158]	GKFGNVYLAR	0.22	5.3	Tyr-155
[99-113]	NPQQTSHSSTPNVEK[a]	0.12	4.3	Thr-103
[7-25]	ENHKPSNVKIFHPMTEGAK	0.08	3.1	Thr-21
[16-25]	IFHPMTEGAK	0.43	2.1	Thr-21
[246-257]	QLAEALLYCHSK[b]	0.21	<0.5	-
[228-234]	ELQKCTR	0.00	1.3	-
[134-148]	QWCLEDFEIGRPLGK	-0.31	1.1	-
[234-245]	FDDQRSAMYIK	-0.10	1	-
[263-278]	DIKPENLLLGSNGELK	-0.01	1	-
[170-178]	VLFKSQLEK	-0.03	0.9	-
[279-292]	IADFGWSVHAPSSR	-0.47	0.8	-
[279-293]	IADFGWSVHAPSSRR	-0.17	0.5	-
[197-202]	HPNILR	0.00	<0.5	-
[383-407]	GVLEHPWIIKNSQLKKKDEPLPGAQ	0.00	<0.5	-
[213-227]	VYLILDYAPGGELFR	-0.06	<0.5	-
[179-186]	AGVEHQLR	-0.09	<0.5	-
[351-364]	VEFQYPPYVSEEAR	-0.27	<0.5	-
[161-169]	ESKFILALK	-0.36	<0.5	-
[203-212]	LYGYFHDASR	-0.46	<0.5	-
[351-369]	VEFQYPPYVSEEARDLVSK	-0.61	<0.5	-
[27-48]	IPVNQPQSTQFRPPGTAVSAQR	-0.02	<0.5	-
[59-98]	VLAQAQKPILSSQKPTTQIPLRPATQGHQSSKPQGPNENR	-	-	-
[312-346]	MHDETVDLWSLGVLCYEFLVGKPPFETDTHQETYR	-	-	-

[a] Phosphorylation sites could not be localized by ms-ms, but have been previously described

[b] False positive

Figure 4.7. Determination of Aurora-A autophosphorylation sites. (A) Recombinant *Xenopus* Aurora-A displays reduced mobility in SDS-PAGE upon incubation with ATP. (B) Autophosphorylation sites of Aurora-A were found by MS phosphopeptide fingerprinting and confirmed by MS-MS and MS-MS-MS. The S/Ns for all unmodified Aurora-A peptides are shown in the table, along with the S/Ns for the peaks corresponding to the loss of phosphoric acid in the MS-MS of the corresponding phosphopeptides. The residues that were found to be phosphorylated are indicated in red.

4.5 *Comparison to Other Methods*

We compared our MS phosphopeptide fingerprinting approach to two other established methods using phosphorylated Aurora A as a test case, and found that it was the most efficient for finding phosphopeptides (Figure 4.8). Our method found all 9 phosphopeptides in the first 10 peptides tested. By comparison, analysis of all hypothesized Aurora A phosphopeptides in mass order (i.e., the hypothesis-driven multiple-stage MS approach (Chang et al., 2004) yielded all nine phosphopeptides in the

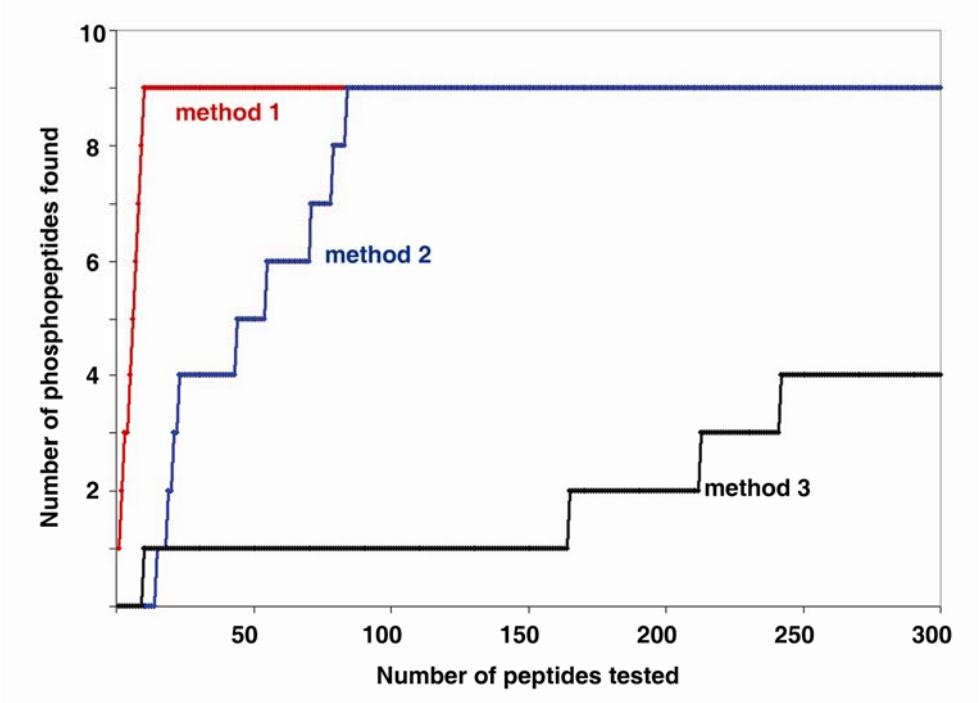

Figure 4.8. Comparison of MS phosphopeptide fingerprinting to other methods. MS phosphopeptide fingerprinting (method 1, red) identifies phosphopeptides more efficiently than hypothesis-driven multistage MS (method 2, blue) and fragmentation of the 300 most intense peaks in the spectrum (method 3, black).

sample, but only after examining 84 peptides. A neutral loss scan approach that analyzed the top 300 most intense peaks in the spectrum found only 4 of the 9 phosphopeptides, indicating that many phosphopeptides are not well-detected directly by MS.

4.6 *Discussion*

In summary, we show that chemical dephosphorylation is an effective method for generating an "MS phosphopeptide fingerprint" that permits rapid identification of phosphopeptides by MS. This approach uses MS data to determine candidate phosphopeptides that can be confirmed with efficient consumption of sample by tandem MS analysis. It takes advantage of the S/N enhancement that is generally observed upon dephosphorylation of phosphopeptides; smaller phosphopeptide signals are converted to larger unphosphorylated peptide signals. We have applied our technique to the analysis of model phosphoproteins, as well as *in vitro* phosphorylated proteins. In the next chapter we will discuss application of this method to *in vivo* samples.

CHAPTER FIVE: IDENTIFICATION OF PHOSPHORYLATION SITES ON VESPERA AND THE AURORA B CHROMOSOME PASSENGER COMPLEX

5.1 *Introduction*

Having validated our method on model phosphoproteins and a known *in vitro* phosphorylation reaction, we wished to apply it to *in vivo* samples. A rapid and efficient method for the identification of phosphorylation is particularly useful in studying mitosis, where phosphorylation signaling appears to be of central importance. The order and timing of events in the cell cycle are coordinated by cyclin-dependent kinases (Cdks), which phosphorylate different substrates, depending on their association with different cyclin binding partners. These phosphorylation events trigger biochemical switches that initiate signaling cascades and thereby direct the progression of the cell through various phases of the cell cycle (Morgan, 1997). Comprehensive knowledge of the phosphorylation sites that are associated with different activities in the cell cycle will be crucial to understanding the cell-cycle control system.

Here, we apply our method to identify *in vivo* phosphorylation sites on four members of the CPC--Aurora B, Incenp, Dasra A, and Survivin—that were immunoprecipitated from *Xenopus* egg extracts using anti-Incenp antibodies. In addition, we observe a cell cycle-dependent mobility shift on Vespera, and we identify phosphorylation sites on immunoprecipitated Vespera that account for this shift. For both Incenp and Vespera, we identify Cdk consensus phosphorylation sites which suggest mitotic regulation of these proteins. We also show that Vespera phosphorylation is not required for its SUMOylation.

5.2 *Identification of Phosphorylation Sites on the Aurora B Chromosome Passenger Complex (CPC)*

We applied the MS phosphopeptide fingerprinting approach to the Chromosome Passenger Complex (CPC), purified from *Xenopus* egg extracts. Aurora B has been previously shown to phosphorylate itself as well as the other CPC complex members by incorporation of ^{32}P, but not all of the *in vivo* phosphorylation sites have been mapped (Bishop and Schumacher, 2002; Honda et al., 2003; Sessa et al., 2005; Wheatley et al., 2004; Yasui et al., 2004). Phosphorylation serves to activate the CPC, which is normally suppressed in the cytoplasm, but active on chromatin. This phosphorylation and activation can be induced either by the addition of phosphatase inhibitors or by clustering of the complex on chromatin (Kelly et al., 2007). We therefore examined the phosphorylation of CPC members in *Xenopus* egg extracts that had been treated with a phosphatase inhibitor (okadaic acid) or a control (DMSO).

Certain of the immunoprecipitated CPC components from extracts that were treated with okadaic acid showed shifts in SDS-PAGE, compared to DMSO control, consistent with phosphorylation (Figure 5.1A). The regions containing the phosphorylated CPC proteins were excised from the gel and the phosphorylated peptides were identified using our MS phosphopeptide fingerprinting method (Figure 5.1B). CPC peptides that yielded a positive phosphopeptide index were subjected to MS-MS and MS-MS-MS analysis, confirming that these peptides were phosphorylated. In several cases, we were also able to identify the precise sites of phosphorylation. Aurora B is known to bind and phosphorylate the C-terminal region of Incenp, resulting in a positive feedback loop that further stimulates Aurora B activity via autophosphorylation of its activation loop

(Bishop and Schumacher, 2002; Yasui et al., 2004). Our analysis indicates that these phosphorylation events occur in *Xenopus* egg extracts, after

A

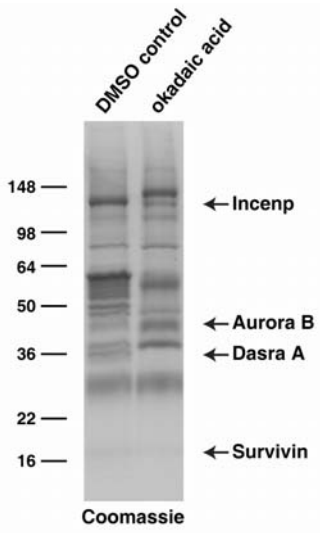

B

residues	peptide sequence	phosphopeptide index	s/n -H_3PO_4	phosphorylation site
Incenp				
[847-862]	RTSSAVWHSPPLSSNR	0.45	79	T848, S849, S850
[275-287]	RASLASQFSLASK	0.18	20	Ser-277
Aurora B				
[2-15]	EYKENLNPSSYTSK	0.62	22	Y3, S10, S11, Y12, T13, or S14
[55-66]	ITPSASSSVPGR	0.17	15	Thr-56
[248-264]	TMCGTLDYLPPEMIEGK	0.20	5.7	Thr-248
Dasra A				
[60-70]	DLESLSTTADK	0.36	5.5	S63, S65, T66, T67
[194-206]	LLVTNSSSKPAQR	0.50	4.3	T197, S199, S200, or S201

Figure 5.1. Chromosome Passenger Complex (CPC) Phosphorylation. (A) CPC was immunoprecipitated from *Xenopus* egg extracts treated with DMSO control or okadaic acid (phosphatase inhibitor), and analyzed by SDS-PAGE. (B) Phosphopeptides were identified for Incenp, Aurora B, and Dasra A.

treatment with okadaic acid, but not DMSO. Incenp was found to be triply-phosphorylated on a peptide containing Thr-848, Ser-849, and Ser-850, and Aurora B was phosphorylated at Thr-248.

In addition to these known sites, we found phosphorylation on Incenp at Ser-277, and on Aurora B at Thr-56. Interestingly, Thr-56 is a cyclin-dependent kinase (Cdk) consensus site, which may indicate Cdk regulation of Aurora B, as has been previously suggested for Incenp (Goto et al., 2006). We also found a peptide in the N-terminal region of Dasra A that was quadruply phosphorylated on Ser-63, Ser-65, Thr-66, and Thr-67, though the functional significance of this non-conserved region has yet to be determined. In addition, two other phosphopeptides (one each for Aurora B and Dasra A) were found and confirmed by MS-MS-MS, but the precise phosphorylation sites within these peptides could not be localized.

5.3 *Identification of Vespera Phosphorylation*

In addition to its SUMOylation upon binding DNA, we observed that Vespera exhibits a DNA-independent mobility shift in mitosis (Figure 5.2A). We speculated that this shift was due to phosphorylation, and mapped three phosphorylation sites on endogenous Vespera using MS phosphopeptide fingerprinting (Figure 5.2B) (Woo et al., 2008). These sites included Ser-183, Ser-226, and Ser-234. We noted that Ser-183 matches an Aurora kinase consensus site, [RX(S/T)], while Ser-226 and Ser-234 are both Cdk consensus sites, [(S/T) P] (see Figure 5.4). We therefore mutated these residues to alanine or acidic residues, and tested the mutants to see if they still displayed a cell cycle-dependent mobility shift. We treated the pair of Cdk consensus sites, Ser-226 and Ser-234, as one unit, mutating them in tandem. When we did the analysis, we observed that Aurora-site (S183)

mutants still shifted in metaphase, like wild-type, but that Cdk-site (S226, S234) mutants no longer did so (Figure 5.3).

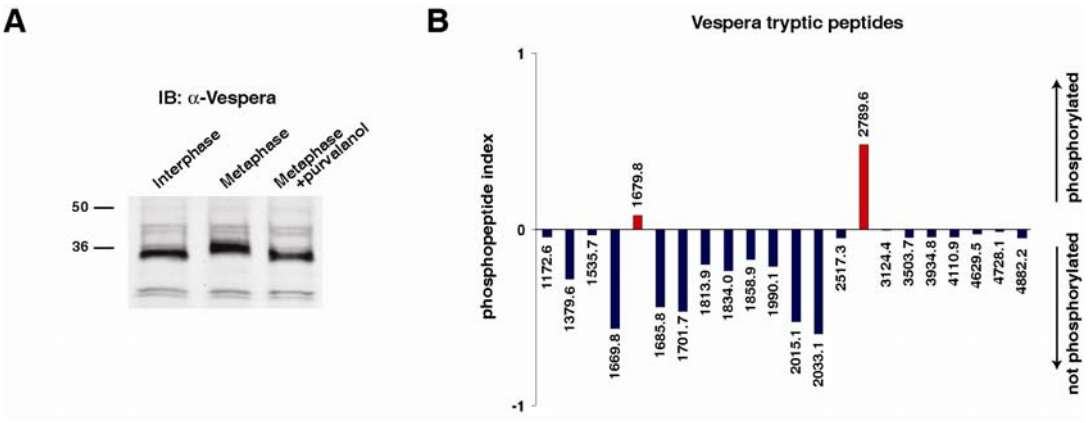

Figure 5.2. Phosphopeptide Mapping of Vespera. (A) Cell-cycle-dependent mobility shift of Vespera. In the absence of DNA, total protein from interphase extract, metaphase extract, and metaphase extract treated with the Cdk inhibitor purvalanol were analyzed by Western blotting using anti-Vespera antibodies. (B) Phosphopeptide finger-printing analysis of immunoprecipitated Vespera from metaphase extract identified two phosphopeptides.

We therefore concluded that phosphorylation of Cdk-consensus S226 and/or S234 is required for the observed mitotic shift of Vespera. This is most likely due directly to Cdk-dependent phosphorylation of these sites.

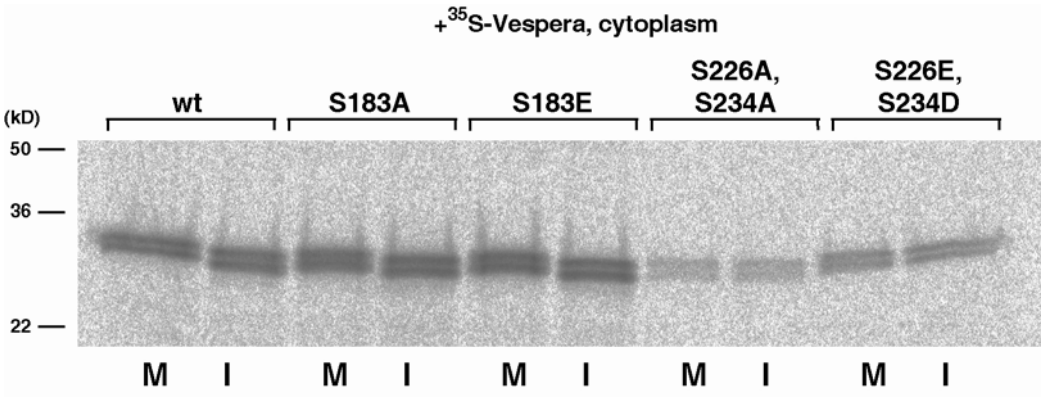

Figure 5.3. Mutational analysis of Vespera phosphorylation sites. ^{35}S-labeled, *in vitro*-translated wild-type or mutant Vespera as indicated was incubated for 45 min at 22°C with CSF extract containing cycloheximide, with (M) or without (I) calcium to induce interphase. For each sample, 0.5µl of extract was analyzed by SDS-PAGE and autoradiography.

In summary, we have identified several modifications on Vespera that cluster in its C-terminus (Figure 5.4). These include a single site required for poly-SUMOylation on chromatin, an Aurora kinase consensus site, and two Cdk consensus sites that are needed for modification of Vespera in metaphase.

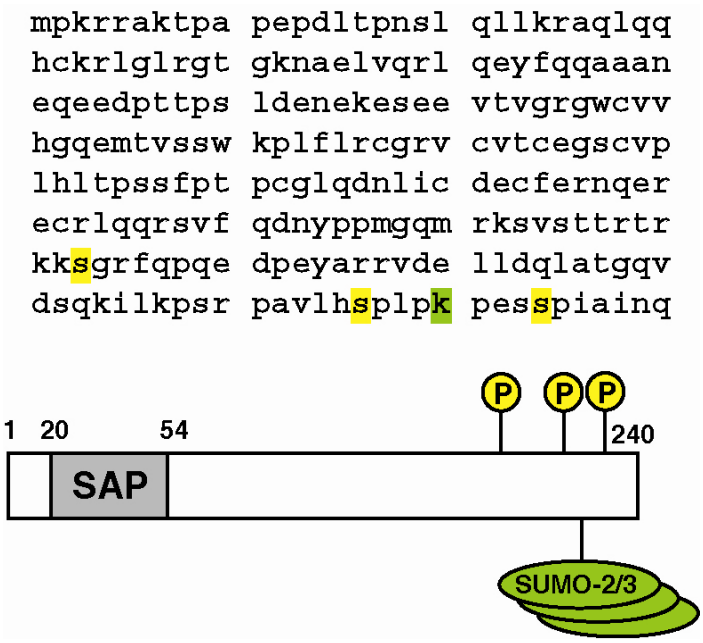

Figure 5.4. Vespera sequence and modifications.

5.4 *Vespera Phosphorylation Is Not Required for its SUMOylation*

SUMOylation of Vespera requires DNA-binding, but we observe the mitotic shift in Vespera in the absence of DNA. Therefore, we infer that Vespera SUMOylation is not required for its phosphorylation. We next asked if SUMOylation of Vespera is dependent on phosphorylation by mutating the phosphorylation sites we had identified and visualizing the chromatin-bound constructs. All of the phosphorylation mutants we tested were SUMOylated on chromatin, so mitotic phosphorylation does not appear to be required for SUMOylation (Figure 5.5). This is consistent with our observation that Vespera SUMOylation is not cell cycle-dependent (see Figure 2.7).

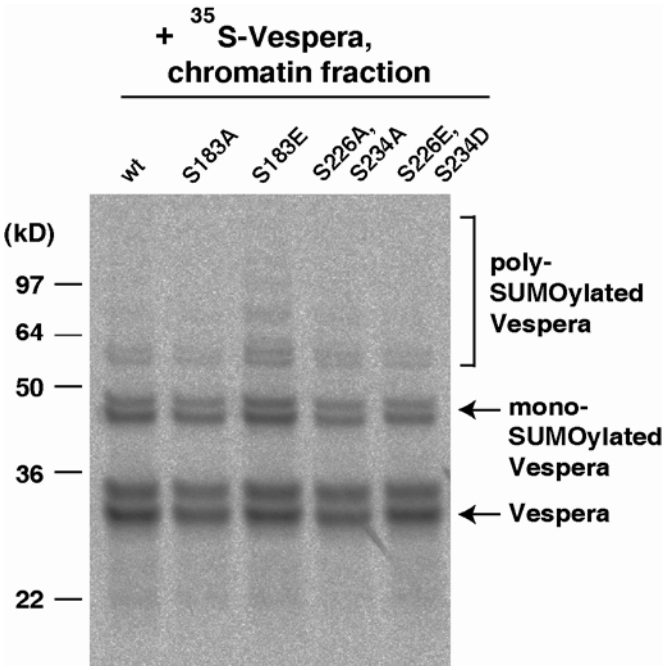

Figure 5.5. Vespera phosphorylation is not required for its SUMOylation. ^{35}S-labeled, *in vitro*-translated wild-type or mutant Vespera proteins were added to metaphase extracts containing cycloheximide and incubated for 40 min at 22°C. DNA-beads were added to the extracts and incubated for an additional 40 min, then isolated and purified. The DNA-beads-associated proteins were visualized by SDS-PAGE and autoradiography. Arrow indicates unmodified Vespera, mono-SUMOylated Vespera, and bracket indicates poly-SUMOylated Vespera. The doublet is an artefact of *in vitro* translation.

5.5 Discussion

From our analysis of the CPC and Vespera purified from *Xenopus* egg extracts, we conclude that MS phosphopeptide fingerprinting can

successfully identify phosphopeptides isolated *in vivo*. Although our method is highly effective for finding phosphopeptides, the confirmation and unambiguous localization of the precise phosphorylation sites can still be very difficult, as observed with members of the CPC. While the neutral loss of phosphoric acid in CID provides useful confirmation of a phosphopeptide, the loss of the phosphate group often makes it difficult to pinpoint its location. In the future, we plan to combine the current approach with fragmentation techniques such as electron transfer dissociation (ETD) or electron capture dissociation (ECD), which promote peptide bond breakage without loss of phosphate groups. We have demonstrated this technique using MALDI, but we believe it should be an effective method for electrospray ionization as well.

A phosphopeptide index can be calculated for any peptide without prior knowledge of the sample. Thus, even when the protein sample is unknown, MS phosphopeptide fingerprinting should be an effective method for the identification of phosphopeptides. The HF-treated samples can also provide additional peptides for protein identification, especially in cases where the identification of a phosphoprotein might be complicated by heavy modification.

Our analysis of CPC and Vespera has identified previously unknown phosphorylation sites. We demonstrated that Vespera phosphorylation is not required for its SUMOylation, and therefore, we would predict, for the SUMOylation-dependent functions we observe. Nevertheless, the sites we identified match known consensus sites for Aurora and Cdk, two kinase families that are important in mitosis, and this suggests that there are cell cycle-regulated roles for these modifications. Future studies are required to elucidate these roles, as well as those for the new phosphorylation sites

identified in Incenp, Aurora B, and Dasra A. Cdk-dependent phosphorylation of Aurora B at Thr-56 may be of particular interest, since direct regulation of Aurora B by Cdk has not yet been described. Finally, though we observed Survivin association with CPC in our immunoprecipitated complexes, we did not observe phosphorylation of Survivin under the conditions of our experiment. Survivin phosphorylation by Aurora B has been reported *in vitro* (Wheatley et al., 2004), and dominant-negative phosphorylation-site mutants produced spindle abnormalities in *Xenopus* egg extracts (Canovas and Guadagno, 2007). More studies of endogenous Survivin are needed to identify the *in vivo* context for Survivin phosphorylation, and its biological functions.

CHAPTER SIX:
GENERAL DISCUSSION

6.1 *Vespera Conservation and Function in Early Development*

We have identified Vespera as a protein that is important for nuclear reassembly in *Xenopus* egg extracts. Nuclear re-formation in telophase is a fundamental process in all eukaryotic cells with an open mitosis, but Vespera is evolutionarily not well conserved. The closest mammalian homologs of Vespera are Dppa2 (Developmental pluripotency associated) and Dppa4, with 21.6% overall identity between the frog and human proteins, much of which is accounted for by their SAP domains (Figure 6.1A). Interestingly, the C terminus of Vespera is also fairly well conserved (Figure 6.1B), as has been reported for the mammalian proteins (Maldonado-Saldivia et al., 2007). This higher level of conservation coincides with the clustering of the modifications we mapped (see Figure 5.4) and may reflect conserved modification patterns.

Dppa2 and Dppa4 expression is restricted to embryonic pluripotent cells, and similarly, we find that expression of Vespera mRNA is restricted to eggs and early embryos (Figure 6.2). The modest sequence conservation and embryonic expression of Vespera raise questions about the generality of its function. Because *Xenopus* eggs and early embryos are substantially larger than their nuclei and spindles, these cells may have a unique requirement for active disassembly of microtubules from chromosomes. *Xenopus* egg extracts can assemble spindles around DNA-beads in the absence of centrosomes, and it has been suggested that the eggs and early embryos have an enhanced ability to promote microtubule polymerization

from chromosomes. We speculate that Vespera may represent a corresponding enhanced ability to destabilize microtubules around chromosomes, to promote proper spindle disassembly in these systems.

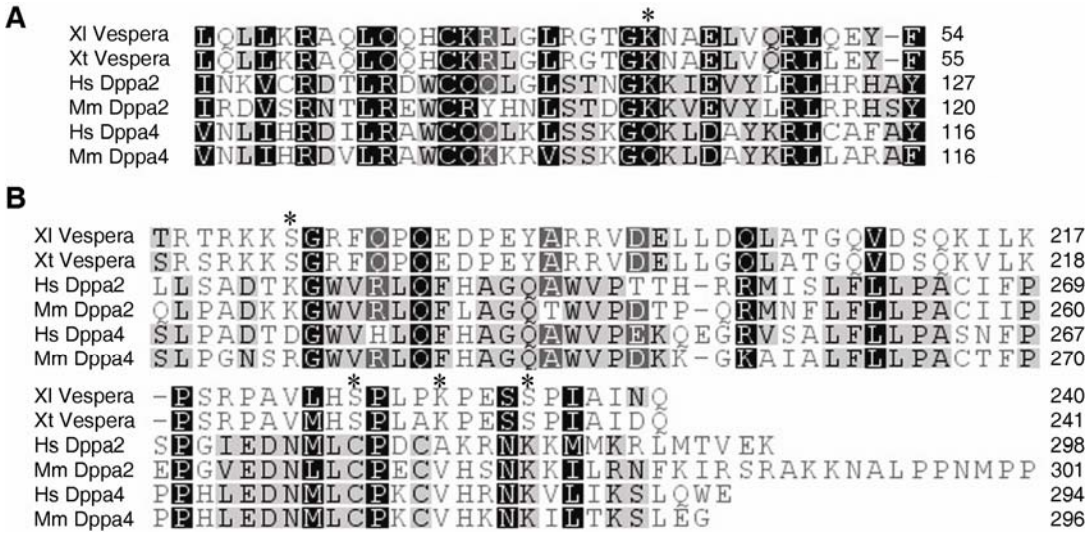

Figure 6.1. Conservation of Vespera. (A) Sequence alignment of the SAP domains of *Xenopus* Vespera and mammalian homologs Dppa2 and Dppa4. Conserved lysine that contacts DNA is marked with an asterisk (*) (B) Sequence alignment of the C termini of *Xenopus* Vespera and mammalian homologs Dppa2 and Dppa4. The identified sites for covalent attachment of phosphate and SUMO modifications are marked with asterisks (*).

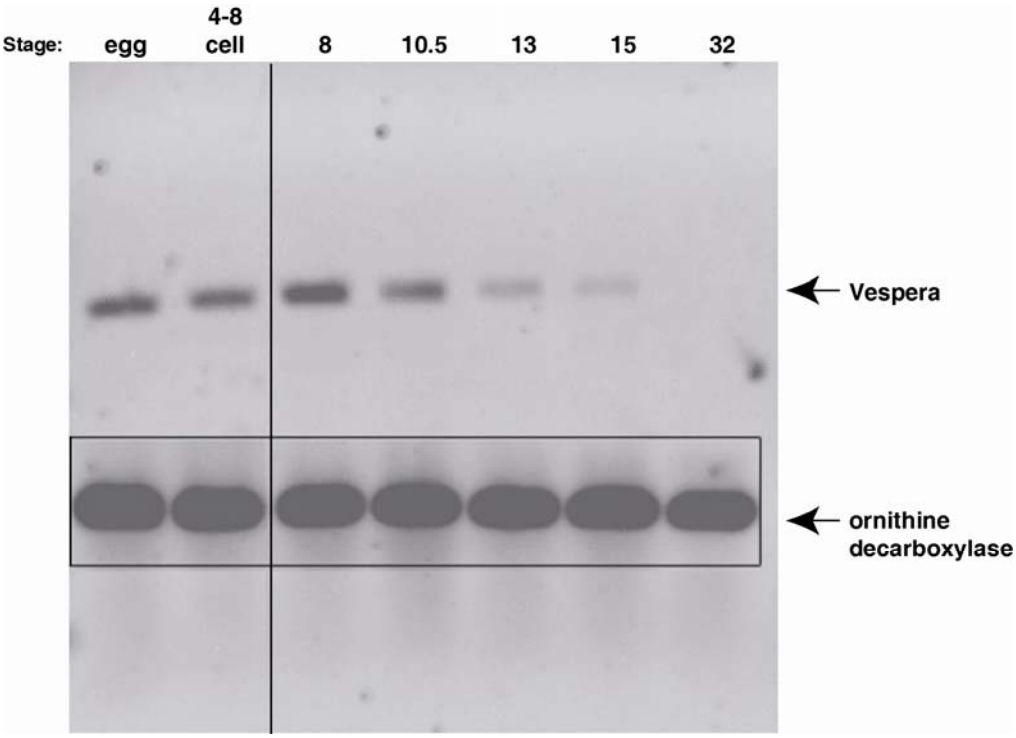

Figure 6.2. Embryonic Expression of Vespera mRNA. Embryos from the indicated stages were collected and RNA was extracted and subjected to RT-PCR analysis using primers for Vespera and ornithine decarboxylase, a loading control for mRNA recovery.

6.2 *Special roles for microtubules in oocytes and eggs*

To facilitate early embryonic divisions, many eggs are large and contain stores of mRNA and proteins needed for initial cell cycles upon fertilization. Furthermore, many meiotic spindles lack centrosomes, and it has been shown that spindle assembly can occur in *Xenopus* egg extracts around DNA-coated beads in the absence of centrosomes (Heald et al., 1996). Therefore, the self-organization of microtubules around chromosomes to form a spindle in oocytes and early embryos often presents a unique challenge for these cells. Studies of acentrosomal spindles in mouse oocytes described a Ran-dependent dramatic increase in microtubule

polymerization following nuclear envelope breakdown in maturing oocytes. These spindles appeared to go through a large "Microtubule Ball" stage before activities of motors like kinesin-5 organized the microtubules into bipolar spindle structures (Schuh and Ellenberg, 2007). It appears that in some systems, at least, microtubule polymerization is particularly active at these stages, in order to nucleate mitotic spindle structures in a relatively large volume of cytoplasm. It follows, then, that specialized microtubule-destabilizing activities might be required to counteract embryonic microtubule polymerization around chromatin, at the appropriate times, and Vespera may represent one such pathway. Interestingly, in starfish oocytes, it was shown that asters are too short to capture chromosomes in these large cells, but that in this case a contracting actin network helps to drive spindle assembly (Lenart et al., 2005). Actin is not required for spindle assembly in mouse oocytes, but apparently these cells have capitalized on enhanced microtubule polymerization to solve the challenge of spindle assembly in large cells (Wassarman and Fujiwara, 1978). Similarly, large amounts of microtubule polymerization appear to facilitate migration and fusion of sperm and egg pronuclei in mouse fertilization (Schatten et al., 1985).

6.3 *Chromosome-Induced SUMOylation in mitosis*

As we have discussed, Vespera is embryonically expressed and poorly conserved. This may reflect a specialized role for this protein in early embryos, but another possibility is that Vespera acts chiefly through its SUMOylation, allowing the Vespera sequence substantial evolutionary flexibility.

Like Aurora B-dependent phosphorylation, SUMOylation has been shown to be stimulated on metaphase chromosomes in *Xenopus* egg extracts (Azuma et al., 2003). Of the chromatin-induced SUMOylation substrates, Topoisomerase II is a major target, but we have now identified Vespera as another one. Like Topo II, SUMOylation of Vespera is dependent on the SUMO E3 ligase PIASy in the *Xenopus* egg extract system. We identified K230 on Vespera as solely required for its SUMOylation, leading us to conclude that this is the attachment site for SUMO chains (though we cannot formally rule out its requirement in SUMOylation of Vespera by another mechanism).

Our findings that SUMO-Vespera has a negative effect on microtubules suggests a chromatin-based mechanism for the local depolymerization of microtubules. This can serve to balance the chromatin-induced microtubule polymerization activities attributed to the Aurora B (CPC) and Ran pathways. In contrast to observations for Aurora B, we find that Vespera is bound to chromatin and SUMOylated throughout the cell cycle, so perhaps Vespera is constantly active on chromatin, with its activity dominating spindle dynamics only when Aurora B is removed from chromatin in anaphase. We provide preliminary evidence that Vespera is involved in recruitment of protein phosphatase PP1 to chromatin, via SUMOylation of Vespera. We note that as a general principle in covalent modification-based signaling, the use of one type of modification to recruit an enzyme that affects a different type of modification (in this case, SUMO recruitment of phosphatase), can be useful, in that the two modules do not interact with one another, resulting in undesirable signal interference.

Although we showed that PIASy-dependent Vespera SUMOylation promotes nuclear formation in *Xenopus* egg extracts, PIASy depletion does

not have an apparent effect on this process (data not shown and (Azuma et al., 2005)). This apparent conflict can be reconciled by our observation that spindle size was reduced in PIASy-depleted extracts (see Figure 2.17), suggesting that PIASy contributes to microtubule stabilization (thereby opposing Vespera), by independent means.

SUMO modifications have been implicated in diverse cellular processes, and the mechanisms are increasingly found to involve recognition of SUMO by proteins containing SUMO-interacting motifs (SIMs). These motifs are characterized by a hydrophobic core flanked by acidic residues (Hecker et al., 2006). Recent large-scale studies have identified yeast PP1 as a SUMO-interacting protein that contains these motifs (Makhnevych et al., 2009), which are conserved in vertebrates. Further studies are required in order to characterize the interaction between SUMOylated Vespera and PP1 or other SIM-containing proteins.

6.4 *Microtubules and the Nuclear Envelope*

Our results indicate a connection between disassembly of spindle microtubules and nuclear re-formation at the end of mitosis. In organisms with an open mitosis, the dynamics of the nuclear envelope and spindle microtubules represent some of the most dramatic structural features of the cell division process. From the earliest high-resolution imaging studies of this process, a relationship has been noted between microtubules and the nuclear envelope.

Electron microscopy studies of nuclear envelope breakdown (NEBD) in prophase revealed that the process was characterized by formation of invaginations in the lamina that were occupied by microtubules (Georgatos et al., 1997). This led to the hypothesis that microtubules participate in

active tearing of membrane fragments to promote NEBD. When cells were treated with nocodazole, however, NEBD still occurred, though the process appeared qualitatively different. More recently, higher-resolution live imaging of microtubules and nuclear envelope components also reported the formation of prophase invaginations, and showed that the first tearing site consistently forms in regions away from chromosomes (Beaudouin et al., 2002). Microtubules were observed to form asters within these invaginations, and these asters were shown to recruit dynein (Salina et al., 2002). Overexpression of dominant-negative dynactin disrupted this dynein localization and delayed NEBD. In contrast to the prior report, nocodazole treatment delayed NEBD in this study. The differences could be explained by varying experimental handling, but normal rat kidney (NRK) cells were used in both cases. Therefore, microtubules appear to play an ill-defined nonessential role in the process of NEBD, perhaps to ensure the timely execution of the process.

If microtubules promote NEBD in prophase, is it possible they provide an obstacle to nuclear re-formation in telophase? In the transition from mitosis to interphase, chromosomes must switch from promoting local microtubule polymerization to attracting components of the nuclear envelope. To some extent this is achieved by signaling pathways. At the end of mitosis, the Triple A-ATPase p97/Cdc48 extracts Aurora B from chromatin and preceding its re-localization to the central spindle, a process that has been shown to be required for proper nuclear re-formation (Ramadan et al., 2007). In yeast, this re-localization is mediated by Cdc14 dephosphorylation of the Aurora-interacting protein Sli15 (homolog of Incenp), and is required for proper spindle disassembly. Therefore, re-localization of the Aurora B Chromosome Passenger Complex (CPC) has

been shown to be required for both spindle disassembly and nuclear re-formation at the end of mitosis. It is possible that Aurora B has central spindle-specific substrates that are required for these events, but the CPC has also been characterized to promote microtubule polymerization from chromosomes (Kelly et al., 2007; Sampath et al., 2004). Therefore a simpler model, given the results to date, is that the CPC must be re-localized in order to suppress its microtubule polymerizing activities from chromosomes at anaphase, when such activities are no longer desirable.

Further clues that spindle microtubules provide a direct challenge for the newly-forming nuclear envelope come from immunofluorescence studies of telophase. Imaging analysis of fluorescently-tagged lamin B receptor, which is recruited to chromatin in the nuclear re-formation process, reported that the protein appears to favor regions of lower microtubule density (Chaudhary and Courvalin, 1993). A higher-resolution version of this study confirmed that nucleation of lamin B receptor begins on the side of the chromatin mass opposite sites of microtubule attachment (Gerlich et al., 2001). Recently, careful timecourse analyses of several nuclear envelope proteins in telophase has revealed that there appear to be two different modes of recruitment of lamina proteins to chromatin (Dechat et al., 2004; Haraguchi et al., 2008). In the first mode, exemplified by lamin B receptor, nuclear envelope components are recruited to regions away from spindle microtubules. In the second mode, displayed by proteins such as LAP2α, emerin, and BAF, recruitment appears localized specifically to the region of chromatin surrounding microtubule attachment (termed the "core" region in these studies). Importantly, these two modes of recruitment appear to reflect differing modes of nuclear re-formation, as the nuclear envelope consistently encloses the surrounding chromatin before the "core"

region (Figure 6.3C). The delay in forming nuclear envelope at the site of spindle attachment further suggests that microtubules present a special

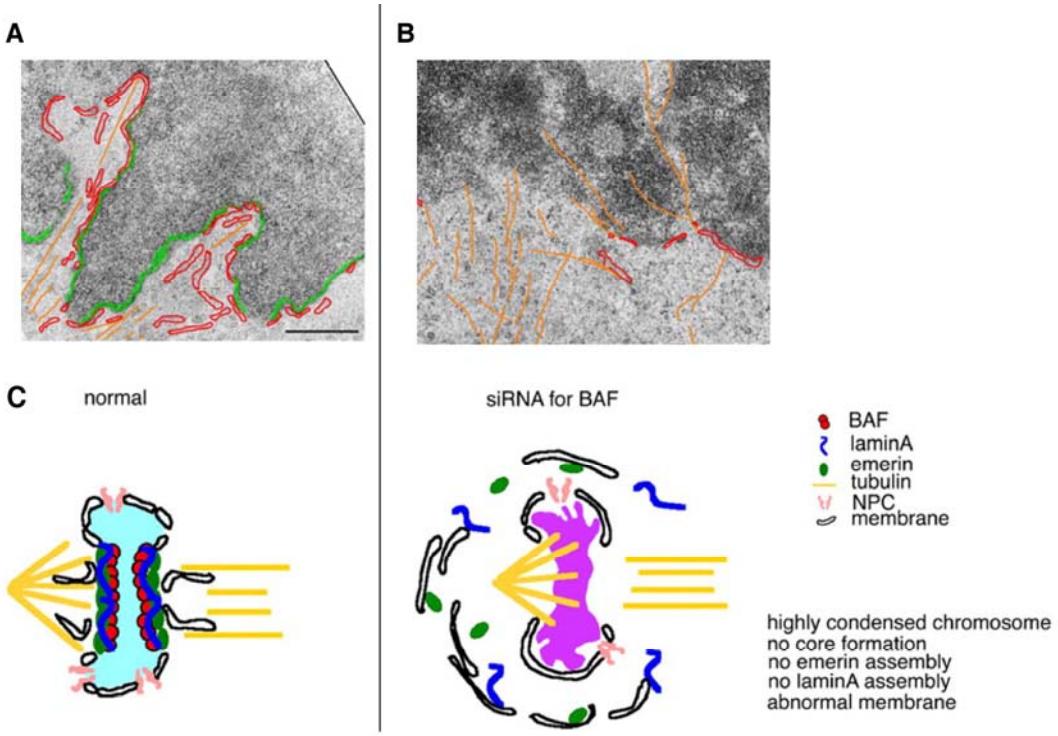

Figure 6.3. Depletion of a chromatin-NE adaptor protein, BAF, results in increased microtubules in the telophase chromatin body, adapted from (Haraguchi et al., 2008). Live-correlated EM analyses of HeLa cells expressing GFP-BAF after siRNA treatment (B) or luciferase siRNA treatment as a control (A). During time-lapse imaging of living HeLa cells expressing GFP-BAF, cells were fixed 7 minutes after the metaphase-anaphase transition and subjected to EM analysis. Drawings are superimposed on the EM images indicating GFP-BAF (green), the NE (red), and MTs (orange). Scale bar, 500 nm. (C) Model of NE formation in the control siRNA-treated (left) and BAF siRNA-treated cell (right).

challenge to that process, and it appears that a specialized "core" complex of proteins is recruited to the region to meet this challenge.

The DNA-binding protein BAF has been shown to be required for recruitment of LEM domain-containing nuclear envelope proteins such as emerin to this chromatin "core" region, and therefore appears to be a key player in forming this structure (Haraguchi et al., 2001). By immunofluorescence, BAF was observed to bind to microtubules prior to its concentration at the "core" region. When cells are treated with nocodazole to depolymerize microtubules, BAF is no longer recruited to telophase chromatin. Based on these observations, the authors of this study postulate that microtubules are required for "core" formation and promote assembly of these proteins on chromatin. This is no doubt demonstrated by their results, but another interpretation is that in the absence of microtubules, "core" complex recruitment is simply not needed, because the "core" complex exists for the special purpose of disrupting chromatin-microtubule attachments. In this model, BAF binds to microtubule for the purpose of navigating to sites of chromatin-microtubule attachment, in order to promote nuclear envelope formation in those regions. More detailed studies of nuclear envelope assembly in the presence of nocodazole are needed to distinguish between different models. For example, it would be useful to know the localization of lamin B receptor in the presence of nocodazole (perhaps it coats the entire chromatin body), as well as the effect of nocodazole treatment on the process of nuclear re-formation as a whole. Our studies in *Xenopus* egg extracts suggest that the formation of functional interphase nuclei is not affected by nocodazole treatment (see Figure 2.19).

Haraguchi et al. have also provided valuable insight into the relationship between microtubules and nuclear envelope formation through

the use of time-resolved electron microscopy (Haraguchi et al., 2008). Four minutes after the metaphase-to-anaphase transition, the core region is not very prominent, nuclear membrane has not yet formed, and microtubules can be observed to penetrate into the chromatin mass. About three minutes later, the core complex can be observed, and nuclear membrane has started to form outside of the core. At this time, microtubules were found in gaps in the core, or seen to extend to the region of core complex and stop, as if the core complex might be inhibiting their further polymerization. Finally, ten minutes following the metaphase-to-anaphase transition, the nuclear membrane is largely formed, with a small remaining region of core accumulation. Again, in this case, it appears that core regions are refractory to microtubules. These studies also revealed dramatic changes upon siRNA depletion of BAF, which appears crucial for core complex formation. In the absence of BAF, the core complex was not observed to form, and relatively long microtubules persisted in the chromatin mass late into anaphase (Figure 6.3A and 6.3B). These observations demonstrate that BAF is required for core complex formation. They suggest that this complex, which is localized on chromatin to regions of spindle-microtubule attachment, plays a role in disassembling microtubules around chromatin in anaphase. Furthermore, the relatively rapid formation of nuclear envelope around regions of chromatin that are devoid of microtubules suggest that chromatin-microtubule attachments impede the recruitment of nuclear envelope components. These results, like those of our study, suggest that microtubules must be depolymerized around chromatin to promote proper nuclear re-formation at the end of mitosis.

6.5 *A Model for the Coordination of Spindle Disassembly and Nuclear Re-formation*

Our review of detailed imaging studies summarizes the circumstantial evidence that microtubules are involved in nuclear envelope formation. It remains unclear from the images whether microtubules contributed positively or negatively to the process, but our analysis of Vespera in *Xenopus* egg extracts suggests that microtubules interfere with nuclear re-formation. In metaphase, chromosomes nucleate microtubule polymerization to promote spindle formation, but in interphase, chromatin attracts nuclear envelope components to promote nuclear formation. A fundamental question, then, is how does chromatin distinguish between these radically different structures at different points in the cell cycle? Our model for the regulation of these chromatin-induced functions is depicted in Figure 6.4, which shows the opposing roles for Aurora B and Vespera in these processes. From prophase to metaphase, Aurora B kinase is localized to chromosomes (see Figure 1.10) where it promotes microtubule polymerization and spindle assembly, and inhibits nuclear formation. Meanwhile, Vespera is SUMOylated on chromatin where it acts to negatively regulate microtubules and promote nuclear formation. While Aurora B is active on chromosomes, it activity dominates, but when Aurora B is re-localized from chromosomes to the spindle midzone at the start of anaphase, Vespera activity dominates. SUMOylated Vespera potentially acts directly on the Aurora B pathway by recruiting PP1 phosphatase to locally dephosphorylate Aurora B substrates around anaphase chromatin. This facilitates microtubule depolymerization around chromatin, thereby permitting proper nuclear formation as the cell proceeds to interphase.

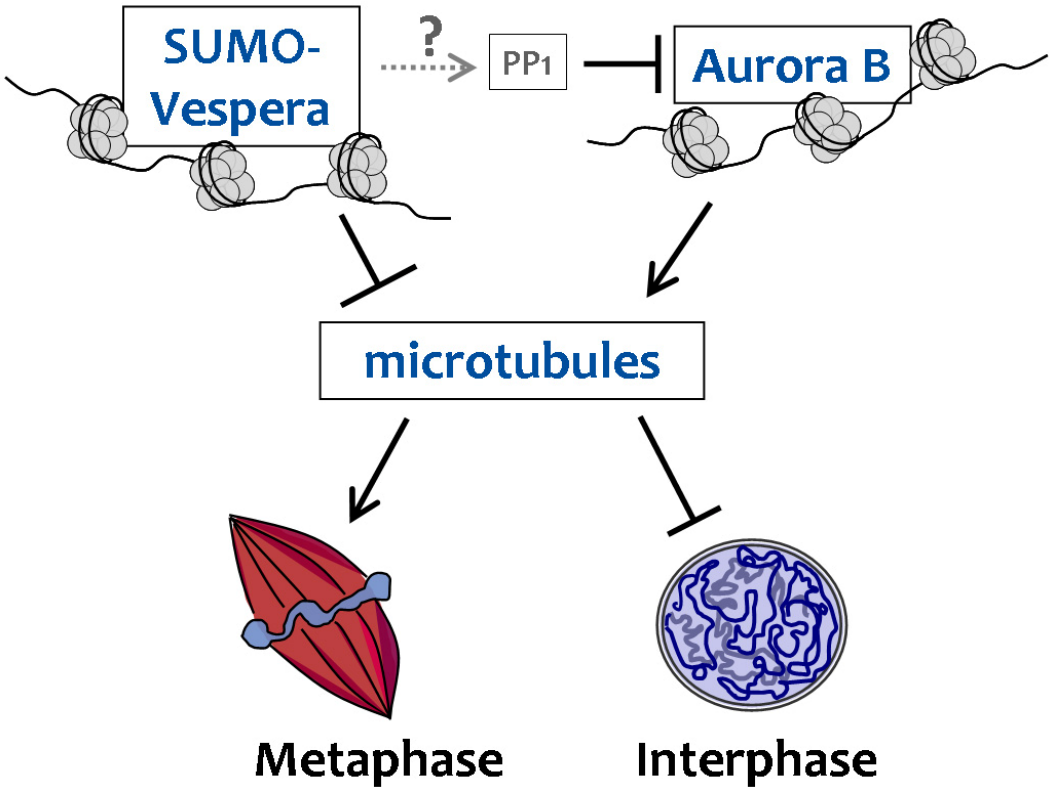

Figure 6.4. A model for opposing action of Vespera and Aurora B on spindle assembly and nuclear formation around chromatin. Aurora B is known to promote chromosome-associate microtubule polymerization, which is required for spindle formation. We have introduced a new protein, Vespera, which is SUMOylated on chromatin and destabilizes microtubules. Taken together, our results suggest that microtubules are inhibitory to nuclear formation. This explains the requirement of Vespera in proper nuclear assembly, and the prior observation that Aurora B inhibits this process. PP1 phosphatases directly opposes Aurora B function by dephosphorylation of its targets, and we provide preliminary evidence that SUMO-Vespera is involved in PP1 recruitment to chromatin.

6.6 *Concluding remarks*

Our results show that, upon completion of mitosis, the disassembly of spindle components and reassembly of nuclear structures must be locally coordinated around chromatin. Previous studies have suggested that an important step in this process is the inactivation of the Aurora B kinase by the Triple A-ATPase Cdc48/p97, which physically extracts the protein from chromatin at anaphase. Aurora B is the catalytic subunit of the CPC, which promotes microtubule polymerization and spindle formation from mitotic chromosomes. We postulate that removal of the CPC from chromosomes at anaphase is required for proper spindle disassembly and nuclear reassembly, and that additionally, an opposing activity is localized to chromatin to promote rapid inactivation of Aurora B activity upon its removal.

Using *Xenopus* egg extracts and mass spectrometry, we discovered Vespera, a protein which is functionally antagonistic to the CPC. We showed that Vespera promotes microtubule depolymerization from chromosomes and is required on chromatin for proper nuclear formation. We initially identified Vespera as a protein that is specifically SUMOylated upon interaction with chromatin, a modification that is dependent on the SUMO E3 ligase, PIASy. Immunodepletion of Vespera from *Xenopus* egg extracts interfered with proper nuclear formation and nuclear transport, and rescue of this defect required Vespera SUMOylation. Addition of excess amounts of Vespera to metaphase extracts disassembled spindle microtubules, and this activity was also dependent on SUMOylation of Vespera and PIASy. Importantly, the Vespera depletion defect in nuclear formation could be rescued by nocodazole or by co-depletion of the CPC. These manipulations depolymerize microtubules, suggesting that the

microtubule-depolymerizing activity of SUMO-Vespera is central to its role in ensuring proper nuclear formation. Our results suggest that microtubules must be actively depolymerized around chromosomes to permit proper nuclear reassembly, a process that is promoted by SUMOylated Vespera.

In conclusion, we have discovered a novel chromatin-localized microtubule disassembly activity, which appears to play an important role in nuclear re-formation at the end of mitosis. The mechanism of this function remains unclear, and further studies will be required to uncover the molecular mechanisms of Vespera activity. MS-based proteomic approaches using SUMOylated Vespera will be valuable in determining if the hypothesized connection between SUMO-Vespera and PP1 is direct. We have also reported a new MS method for the efficient identification of phosphorylation, and application of this method to identification of phosphorylation signaling pathways such as those directed by Aurora B kinase and opposing PP1 phosphatase will be of great use in achieving a more detailed understanding of cell cycle processes.

APPENDIX I:

LIST OF PROTEINS IDENTIFIED BY MASS SPECTROMETRY

I.1 Chromatin-binding proteins found in Interphase

Accession numbers	kD	Gene description
gi|111307761|gb|AAI21193.1	224.14	trans-sialidase, putative
gi|49115532|gb|AAH73439.1	191.43	Clathrin heavy chain
gi|47939759|gb|AAH72193.1	178.62	Topoisomerase II
gi|89514893|gb|AAV35204.2	162.57	fanconia anemia complementation group D2
gi|38173761|gb|AAH60753.1	138.84	Collagen alpha 1(III) chain precursor isoform
gi|47122916|gb|AAH70581.1	131.69	Transcription termination factor 2 (RNA polymerase II termination factor)
gi|49899007|gb|AAH76715.1	122.08	ISWI
gi|50418010|gb|AAH77918.1	104.17	Actinin, alpha 4
gi|108935850|sp|P55861	100.26	MCM2
gi|1621291|gb|AAC60033.1	99.97	ORC1
gi|1002598|gb|AAB01680.1	97.18	Cdc21/MCM4
gi|109940097|sp|P30664	97.12	MCM4-B
gi|82231283|sp|Q5FWY4	92.64	MCM6
gi|109940096|sp|P49739	90.41	MCM-3
gi|868012|dbj|BAA07268.1	90.2	DNA replication licensing; Budding yeast MCM3 and mammalian P1 protein homolog
gi|1469526|gb|AAB17253.1	81.88	MCM-7
gi|82241532|sp|Q7ZXB1	81.73	MCM-7B
gi|27735471|gb|AAH41312.1	81.03	ORC3-like
gi|1753195|dbj|BAA09949.1	80.38	CDC46 MCM
gi|54261462|gb|AAH84208.1	79.83	epithelial protein lost in neoplasm beta isoform 5; LIM domain and actin binding 1
gi|136655|sp|P25979	79.17	upstream binding factor
gi|2749954|gb|AAC60340.1	74.24	DNA-PK
gi|27371247|gb|AAH41201.1	71.19	Heat shock 70 kD protein 8
gi|22653657|sp|Q8UVR5	70.21	ACF bromodomain
gi|68533794|gb|AAH99057.1	69.06	T-SNARE domain containing 1
gi|32766481|gb|AAH54976.1	68.51	ubiquitin
gi|49119345|gb|AAH73454.1	63.77	cortactin Src substrate
gi|2947303|gb|AAC05382.1	62.88	thymopoietin, lamina-associated

I.1 Chromatin-binding proteins found in Interphase, continued

Accession numbers	kD	Gene description
gi|80477560|gb|AAI08503.1	61.68	similar to Ariadne-1 protein homolog (ARI-1) (Ubiquitin-conjugating enzyme E2-binding protein 1) (UbcH7-binding protein)
gi|28278602|gb|AAH44116.1	56.06	keratin
gi|125112|sp|P08776	55.68	keratin
gi|125106|sp|P16878	55.45	keratin
gi|66910686|gb|AAH97521.1	51.96	origin recognition complex, subunit 5-like
gi|47122943|gb|AAH70609.1	50.2	tubulin alpha
gi|401166|sp|P30883	49.82	tubulin beta
gi|68533761|gb|AAH99014.1	48.09	DNA repair protein RAD52 homolog
gi|47939824|gb|AAH72305.1	47.47	keratin
gi|29126978|gb|AAH47983.1	47.29	ARP3 actin-related protein 3 homolog
gi|47682287|gb|AAH70682.1	45.35	keratin
gi|27696928|gb|AAH43992.1	44.66	ARP2 actin-related protein 2-like
gi|27924422|gb|AAH45004.1	42.75	ubiquitin
gi|1703123|sp|P53505	41.85	actin
gi|80477601|gb|AAI08544.1	41.8	actin
gi|41016788|sp|O93400	41.77	actin
gi|27371277|gb|AAH41267.1	41.57	actin related protein 2/3 complex, subunit 1A
gi|27924181|gb|AAH44969.1	35.3	zinc-finger protein NOA 36
gi|47506888|gb|AAH70989.1	34.34	actin related protein 2/3 complex, subunit 2, 34kDa
gi|49117926|gb|AAH72853.1	32.9	F-actin capping protein alpha-2 subunit (CapZ alpha-2)
gi|27370869|gb|AAH41233.1	30.65	actin capping protein beta subunit, isoform 2; capZ
gi|54035281|gb|AAH84065.1	30.41	linker histone B4
gi|77748204|gb|AAI06701.1	29.66	ribosomal protein s4 x linked
gi|115594|sp|P25229	29.43	Actin-binding protein chain A
gi|114795|sp|P15308	29.31	B4
gi|45360795|ref|NP_989071.1	28.04	proteasome subunit
gi|47937622|gb|AAH72203.1	27.65	Novel glutathione S-transferase theta protein
gi|54261501|gb|AAH84423.1	27.34	proteasome (prosome macropain) subunit alpha type 6
gi|66910988|gb|AAH97923.1	27.19	similar to Developmental pluripotency associated 2 (Vespera)

I.1 Chromatin-binding proteins found in Interphase, continued

Accession numbers	kD	Gene description
gi|232034|sp|P30151	25.18	EF-1-beta
gi|32450305|gb|AAH54309.1	25.07	peroxiredoxin 6 isoform 2
gi|51338726|sp|P52301	24.4	Ran
gi|27735390|gb|AAH41293.1	24.34	GTP-binding nuclear protein Ran (GTPase Ran) (Ras-like protein TC4)
gi|28436776|gb|AAH46569.1	24.06	ribosomal protein L15
gi|33416674|gb|AAH56034.1	20.6	ARP2/3 complex 21 kD subunit (p21-ARC)
gi|33416674|gb|AAH56034.1	20.6	Arpc3
gi|44968390|gb|AAS49590.1	20.34	ribosomal protein L13
gi|52345592|ref|NP_001004844.1	19.69	actin related protein 2/3 complex, subunit 4
gi|2118960|pir||I51568	18.8	ubiquitin
gi|27807503|ref|NP_777203.1	17.96	ubiquitin
gi|50414831|gb|AAH77328.1	17.14	Arpc5
gi|34785262|gb|AAH56660.1	14.86	Histone H2A.x or H2A
gi|4507761|ref|NP_003324.1	14.73	ubiquitin
gi|52346108|ref|NP_001005097.1	13.49	Histone H2A.Z-like
gi|52345610|ref|NP_001004853.1	10.71	SUMO
gi|51701919|sp|P63049	8.56	ubiquitin

I.2 Chromatin-binding proteins found in Metaphase

Accession numbers	kD	Gene description
gi|49115532|gb|AAH73439.1	191.43	clathrin, heavy polypeptide
gi|47939759|gb|AAH72193.1	178.62	topoisomerase II
gi|28881882|dbj|BAC65235.1	169.17	topoisomerase II binding protein topBP1
gi|89514893|gb|AAV35204.2	162.57	Fanconi anemia complementation group D2
gi|49118127|gb|AAH73087.1	161.13	werner helicase
gi|30172983|sp|Q9YHY6	154.19	condensin XCAP-D2
gi|1722855|sp|P50532	146.99	SMC-4
gi|1722856|sp|P50533	136.34	SMC-2
gi|37748213|gb|AAH59308.1	130.09	pyruvate carboxylase isoform 2
gi|28277299|gb|AAH44276.1	129.51	topoisomerase II
gi|49899007|gb|AAH76715.1	122.08	ISWI
gi|11874759|dbj|BAB19357.1	117.97	ubiquitin-activating enzyme E1
gi|71681279|gb|AAI00246.1	106.53	SWI/SNF-related matrix-associated actin-dependent regulator of chromatin a-like 1 (HARP)
gi|2231169|gb|AAC60223.1	100.26	MCM-2
gi|1621291|gb|AAC60033.1	99.97	ORC-1
gi|52430485|gb|AAH82952.1	97.89	glycogen phosphorylase
gi|109940097|sp|P30664	97.12	mcm4
gi|48734665|gb|AAH72348.1	94.49	Loss of heterozygosity 11 chromosomal region 2 gene A protein homolog (Mast cell surface antigen 1) (Masa-1)
gi|82231283|sp|Q5FWY4	92.64	mcm6
gi|868012|dbj|BAA07268.1	90.2	mcm3
gi|54038573|gb|AAH84223.1	84.24	DNA repair protein RAD50
gi|50603918|gb|AAH77195.1	82.96	hsp90
gi|6016534|sp|P55862	82.44	mcm5
gi|27503844|gb|AAH42232.1	82.03	Nucleolar transcription factor 1-B (Upstream-binding factor 1-B)
gi|65265|emb|CAA42523.1	82.01	upstream binding factor
gi|1469526|gb|AAB17253.1	81.88	MCM7
gi|136655|sp|P25979	79.17	nucleolar transcription factor 1A
gi|14330668|emb|CAC41092.1	74.97	HIRA
gi|49118978|gb|AAH73609.1	74.53	SRP
gi|50417653|gb|AAH77757.1	72.67	Heat shock 70 kD protein 5

I.2 Chromatin-binding proteins found in Metaphase, continued

Accession numbers	kD	Gene description
gi|27371247|gb|AAH41201.1	71.19	hsp70
gi|28374367|gb|AAH46262.1	70.79	Hsc70 protein
gi|22653657|sp|Q8UVR5	70.21	ACF
gi|4630797|dbj|BAA76953.1	69.28	ku70
gi|68533794|gb|AAH99057.1	69.06	T-SNARE domain containing 1
gi|32766481|gb|AAH54976.1	68.51	ubiquitin
gi|49118613|gb|AAH73637.1	68.33	novel protein similar to guanylate binding protein 4
gi|8515825|gb|AAF76194.1	67.45	transketolase
gi|400975|sp|Q01588	67.09	RPA p70
gi|47122884|gb|AAH70559.1	66.9	RPA
gi|12230782|sp|Q9W7F2	66.09	WD repeat actin interacting
gi|48734658|gb|AAH72321.1	64.33	5-aminoimidazole-4-carboxamide ribonucleotide formyltransferase/IMP cyclohydrolase
gi|54038187|gb|AAH84353.1	62.83	ORC2
gi|49115344|gb|AAH73315.1	62.11	glucose phosphate isomerase
gi|13111394|dbj|BAB32829.1	59.94	keratin
gi|27924333|gb|AAH44997.1	59.59	Chaperonin containing TCP1, subunit 5
gi|2497536|sp|Q92122	57.53	pyruvate kinase
gi|28278602|gb|AAH44116.1	56.06	keratin
gi|125106|sp|P16878	55.45	keratin
gi|51895961|gb|AAH81233.1	53.7	Dihydrolipoyllysine-residue Dihydrolipoamide branched chain transacylase (BCKAD E2)
gi|66910686|gb|AAH97521.1	51.96	origin recognition complex, subunit 5-like
gi|119140|sp|P17508	50.2	elongation factor 1
gi|54648594|gb|AAH84938.1	50.07	tubulin, alpha 2
gi|401166|sp|P30883	49.82	tubulin
gi|68533761|gb|AAH99014.1	48.09	similar to DNA repair protein RAD52 homolog
gi|32766495|gb|AAH54993.1	48	keratin
gi|33585662|gb|AAH56110.1	47.62	glutamic-oxaloacetic transaminase 2, mitochondrial (aspartate aminotransferase 2); Got2
gi|27371000|gb|AAH41279.1	47.46	Alpha-enolase (2-phosphoglycerate dehydratase)

I.2 Chromatin-binding proteins found in Metaphase, continued

Accession numbers	kD	Gene description
gi|27924422|gb|AAH45004.1	42.75	ubiquitin
gi|27924422|gb|AAH45004.1	42.75	ubiquitin
gi|47124885|gb|AAH70578.1	42.73	hyaluronan binding protein 4
gi|54038179|gb|AAH84215.1	41.97	dual specificity phosphatase 6
gi|1703123|sp|P53505	41.85	actin
gi|41016788|sp|O93400	41.77	actin
gi|50414850|gb|AAH77339.1	41.74	aurora B
gi|76780024|gb|AAI06623.1	39.41	aldolase
gi|1944025|dbj|BAA19524.1	39.39	aldolase
gi|3928511|dbj|BAA34671.1	39.27	aldolase
gi|125504|sp|P12965	39.16	Serine/threonine-protein kinase mos (pp39-mos)
gi|82186776|sp|Q6PAB3	36.43	malate dehydrogenase
gi|50415703|gb|AAH77642.1	36.23	annexin A5
gi|50882324|gb|AAT85637.1	35.79	malate dehydrogenase
gi|1016758|gb|AAA91456.1	35.5	transcription factor A; HMG box mitochondrial transcription factor
gi|6680047|ref|NP_032169.1	35.08	guanine nucleotide binding protein (G protein), beta polypeptide 2 like 1
gi|132983|sp|P15125	34.11	60S ribosomal protein L5-A
gi|51593227|gb|AAH78560.1	31.7	esterase D/formylglutathione hydrolase isoform 3
gi|54035281|gb|AAH84065.1	30.41	B4
gi|33417132|gb|AAH56066.1	30.27	ribosomal protein S2
gi|82210070|sp|Q801S3	29.94	40S ribosomal protein S3a
gi|49255981|gb|AAH72834.1	29.87	60S ribosomal protein L7a
gi|49255981|gb|AAH72834.1	29.87	similar to 60S ribosomal protein L7a
gi|77748204|gb|AAI06701.1	29.66	ribosomal protein s4 x linked
gi|90120317|sp|P49401	29.65	40S ribosomal protein S4
gi|48734630|gb|AAH72101.1	29.45	RPA
gi|9789803|sp|Q9YGP6	28.9	histone RNA stem-loop-binding protein2
gi|7248365|dbj|BAA92700.1	28.81	PCNA
gi|47937622|gb|AAH72203.1	27.65	Glutathione S-transferase theta 1
gi|66910988|gb|AAH97923.1	27.19	developmental pluripotency associated 2, isoform CRA_b (Vespera)
gi|28461382|gb|AAH46864.1	26.76	triosephosphate isomerase 1
gi|32484222|gb|AAH54171.1	25.39	glutathione S-transferase M1

I.2 Chromatin-binding proteins found in Metaphase, continued

Accession numbers	kD	Gene description
gi|51338726|sp|P52301	24.4	Ran
gi|33417168|gb|AAH56115.1	24.27	unknown protein, might have homology to similar to Tumor necrosis factor receptor
gi|32450087|gb|AAH53774.1	22.74	glutathione s-transferase
gi|27735416|gb|AAH41242.1	22.58	Ribosomal protein S9
gi|48734656|gb|AAH72318.1	22.44	peroxiredoxin 2
gi|134026|sp|P02362	22.18	ribosomal S7
gi|62185728|gb|AAH92331.1	21.69	Sorcin
gi|50604065|gb|AAH77192.1	21.4	60S ribosomal protein L17
gi|27882415|gb|AAH44685.1	20.92	Ferritin heavy chain, oocyte isoform (A-ferritin)
gi|27769162|gb|AAH42256.1	20.78	ribosomal protein L18a
gi|51873961|gb|AAH78513.1	20.18	ribosomal protein L11
gi|929913|emb|CAA24703.1	19.46	ribosomal protein S8
gi|1168995|sp|P45593	19.12	cofilin
gi|585934|sp|Q07254	18.88	40S ribosomal protein S10
gi|2118960|pir|	18.8	ubiquitin
gi|49255998|gb|AAH73305.1	18.66	Ribosomal protein L21
gi|49255998|gb|AAH73305.1	18.66	60S ribosomal protein L23a
gi|730626|sp|P41115	18.42	ribosomal
gi|27807503|ref|NP_777203.1	17.96	ubiquitin
gi|52346118|ref|NP_001005104.1	17.19	ribosomal
gi|4507761|ref|NP_003324.1	14.73	ubiquitin
gi|16974922|pdb|1K5J	13.74	nucleoplasmin
gi|49256565|gb|AAH72995.1	10.87	smt3
gi|51701919|sp|P63049	8.56	ubiquitin

I.3 Background proteins that bind to streptavidin-beads

Accession numbers	kD	Gene description
gi|111307761|gb|AAI21193.1	224.14	trans-sialidase
gi|28422180|gb|AAH46866.1|	214.69	chromodomain helicase DNA binding protein 4
gi|12057014|emb|CAC19793.1|	190.13	53BP1 protein
gi|47939759|gb|AAH72193.1	178.62	topoisomerase (DNA) II alpha
gi|29387027|gb|AAH48220.1	170.24	plectin 1
gi|50927228|gb|AAH79780.1	164.81	Microtubule-associated serine/threonine-protein kinase 3
gi|54648598|gb|AAH84946.1|	160.3	polybromo 1
gi|1722855|sp|P50532|SMC4_XENLA	146.99	Structural maintenance of chromosome 4 (Chromosome-associated protein C) (Chromosome assembly protein XCAP-C)
gi|49522205|gb|AAH74479.1	145.8	flightless I homolog
gi|49115497|gb|AAH73405.1	141.58	Apoptotic protease activating factor 1 (Apaf-1)
gi|49115413|gb|AAH73356.1	137.94	DNA mismatch repair protein Mlh3 (MutL protein homolog 3)
gi|55250671|gb|AAH86289.1	136.88	androgen-induced prostate proliferative shutoff associated
gi|37748213|gb|AAH59308.1	130.09	Pyruvate carboxylase
gi|37748213|gb|AAH59308.1	130.09	Pyruvate carboxylase, mitochondrial precursor
gi|39645073|gb|AAH63719.1	124.66	Nuclear receptor-interacting protein 1 (Nuclear factor RIP140)
gi|71052228|gb|AAH98986.1	122.56	ubiquitination factor E4A
gi|50415131|gb|AAH77364.1	120.68	vacuolar protein sorting 13A isoform A
gi|49118072|gb|AAH73023.1	119.13	Bub1b protein
gi|29165659|gb|AAH49176.1	115.4	Atp12a-prov
gi|82243533|sp|Q8JI28|TLL1_XENLA	114.37	Tolloid-like protein 1 precursor (*Xenopus* tolloid-like protein 1) (Metalloprotease xolloid-like) (Xlr)
gi|51895934|gb|AAH81001.1	111.5	cis-Golgi matrix protein GM130
gi|46250354|gb|AAH68936.1	109.64	Ext2-prov protein
gi|54648511|gb|AAH85055.1	109.59	alanyl (membrane) aminopeptidase
gi|47506906|gb|AAH70993.1	104.47	DNA ligase III isoform alpha
gi|47124802|gb|AAH70795.1	103.08	M-phase phosphoprotein 1
gi|47124776|gb|AAH70757.1	101.9	exosome component 10
gi|28422362|gb|AAH46949.1	101.05	transportin 2
gi|80476351|gb|AAI08521.1	99.69	Mycbp associated protein
gi|46249663|gb|AAH68957.1	99.31	similar to proteasome 26S non-ATPase subunit 2
gi|38014398|gb|AAH60445.1	97.89	glycogen phosphorylase

I.3 Background proteins that bind to streptavidin-beads, continued

Accession numbers	kD	Gene description
gi|60688087|gb|AAH91631.1	96.29	3-hydroxy-3-methylglutaryl-coenzyme A reductase (HMG-CoA reductase)
gi|50927226|gb|AAH79778.1	95.51	Ubiquitin specific peptidase 5 (isopeptidase T)
gi|27882475|gb|AAH44327.1	95.43	Eef2-prov protein
gi|28422362|gb|AAH46949.1	89.21	Vcp-prov
gi|28422362|gb|AAH46949.1	89.21	Vcp-prov
gi|50414847|gb|AAH77338.1	85.48	eukaryotic translation initiation factor 4E nuclear import factor 1
gi|82235865|sp|Q6DFJ6|TBK1	83.27	Serine/threonine-protein kinase TBK1
gi|50603918|gb|AAH77195.1	82.96	Hsp90beta protein
gi|27881752|gb|AAH44703.1|	82.08	Complement factor I
gi|228024|prf||1715211A	82	ribosomal transcription factor xUBF2
gi|52430485|gb|AAH82952.1	81.73	DNA replication licensing factor mcm7-B
gi|56270045|gb|AAH87496.1	80.56	Leucine-rich repeat and fibronectin type-III domain-containing protein 2
gi|54035194|gb|AAH84059.1	80.5	gelsolin
gi|49116037|gb|AAH73703.1|	79.33	discoidin, CUB and LCCL domain containing 1
gi|59862015|gb|AAH90253.1	78.45	Propionyl-Coenzyme A carboxylase
gi|50414914|gb|AAH77828.1	77.18	dsRNA-binding protein 4F.1
gi|54647570|gb|AAH84933.1	76.3	Leucine zipper, putative tumor suppressor 2
gi|5421757|dbj|BAA82338.1	75.21	Tbx2
gi|28302215|gb|AAH46732.1|	74.99	Stau2-a
gi|66912037|gb|AAH97633.1	74.05	Arginyl-tRNA synthetase, cytoplasmic
gi|57921040|gb|AAH89141.1	72.64	centrosomal protein 70 kD
gi|46250301|gb|AAH68696.1|	72.29	Hsl7 protein
gi|27371247|gb|AAH41201.1	71.19	Heat shock 70 kD
gi|27371247|gb|AAH41201.1	71.19	Hsc70 protein
gi|213926|gb|AAA02822.1	71.01	LReO_3
gi|28374367|gb|AAH46262.1	70.79	Hsc70 protein
gi|28374367|gb|AAH46262.1	70.79	Hsc70 protein
gi|13540314|gb|AAK29408.1|AF338225_1	70.72	embryonic poly(A) binding protein

I.3 Background proteins that bind to streptavidin-beads, continued

Accession numbers	kD	Gene description
gi|54038353|gb|AAH84637.1	70.46	similar to breast cancer anti-estrogen resistance 1
gi|115528349|gb|AAI24971.1	70.37	unknown
gi|47718038|gb|AAH70981.1	69.31	FUSE binding protein-like protein
gi|50604152|gb|AAH77445.1	69.27	Ku70
gi|47940320|gb|AAH72359.1	68.53	novel protein
gi|32766481|gb|AAH54976.1	68.51	Ubc-prov
gi|49118613|gb|AAH73637.1	68.33	guanylate binding protein 4
gi|63100234|gb|AAH95915.1	64.99	extracellular signal-regulated kinase 7
gi|49115557|gb|AAH73457.1	64.96	Fragile X mental retardation syndrome-related protein 1
gi|50414890|gb|AAH77811.1	64.81	Nars-prov
gi|48734658|gb|AAH72321.1	64.33	5-aminoimidazole-4-carboxamide ribonucleotide formyltransferase/IMP cyclohydrolase
gi|110278982|sp|Q2KHP9|FMR1B	63.86	Fragile X mental retardation protein 1 homolog-B
gi|49114811|gb|AAH72755.1	62.02	mannosyl (alpha-1,3-)-glycoprotein beta-1,4-N-acetylglucosaminyltransferase, isoenzyme A isoform 2
gi|54035212|gb|AAH84097.1	61.48	YTH domain family, member 1
gi|51258451|gb|AAH80087.1	60.97	Synaptotagmin-14 (Synaptotagmin XIV) (SytXIV)
gi|115528345|gb|AAI24968.1	60.83	unknown
gi|27696390|gb|AAH43885.1	60.36	Tn3 protein
gi|52139070|gb|AAH82625.1	60.35	tyrosine phosphatase Cdc25A
gi|50418025|gb|AAH77347.1	60.31	golgin 97
gi|37748655|gb|AAH59999.1	60.14	disabled homolog 2
gi|13111394|dbj|BAB32829.1	59.94	larval keratin XLK
gi|83318223|gb|AAI08628.1	59.68	Transcription intermediary factor 1-gamma (TIF1-gamma) (Tripartite motif-containing protein 33)
gi|49115856|gb|AAH73593.1	57.47	proteasome 26S non-ATPase subunit 3
gi|50925193|gb|AAH79694.1	57.32	hydroxymethylglutaryl-CoA synthase
gi|27694844|gb|AAH44037.1	57.24	DnaJ (Hsp40) homolog, subfamily C, member 3
gi|51703900|gb|AAH81073.1	56.94	M-phase phosphoprotein 1
gi|28278602|gb|AAH44116.1	56.06	Krt8-prov

I.3 Background proteins that bind to streptavidin-beads, continued

Accession numbers	kD	Gene description
gi|125112|sp|P08776|K2C8	55.68	Keratin, type II cytoskeletal 8
gi|125106|sp|P16878|K2C5	55.45	Keratin, type II cytoskeletal
gi|58402678|gb|AAH89255.1	55.11	Protein C6orf182
gi|55953148|dbj|BAD72829.1|	54.76	transcription factor Glial cells missing-2
gi|1709533|sp|P54824|DDX6	54.09	Probable ATP-dependent RNA helicase DDX6
gi|50415415|gb|AAH78086.1	54	annexin VII
gi|50415415|gb|AAH78086.1	54	annexin VII
gi|50415295|gb|AAH77476.1	53.27	Ina-A-prov
gi|50415295|gb|AAH77476.1	53.27	Ina-A-prov protein
gi|115528666|gb|AAI24898.1	53.21	unknown
gi|26106079|dbj|BAC41520.1	51.9	adult keratin XAK-C
gi|47124798|gb|AAH70789.1	51.75	similar to R3H domain (binds single-stranded nucleic acids) isoform 2
gi|76780035|gb|AAI06644.1	50.49	FGFR1 oncogene partner
gi|67678009|gb|AAH97795.1	50.27	Nucleoporin-like 2
gi|62471477|gb|AAH93575.1	50.05	galactosidase, beta 1-like
gi|27735425|gb|AAH41186.1	49.85	proteasome (prosome, macropain) 26S subunit, ATPase 2
gi|50417476|gb|AAH77344.1	49.47	adaptor-related protein complex 4, mu 1 subunit
gi|32484378|gb|AAH54287.1	49.15	proteasome (prosome, macropain) 26S subunit, ATPase, 1
gi|3024672|sp|Q91604|STK11_XENLA	49.07	Serine/threonine-protein kinase 11
gi|33585662|gb|AAH56110.1	47.62	Got2-prov protein
gi|37994750|gb|AAH60362.1	47.39	Psmc4
gi|785052|emb|CAA60136.1|	47.25	POU-60
gi|27371295|gb|AAH41276.1	47.17	phosphoribosylaminoimidazole carboxylase
gi|49255977|gb|AAH72829.1	46.52	proteasomal ATPase (SUG1)
gi|66912074|gb|AAH97800.1	46.19	Stromal membrane-associated protein 1-like
gi|52139072|gb|AAH82626.1	45.77	Solute carrier family 30 (zinc transporter), member 4

I.3 Background proteins that bind to streptavidin-beads, continued

Accession numbers	kD	Gene description
gi|58702032|gb|AAH90247.1	45.75	CG12822-PA
gi|54038456|gb|AAH84351.1	45.56	proteasome (prosome, macropain) 26S subunit, non-ATPase, 6
gi|22000680|gb|AAM88215.1|AF468029_1	45.29	IAP-like protein
gi|27696928|gb|AAH43992.1	44.66	Similar to ARP2 actin-related protein 2 homolog
gi|49258183|gb|AAH73644.1|	44.58	Psmc6 protein
gi|50416416|gb|AAH77781.1|	44.58	Pgk2-prov
gi|46249540|gb|AAH68755.1	44.13	mitochondrial acetoacetyl-CoA thiolase
gi|50414512|gb|AAH77742.1	43.99	nexin-1
gi|6138954|gb|AAF04406.1|AF057166_1	43.52	gag-like protein
gi|56269237|gb|AAH87502.1	43.39	galactose-1-phosphate uridylyltransferase
gi|76780144|gb|AAI06431.1	42.98	keratin 18
gi|51261513|gb|AAH80105.1	42.98	TIA1 cytotoxic granule-associated RNA binding protein
gi|27924422|gb|AAH45004.1	42.75	UBC protein
gi|27924422|gb|AAH45004.1	42.75	UBC
gi|27924422|gb|AAH45004.1	42.75	ubiquitin C
gi|4902905|emb|CAB43617.1	42.05	Actin
gi|32450257|gb|AAH54262.1	41.88	Actin, alpha sarcomeric/skeletal
gi|71679779|gb|AAI00175.1	41.87	FAM61B
gi|1703127|sp|P53506|ACT8	41.85	Actin, cytoplasmic type 8
gi|76779973|gb|AAI06448.1	41.69	family 53, member C protein
gi|76779973|gb|AAI06448.1	41.69	similar to family 53, member C protein
gi|12003372|gb|AAG43543.1|AF212298_1	40.93	septin A
gi|1944025|dbj|BAA19524.1	39.39	aldolase
gi|47124806|gb|AAH70798.1	39.32	similar to cyclin fold protein 1
gi|50418209|gb|AAH77241.1	38.6	Protein KIAA0174
gi|56270048|gb|AAH87497.1	38.58	Cyclin N-terminal domain containing 1

I.3 Background proteins that bind to streptavidin-beads, continued

Accession numbers	kD	Gene description
gi|56270048|gb|AAH87497.1	38.58	similar to Serine/threonine-protein kinase WNK4 (Protein kinase with no lysine 4) (Protein kinase, lysine-deficient 4) (Liver regeneration-related protein LRRG120)
gi|52139097|gb|AAH82713.1	37.93	cdc25 protein
gi|115292033|gb|AAI22496.1	37.77	unknown
gi|27371273|gb|AAH41257.1	37.52	Ags3-prov protein
gi|27371273|gb|AAH41257.1	37.52	Ags3-prov protein
gi|214157|gb|AAA49716.1	37.23	Y-box-binding protein 2-B
gi|51703920|gb|AAH81139.1	36.61	Psmd7 protein
gi|57032700|gb|AAH88936.1	36.54	fubp1
gi|82186776|sp|Q6PAB3|MDHC	36.43	Malate dehydrogenase, cytoplasmic
gi|2498255|sp|Q91653|CRHBP	36.29	Corticotropin-releasing factor-binding protein precursor
gi|55250533|gb|AAH86269.1	36.01	ELAV (embryonic lethal, abnormal vision, Drosophila)-like 1 (Hu antigen R)
gi|50882324|gb|AAT85637.1	35.79	mitochondrial malate dehydrogenase 2a
gi|49255952|gb|AAH71073.1|	35.71	mitochondrial malate dehydrogenase 2b
gi|50925082|gb|AAH79812.1	35.33	Solute carrier family 25 member 44
gi|38540890|gb|AAH61930.1|	34.86	ubiquitin fusion degradation 1-like
gi|27924246|gb|AAH45094.1	34.57	Psmd14-prov protein
gi|71682415|gb|AAI00234.1	33.46	fused toes homolog
gi|3334381|sp|Q91836|TRBP_XENLA	32.85	Double-stranded RNA-binding protein A (XlRBPA)
gi|3334381|sp|Q91836|TRBP_XENLA	32.85	Double-stranded RNA-binding protein A
gi|76779636|gb|AAI06582.1	32.36	Valacyclovir hydrolase precursor (VACVase) (Biphenyl hydrolase-like protein) (Biphenyl hydrolase-related protein) (Bph-rp)
gi|47940223|gb|AAH72042.1	32.1	DnaJ (Hsp40) homolog,
gi|50603800|gb|AAH77738.1	31.56	Pura-prov protein

I.3 Background proteins that bind to streptavidin-beads, continued

Accession numbers	kD	Gene description
gi|46329485|gb|AAH68763.1	30.98	Proteasome (prosome, macropain) 26S subunit, non-ATPase, 8
gi|32450017|gb|AAH54141.1	30.48	Drng-A-prov
gi|82210070|sp|Q801S3|RS3A_XENLA	29.94	40S ribosomal protein S3a
gi|34849610|gb|AAH58201.1	28.44	Psma3-prov protein
gi|27884299|dbj|BAC55886.1	28.33	galectin family galectin-VIIa
gi|45360795|ref|NP_989071.1	28.04	proteasome (prosome, macropain) subunit, alpha type 7
gi|12229929|sp|Q9PVQ1|PSA7B_XENLA	27.94	Proteasome subunit alpha type 7-B (Proteasome subunit alpha 4-B)
gi|49257961|gb|AAH71115.1	27.48	Myeloid leukemia factor 2
gi|50603942|gb|AAH77442.1	27.46	Psma6-prov protein
gi|54038683|gb|AAH84334.1	27.11	DnaJ homolog subfamily B member 6
gi|27697097|gb|AAH43976.1	26.43	Rpl13a-prov protein
gi|54035222|gb|AAH84116.1	26.17	ubiquitin carboxyl-terminal esterase
gi|62858493|ref|NP_001016382.1	25.83	Psma2 protein
gi|28422711|gb|AAH46936.1	25.49	Dnajb9-prov protein
gi|77748321|gb|AAI06643.1	24.86	Ubiquitin carboxyl-terminal esterase L1 (ubiquitin thiolesterase)
gi|57921028|gb|AAH89136.1	24.61	eIF-4E protein
gi|49256355|gb|AAH74452.1	24.36	tissue inhibitor of mettaloproteinase 2
gi|73535301|pdb|1U20|A	24.35	Nudix Hydrolase Nuclear Snorna Decapping Protein X29
gi|49114954|gb|AAH72812.1	24.03	Seb4-A-prov
gi|56270462|gb|AAH87395.1	23.04	proteasome (prosome, macropain) subunit, beta type 3
gi|32450087|gb|AAH53774.1|	22.74	XlGSTS1-1 protein
gi|49119183|gb|AAH72908.1	22.61	proteasome (prosome macropain) subunit beta type 2
gi|52138931|gb|AAH82679.1	22.55	within bgcn homolog
gi|48734656|gb|AAH72318.1|	22.44	peroxiredoxin 2
gi|134026|sp|P02362|RS7_XENLA	22.18	40S ribosomal protein S7 (S8)
gi|13124486|sp|Q9YGP5|RBPMS_XENLA	21.68	RNA-binding protein with multiple splicing homolog (RBP-MS) (Heart, RRM Expressed Sequence) (Hermes)

I.3 Background proteins that bind to streptavidin-beads, continued

Accession numbers	kD	Gene description
gi|49256167|gb|AAH73601.1	19.92	40S ribosomal protein S10
gi|32450483|gb|AAH53796.1	18.86	signal sequence receptor delta
gi|2118960|pir||I51568	18.8	polyubiquitin
gi|27807503|ref|NP_777203.1	17.96	ribosomal protein S27a
gi|51873786|gb|AAH78526.1	17.67	similar to 60S ribosomal protein L23a
gi|6225751|sp|P70010|NDKA1_XENLA	17.49	Nucleoside diphosphate kinase A1 (NDK A1) (NDP kinase A1) (NM23/nucleoside diphosphate kinase A1)
gi|82180497|sp|Q5XHI2|K1143	17.14	KIAA1143
gi|54647585|gb|AAH84940.1|	14.76	myeloid leukemia factor 2
gi|4507761|ref|NP_003324.1	14.73	ubiquitin and ribosomal protein L40 precursor
gi|51701919|sp|P63049|UBIQ_CANFA	8.56	Ubiquitin
gi|998831|gb|AAB34537.1	2.9	Tyrosine kinase catalytic domain, clone Xltk27

MATERIAL AND METHODS

Antibodies

Vespera antibodies were raised in rabbits against full-length recombinant Vespera protein. PP1α antibodies were raised against the C-terminal peptide CPTVTPPRGMITKQAKK (a gift of J. Rosenberg). Antibodies were affinity-purified after coupling of the protein antigen to SulfoLink Coupling Gel (Pierce) according to the manufacturer's instructions. Bound antibodies were eluted with 100mM glycine (pH 2.3) into neutralizing Tris base, and peak fractions were pooled and dialyzed serially against PBS/50% glycerol, PBS, and PBS/50% glycerol. Affinity-purified antibodies were stored at -20°C.

X. *laevis* Egg Extracts and Chromatin Bead Purification

Meiotic metaphase II-arrested (CSF) *Xenopus laevis* egg extracts were prepared as previously described (Murray, 1991). DNA-beads without DNA ends were prepared from pBluescript SK+ plasmid as previously described (Postow et al., 2008). Briefly, the plasmid was digested with BamHI, and the overhangs were filled in with biotinylated nucleotides using Klenow reaction (New England Biolabs, Inc.). The biotinylated DNA was then coupled to streptavidin M280 Dynabeads (Invitrogen). Metaphase

spindles were assembled in egg extracts around DNA-beads, as described (Heald et al., 1996). The metaphase chromatin beads were then collected on a magnet in the presence of 10 μg/ml nocodazole, washed five times with 30SDB2+150 mM NaCl (10 mM Hepes, 150 mM NaCl, 10 mM β-glycerophosphate, 50 mM NaF, 20 mM EGTA, 2 mM EDTA, 0.5 mM spermin, 30% sucrose, and 0.05% Triton X-100), transferred to a new Eppendorf tube, and proteins were eluted with SDS-PAGE sample buffer . Interphase chromatin beads were produced by incubation of DNA-beads in CSF extracts plus 0.3 mM calcium and 100 μg/ml cycloheximide for 80 min at 22°C. To purify these beads, nuclear membranes we re first disrupted by addition of 2.5 volumes of ice-cold DB2+Triton (10 mM Hepes, 10 mM β-glycerophosphate, 50 mM NaF, 20 mM EGTA, 2 mM EDTA, 0.5 mM spermin, 0.1% Triton X-100) to the extracts containing beads, and incubation for 10 min on ice. This mixture was layered on top of 400 μL of 60SDB2+Triton (10 mM Hepes, 10 mM β-glycerophosphate, 50 mM NaF, 20 mM EGTA, 2 mM EDTA, 0.5 mM spermin, 60% sucrose , 0.1% Triton X-100) and spun at 4000g for 10 min at 4°C in a centrifuge with a swinging bucket rotor. The sucrose interface was washed twice with DB2+Triton. The supernatant was removed, and the beads were collected on a magnet. The

beads were then washed five times with DB2+Triton, placed in a fresh Eppendorf tube, and proteins were eluted with SDS-PAGE sample buffer.

Identification of Vespera SUMOylation

To identify the modification of Vespera, 35S-labeled Vespera was translated *in vitro* using a cDNA clone in pBluescript SK- (Open Biosystems) and a coupled transcription-translation system in rabbit reticulocyte lysate (T7 promoter, Promega). For each sample, 2 μL of labeled protein reaction was added to 50 μL of CSF extract containing cycloheximide and nocodazole, and incubated for 40 min at 22°C, along with 2 μL buffer (50 mM HEPES pH 8.0, 150 mM NaCl, 1 mM DTT) or 50 μg/ml 6His-SUMO-1, 6His-SUMO-2, 6His-SUMO-3 (Boston Biochem), or 6His-Ubiquitin (Postow et al., 2008). DNA-beads (equivalent to 1 μg DNA) were then added to each sample and incubated for an additional 40 min at 22°C, along with 7 μL of streptavidin-beads, to facilitate beads' recovery. The beads were collected on a magnet, washed five times with 30SDB2+150mM NaCl, transferred to a new Eppendorf tube, and proteins were eluted with SDS-PAGE sample buffer. Proteins were separated by SDS-PAGE, and the gel was dried and visualized by autoradiography using a phosphorimager (Fujifilm).

In vitro Translation and Mutational Analysis

To identify the SUMOylation site of Vespera, all thirteen of its lysine residues were individually mutated to arginine. The resulting cDNA clones were transcribed and translated *in vitro* to produce 35S-labeled proteins. Labeled proteins were added to extract, and analyzed for SUMOylation using chromatin beads, as described above. This analysis was also conducted for the following phosphorylation site mutants: S183A; S183D; S226A, S234A (double mutant); S226E, S234D (double mutant).

Protein Purification

Flag-tagged wild-type and mutant Vespera proteins were expressed as GST-fusions in BL21 bacteria from pGEX-6P-1 plasmid (GE Lifesciences). Bacteria were grown to OD 0.6, induced with 0.5 mM IPTG for 7 h at 30°C, and harvested by centrifugation. Bacterial pellets were resuspended in lysis buffer (PBS, 1 mM DTT, 150 mM NaCl, 0.1% Triton-X, protease inhibitors) and lysed by sonication. The sonicates were treated with 1 mg/ml lysozyme and 0.04 mg/ml DNase I for 15 min at room temperature. Insoluble material was pelleted by centrifugation for 20 min at 16k rpm and 4°C in SS-34 rotor (Sorvall). Clarified lysates were incubated with glutathione-sepharose 4b (GE Lifesciences) to bind GST-fusion proteins, and the resin was washed on

a column with 1 L of PBS + 1 mM DTT and protease inhibitors. GST-tagged proteins were eluted with 2 column volumes of PBS+15mM glutathione, and the GST tag was cleaved with Prescission Protease (GE Lifesciences) for 10-16 h at 4°C. Simultaneously, the protein was dialyzed into PBS + 1 mM DTT to remove glutathione. Excess GST, Prescission Protease, and nonspecific glutathione-sepharose binding proteins were then removed by an additional incubation with glutathione-sepharose.

Immunodepletions

Egg extracts were immunodepleted using antibodies bound to Protein A-Dynabeads (Invitrogen). Prior to antibody binding, beads were washed three times with TBS. Antibody was then bound to beads at a final concentration of 0.1 mg/ml (volume of beads slurry as provided by the manufacturer), with incubation for 10-30 min with rotation at room temperature. Following binding, beads were again washed three times with TBS, and stored for up to a week at 4°C. Before addition to extract, beads were washed with Sperm Dilution Buffer (5 mM K-HEPES [pH 7.7], 1mM $MgCl_2$, 100 mM KCl, 150 mM sucrose), and isolated, dry, on magnet. The volume of beads was determined prior to buffer removal. For Vespera depletion, ½ volume of beads were added to 1 volume of extract, for one

hour on ice. These beads were then collected on a magnet, and a second round of depletion was carried out, identical to the first. For control and Incenp depletions, this procedure was repeated using IgG beads and anti-Incenp beads, respectively. For Incenp and Vespera co-depletion, ½ volume each of anti-Vespera and anti-Incenp beads were added to extract in two rounds. For PIASy depletion, the first depletion was carried out for 15 min at room temperature, and the second depletion was for one hour on ice.

Immunofluorescence Microscopy

Chromatin structures produced in egg extracts were processed for immunofluorescence as described (Funabiki and Murray, 2000). 20 μL of extracts containing metaphase spindles or 10 μL of extracts containing interphase nuclei (500/μL) were fixed and spun down on glass coverslips. Affinity-purified Vespera antibodies were used at 200 ng/ml in AbDil (TBS/0.1% Triton X-100 + 2% BSA) for 1 h. Phospho-histone H3 (Ser10) antibodies (Millipore) were used at 1 μg/ml in AbDil for 1 h. Binding was visualized with Alexa 488-conjugated goat anti-rabbit antibodies (Invitrogen). DNA was counterstained with 0.25 μg/ml Hoechst in AbDil and mounted in mounting medium (90% glycerol, 20mM Tris-HCl [pH 8.8]).

Nuclear Assembly Reactions and Nuclear Import Assay

Demembranated X. *laevis* sperm nuclei were added to egg extracts on ice, then moved to 22°C. Nuclear assembly was initiated by the addition of 0.3 mM calcium chloride, either immediately after adding sperm, or after 45 min prior incubation of sperm in extract at 22°C. Nuclear import was analyzed by the addition of 50 μg/ml green fluorescent protein tagged with nuclear localization signal (GFP-NLS)

Spindle Assembly Reactions

In a typical spindle assembly reaction, 0.3 mM calcium chloride was added to 40 μL of CSF extract containing 500 sperm/μL, cycloheximide, and rhodamine tubulin. This reaction was incubated for 80 min at 22°C to permit sperm remodeling and the completion of interphase. An additional 40 μL of CSF was then added to induce metaphase, and this reaction was incubated for 30-60 min more for spindle formation. For excess Vespera experiments, recombinant protein was added to a final concentration of 4.5 μM in extract, an estimated 10-fold excess over the endogenous concentration.

Chromosome Biotinylation and Purification

Chromosomes were biotinylated and purified from control and Vespera-depleted extracts as previously described (Funabiki and Murray, 2000; Sampath et al., 2004). Briefly, biotin was incorporated from biotin-dUTP during replication in interphase. After cycling to metaphase, chromosomes were pelleted from the extract through a sucrose cushion and affinity purified using streptavidin-Dynabeads (Invitrogen). Beads were washed with 30SDB2 (10 mM Hepes, 10 mM β -glycerophosphate, 50 mM NaF, 20 mM EGTA, 2 mM EDTA, 0.5 mM spermin, 30% sucrose, and 0.05% Triton X-100) and proteins were eluted with SDS-PAGE sample buffer.

Western Blots

Immunoblots were blocked with PBS/4% nonfat dry milk for 15-30 min at RT or overnight at 4°C. Primary antibodies were diluted in AbDil at the following concentrations: 5 μg/ml anti-Vespera, 5 μg/ml anti-xIncenp, 3 μg/ml anti-Xkid, 5 μg/ml anti-PP1 μg/ml anti-phosphohistone-H3S10 (Millipore), 1:1000 anti-phosphohistone-H3T3 (Cell Signaling), 0.2 μg/ml

anti-Op18 (a gift of R. Heald), 1 μg/ml anti-PIASy antibody (a gift of Y. Azuma).

For secondary antibodies, IRDye 680 goat anti-rabbit IgG (Li-Cor) and IRDye 800CW goat anti-mouse IgG (Li-Cor) were diluted in PBS/4% nonfat dry milk + 0.1% Tween-20. The Odyssey Infrared Imaging System (Li-Cor) was used for detection.

Interphase and Metaphase Analysis of Vespera

Vespera modifications in interphase and metaphase in the absence of DNA were examined by Western blotting with anti-Vespera antibodies. After 30 min incubation at 22°C, total protein samples were collected from 20 μl CSF extract (metaphase), CSF extract with 0.3 mM calcium (interphase), or CSF extract with 0.3 mM calcium and the Cdk inhibitor purvalanol (1 μM, Sigma). Vespera modifications on DNA in interphase and metaphase were examined using 35S-labeled protein bound to chromatin beads. *In vitro* translated 35S-labeled Vespera was incubated in 50 μl CSF extract (metaphase) or CSF extract containing 0.3 mM calcium (interphase) for 40 min at 22°C. DNA-beads (1 μg DNA equivalent) were then added to the extract for another 40 min, along with 7 μl streptavidin-Dynabeads to facilitate beads' recovery. The beads were collected on a magnet and

washed, and the proteins were eluted by SDS sample buffer and analyzed by SDS-PAGE and autoradiography.

Immunoprecipitation of Vespera

Vespera was immunoprecipitated from 100 μl of CSF extract using 50 μl of crosslinked anti-Vespera beads. The beads were prepared as previously described , using dimethyl pimelimidate (DMP) crosslinker (Pierce). Beads were washed five times with 30SDB2+150 mM NaCl, transferred to a new tube, and proteins were eluted by SDS-PAGE sample buffer.

Sperm Centrosome Aster Analysis

Sperm nuclei and 0.3 mM calcium chloride were added to CSF extracts containing rhodamine-tubulin and incubated at 20°C. After 12 minutes, asters were fixed and visualized by fluorescence microscopy. Aster intensity was calculated using Metamorph software (Molecular Devices) by measuring the integrated intensity of a circle surrounding the aster and subtracting a background region in the same frame of equal dimensions.

In-gel Chemical Dephosphorylation

All peptides were produced by solid-phase peptide synthesis. Bovine casein was purchased from Sigma. Peptides or proteins were separated and immobilized in Tris-glycine gels (Invitrogen) by SDS-PAGE, followed by fixation for at least ten minutes in 20% methanol/5% acetic acid solution. Fixation was sufficient to visualize precipitated peptides within the gel without the need to use stains. Protein bands were visualized by colloidal Coomassie GelCode Blue stain (Pierce). Bands were excised from the gel and destained in 400 μL 55% 100 mM ammonium bicarbonate/45% acetonitrile. Gel slices were then dehydrated in 300 μL acetonitrile (HPLC-grade from Pierce) and dried in a Speedvac (Thermo Savant). The dry gel slices were immersed in 70 μL 70% HF-pyridine (Sigma) and incubated on ice for one hour, then washed twice with 150 μL acetic acid and twice with 150 μL water. Washed gel slices were soaked in 300 μL 0.5M ammonium bicarbonate to raise the pH to ~8.5 before digestion with trypsin or Glu-C (Roche).

Safety Considerations for Using Hydrofluoric Acid (HF)

Note that HF is an extremely corrosive substance and should be handled in a fume hood with appropriate care, including use of a lab coat, nitrile gloves

and safety goggles. After use, the HF solution and pipet tips were neutralized in calcium chloride solution prior to disposal.

Mass Spectrometric Identification of Proteins

To identify proteins associating with interphase and metaphase chromatin beads, proteins were separated by SDS-PAGE and the entire gel lane was cut into 1 mM slices using a gel slicer (Brinkman Instruments, Inc.). A comprehensive protocol for matrix-assisted laser desorption ionization (MALDI) sample preparation is available online at http://www.rockefeller.edu/labheads/chait/. Briefly, proteins were alkylated in-gel with 25 mM iodoacetamide, then digested with trypsin (Roche). Peptides were extracted from the gel slices with a slurry of 25 μg/μl POROS R2 20 reversed-phase resin (Applied Biosystems) in 5% formic acid/0.2% trifluoroacetic acid (TFA) at 4°C for 6 h. The slurry was transferred to C18 Ziptips (Millipore) and washed with 0.1% TFA. Peptides were eluted on a metal plate with saturated α-cyano-4-hydroxycinnamic acid (4-HCCA) in two parts water, one part acetonitrile. MALDI-MS was performed with a prOTOF 2000 MALDI-time-of-flight (MALDI-TOF) mass spectrometer (Perkin-Elmer). Tandem mass spectrometry (MS/MS) was performed using

a vMALDI-LTQ instrument (Thermo Scientific). The xproteo program (http://www.xproteo.com) was used for data analysis.

Mass Spectrometric Data Analysis

We have devised a simple method for determining the smooth background in our mass spectra. This is accomplished by iteratively calculating the average root mean square deviation (RMSD) in moving windows across the mass spectrum, excluding the peaks. Initially, the RMSD is calculated across the entire spectrum in windows of 1.0 m/z units, with steps of 0.5 m/z units. The spectrum is then divided into 30 intervals and the average RMSD is calculated for each of these intervals. The average RMSD is then re-calculated for each of the 30 intervals by excluding all values that deviate by more than a factor of 1.3 from the average RMSD. This re-calculation is then repeated two more times to remove interference from all the peaks. The final background is the average RMS in each of the 30 intervals after the fourth iteration, meaning that one value is calculated for each ~100 m/z units. Masses and signal-to-noise ratios (S/N) are then assigned to all peaks. The program for this analysis is available online at http://www.rockefeller.edu/labheads/chait/.

Peaks were assigned in the above manner for spectra from samples that were untreated or treated with HF, with those with a S/N threshold above 1.1 considered for further analysis. For each peak, the ratio of S/N for treated versus untreated was computed, and the log of this ratio was scored as the "phosphopeptide index". A positive value for the phosphopeptide index indicates that the peptide is predicted to be phosphorylated, while a negative value indicates that the peptide is predicted to be unphosphorylated.

Aurora A preparation and *in vitro* kinase assay

Xenopus Aurora A coding sequence was amplified by PCR from a full-length cDNA clone (Open Biosystems, clone ID#6318106) and cloned into pET28a vector at BamHI and XhoI sites. Hexahistidine-tagged Aurora A was expressed in *E. coli* and purified as described (Roghi et al., 1998). Autophosphorylation occurred upon incubation for 30 minutes at 30°C in kinase buffer (20 mM HEPES, pH 7.7, 150 mM NaCl, 10 mM MgCl2, 1 mM DTT, 300 μM ATP). The reaction was stopped by boiling in SDS sample buffer, and reaction products were analyzed by SDS-PAGE.

Immunoisolation of *Xenopus* Chromosome Passenger Complex

150 μL of CSF-arrested *Xenopus laevis* egg extract was treated with DMSO (0.5% v/v) or okadaic acid (0.5 μM) for 30 minutes at 20°C, treated with nocodazole (10 μg/ml) for 10 minutes at 20°C, then cooled to 4°C for 10 min before immunoprecipitation of the CPC for 75 min on ice by incubation with affinity-purified anti-xIncenp rabbit polyclonal antibodies crosslinked to magnetic beads (Dynal). Complexes were washed five times with wash buffer (20 mM HEPES, pH 7.7, 150 mM KCl, 1 mM MgCl2, 0.1% Triton-X100, 1 mM DTT, and phosphatase inhibitor cocktail), transferred to new tubes, and eluted with 30 μL SDS sample buffer. Immunoprecipitated complexes were separated by SDS-PAGE.

REFERENCES

Adams, R.R., Maiato, H., Earnshaw, W.C., and Carmena, M. (2001). Essential roles of Drosophila inner centromere protein (INCENP) and aurora B in histone H3 phosphorylation, metaphase chromosome alignment, kinetochore disjunction, and chromosome segregation. J Cell Biol *153*, 865-880.

al-Khodairy, F., Enoch, T., Hagan, I.M., and Carr, A.M. (1995). The Schizosaccharomyces pombe hus5 gene encodes a ubiquitin conjugating enzyme required for normal mitosis. J Cell Sci *108 (Pt 2)*, 475-486.

Anderson, D.J., and Hetzer, M.W. (2007). Nuclear envelope formation by chromatin-mediated reorganization of the endoplasmic reticulum. Nat Cell Biol *9*, 1160-1166.

Andrews, P.D., Ovechkina, Y., Morrice, N., Wagenbach, M., Duncan, K., Wordeman, L., and Swedlow, J.R. (2004). Aurora B regulates MCAK at the mitotic centromere. Dev Cell *6*, 253-268.

Aravind, L., and Koonin, E.V. (2000). SAP - a putative DNA-binding motif involved in chromosomal organization. Trends Biochem Sci *25*, 112-114.

Azuma, Y., Arnaoutov, A., Anan, T., and Dasso, M. (2005). PIASy mediates SUMO-2 conjugation of Topoisomerase-II on mitotic chromosomes. EMBO J *24*, 2172-2182.

Azuma, Y., Arnaoutov, A., and Dasso, M. (2003). SUMO-2/3 regulates topoisomerase II in mitosis. J Cell Biol *163*, 477-487.

Baur, T., Ramadan, K., Schlundt, A., Kartenbeck, J., and Meyer, H.H. (2007). NSF- and SNARE-mediated membrane fusion is required for nuclear envelope formation and completion of nuclear pore complex assembly in Xenopus *laevis* egg extracts. J Cell Sci *120*, 2895-2903.

Beaudouin, J., Gerlich, D., Daigle, N., Eils, R., and Ellenberg, J. (2002). Nuclear envelope breakdown proceeds by microtubule-induced tearing of the lamina. Cell *108*, 83-96.

Biggins, S., and Murray, A.W. (2001). The budding yeast protein kinase Ipl1/Aurora allows the absence of tension to activate the spindle checkpoint. Genes Dev *15*, 3118-3129.

Biggins, S., Severin, F.F., Bhalla, N., Sassoon, I., Hyman, A.A., and Murray, A.W. (1999). The conserved protein kinase Ipl1 regulates microtubule binding to kinetochores in budding yeast. Genes Dev *13*, 532-544.

Bishop, J.D., and Schumacher, J.M. (2002). Phosphorylation of the carboxyl terminus of inner centromere protein (INCENP) by the Aurora B Kinase stimulates Aurora B kinase activity. J Biol Chem *277*, 27577-27580.

Burke, B., and Ellenberg, J. (2002). Remodelling the walls of the nucleus. Nat Rev Mol Cell Biol *3*, 487-497.

Buvelot, S., Tatsutani, S.Y., Vermaak, D., and Biggins, S. (2003). The budding yeast Ipl1/Aurora protein kinase regulates mitotic spindle disassembly. J Cell Biol *160*, 329-339.

Canovas, P.M., and Guadagno, T.M. (2007). Functional analysis of Survivin in spindle assembly in Xenopus egg extracts. J Cell Biochem *100*, 217-229.

Cao, K., Nakajima, R., Meyer, H.H., and Zheng, Y. (2003). The AAA-ATPase Cdc48/p97 regulates spindle disassembly at the end of mitosis. Cell *115*, 355-367.

Carr, S.A., Annan, R.S., and Huddleston, M.J. (2005). Mapping posttranslational modifications of proteins by MS-based selective detection: application to phosphoproteomics. Methods Enzymol *405*, 82-115.

Casado-Vela, J., Ruiz, E.J., Nebreda, A.R., and Casal, J.I. (2007). A combination of neutral loss and targeted product ion scanning with two enzymatic digestions facilitates the comprehensive mapping of phosphorylation sites. Proteomics *7*, 2522-2529.

Chang, E.J., Archambault, V., McLachlin, D.T., Krutchinsky, A.N., and Chait, B.T. (2004). Analysis of protein phosphorylation by hypothesis-driven multiple-stage mass spectrometry. Anal Chem *76*, 4472-4483.

Chaudhary, N., and Courvalin, J.C. (1993). Stepwise reassembly of the nuclear envelope at the end of mitosis. J Cell Biol *122*, 295-306.

Cheeseman, I.M., and Desai, A. (2008). Molecular architecture of the kinetochore-microtubule interface. Nat Rev Mol Cell Biol *9*, 33-46.

Cronshaw, J.M., Krutchinsky, A.N., Zhang, W., Chait, B.T., and Matunis, M.J. (2002). Proteomic analysis of the mammalian nuclear pore complex. J Cell Biol *158*, 915-927.

Davis, L.I., and Blobel, G. (1986). Identification and characterization of a nuclear pore complex protein. Cell *45*, 699-709.

Dawlaty, M.M., Malureanu, L., Jeganathan, K.B., Kao, E., Sustmann, C., Tahk, S., Shuai, K., Grosschedl, R., and van Deursen, J.M. (2008). Resolution of sister centromeres requires RanBP2-mediated SUMOylation of topoisomerase IIalpha. Cell *133*, 103-115.

De Souza, C.P., Osmani, A.H., Hashmi, S.B., and Osmani, S.A. (2004). Partial nuclear pore complex disassembly during closed mitosis in Aspergillus nidulans. Curr Biol *14*, 1973-1984.

De Souza, C.P., and Osmani, S.A. (2007). Mitosis, not just open or closed. Eukaryot Cell *6*, 1521-1527.

Dechat, T., Gajewski, A., Korbei, B., Gerlich, D., Daigle, N., Haraguchi, T., Furukawa, K., Ellenberg, J., and Foisner, R. (2004). LAP2alpha and BAF transiently localize to telomeres and specific regions on chromatin during nuclear assembly. J Cell Sci *117*, 6117-6128.

Desai, A., and Mitchison, T.J. (1997). Microtubule polymerization dynamics. Annu Rev Cell Dev Biol *13*, 83-117.

Ellenberg, J., Siggia, E.D., Moreira, J.E., Smith, C.L., Presley, J.F., Worman, H.J., and Lippincott-Schwartz, J. (1997). Nuclear membrane dynamics and reassembly in living cells: targeting of an inner nuclear membrane protein in interphase and mitosis. J Cell Biol *138*, 1193-1206.

Emanuele, M.J., Lan, W., Jwa, M., Miller, S.A., Chan, C.S., and Stukenberg, P.T. (2008). Aurora B kinase and protein phosphatase 1 have opposing roles in modulating kinetochore assembly. J Cell Biol *181*, 241-254.

Forbes, D.J., Kirschner, M.W., and Newport, J.W. (1983). Spontaneous formation of nucleus-like structures around bacteriophage DNA microinjected into Xenopus eggs. Cell *34*, 13-23.

Francisco, L., Wang, W., and Chan, C.S. (1994). Type 1 protein phosphatase acts in opposition to IpL1 protein kinase in regulating yeast chromosome segregation. Mol Cell Biol *14*, 4731-4740.

Funabiki, H., and Murray, A.W. (2000). The Xenopus chromokinesin Xkid is essential for metaphase chromosome alignment and must be degraded to allow anaphase chromosome movement. Cell *102*, 411-424.

Gadde, S., and Heald, R. (2004). Mechanisms and molecules of the mitotic spindle. Curr Biol *14*, R797-805.

Gadea, B.B., and Ruderman, J.V. (2005). Aurora kinase inhibitor ZM447439 blocks chromosome-induced spindle assembly, the completion of chromosome condensation, and the establishment of the spindle integrity checkpoint in Xenopus egg extracts. Mol Biol Cell *16*, 1305-1318.

Gant, T.M., and Wilson, K.L. (1997). Nuclear assembly. Annu Rev Cell Dev Biol *13*, 669-695.

Geiss-Friedlander, R., and Melchior, F. (2007). Concepts in sumoylation: a decade on. Nat Rev Mol Cell Biol *8*, 947-956.

Georgatos, S.D., Pyrpasopoulou, A., and Theodoropoulos, P.A. (1997). Nuclear envelope breakdown in mammalian cells involves stepwise lamina disassembly and microtubule-drive deformation of the nuclear membrane. J Cell Sci *110 (Pt 17)*, 2129-2140.

Gerlich, D., Beaudouin, J., Gebhard, M., Ellenberg, J., and Eils, R. (2001). Four-dimensional imaging and quantitative reconstruction to analyse complex spatiotemporal processes in live cells. Nat Cell Biol *3*, 852-855.

Gorjanacz, M., Klerkx, E.P., Galy, V., Santarella, R., Lopez-Iglesias, C., Askjaer, P., and Mattaj, I.W. (2007). Caenorhabditis elegans BAF-1 and its kinase VRK-1 participate directly in post-mitotic nuclear envelope assembly. EMBO J *26*, 132-143.

Goto, H., Kiyono, T., Tomono, Y., Kawajiri, A., Urano, T., Furukawa, K., Nigg, E.A., and Inagaki, M. (2006). Complex formation of Plk1 and INCENP required for metaphase-anaphase transition. Nat Cell Biol *8*, 180-187.

Guttinger, S., Laurell, E., and Kutay, U. (2009). Orchestrating nuclear envelope disassembly and reassembly during mitosis. Nat Rev Mol Cell Biol *10*, 178-191.

Hagting, A., Jackman, M., Simpson, K., and Pines, J. (1999). Translocation of cyclin B1 to the nucleus at prophase requires a phosphorylation-dependent nuclear import signal. Curr Biol *9*, 680-689.

Haraguchi, T., Kojidani, T., Koujin, T., Shimi, T., Osakada, H., Mori, C., Yamamoto, A., and Hiraoka, Y. (2008). Live cell imaging and electron microscopy reveal dynamic processes of BAF-directed nuclear envelope assembly. J Cell Sci *121*, 2540-2554.

Haraguchi, T., Koujin, T., Segura-Totten, M., Lee, K.K., Matsuoka, Y., Yoneda, Y., Wilson, K.L., and Hiraoka, Y. (2001). BAF is required for emerin assembly into the reforming nuclear envelope. J Cell Sci *114*, 4575-4585.

Hauf, S., and Watanabe, Y. (2004). Kinetochore orientation in mitosis and meiosis. Cell *119*, 317-327.

Haydon, C.E., Eyers, P.A., Aveline-Wolf, L.D., Resing, K.A., Maller, J.L., and Ahn, N.G. (2003). Identification of novel phosphorylation sites on Xenopus *laevis* Aurora A and analysis of phosphopeptide enrichment by immobilized metal-affinity chromatography. Mol Cell Proteomics *2*, 1055-1067.

Heald, R., and McKeon, F. (1990). Mutations of phosphorylation sites in lamin A that prevent nuclear lamina disassembly in mitosis. Cell *61*, 579-589.

Heald, R., Tournebize, R., Blank, T., Sandaltzopoulos, R., Becker, P., Hyman, A., and Karsenti, E. (1996). Self-organization of microtubules into bipolar spindles around artificial chromosomes in Xenopus egg extracts. Nature *382*, 420-425.

Hecker, C.M., Rabiller, M., Haglund, K., Bayer, P., and Dikic, I. (2006). Specification of SUMO1- and SUMO2-interacting motifs. J Biol Chem *281*, 16117-16127.

Hetzer, M., Meyer, H.H., Walther, T.C., Bilbao-Cortes, D., Warren, G., and Mattaj, I.W. (2001). Distinct AAA-ATPase p97 complexes function in discrete steps of nuclear assembly. Nat Cell Biol *3*, 1086-1091.

Hetzer, M.W., Walther, T.C., and Mattaj, I.W. (2005). Pushing the envelope: structure, function, and dynamics of the nuclear periphery. Annu Rev Cell Dev Biol *21*, 347-380.

Hirano, T. (2005). Condensins: organizing and segregating the genome. Curr Biol *15*, R265-275.

Hirschberg, D., Jagerbrink, T., Samskog, J., Gustafsson, M., Stahlberg, M., Alvelius, G., Husman, B., Carlquist, M., Jornvall, H., and Bergman, T. (2004). Detection of phosphorylated peptides in proteomic analyses using microfluidic compact disk technology. Anal Chem *76*, 5864-5871.

Honda, R., Korner, R., and Nigg, E.A. (2003). Exploring the functional interactions between Aurora B, INCENP, and survivin in mitosis. Mol Biol Cell *14*, 3325-3341.

Hopfner, K.P. (2003). Chromosome cohesion: closing time. Curr Biol *13*, R866-868.

Hoppe, T., Matuschewski, K., Rape, M., Schlenker, S., Ulrich, H.D., and Jentsch, S. (2000). Activation of a membrane-bound transcription factor by regulated ubiquitin/proteasome-dependent processing. Cell *102*, 577-586.

Hsu, J.Y., Sun, Z.W., Li, X., Reuben, M., Tatchell, K., Bishop, D.K., Grushcow, J.M., Brame, C.J., Caldwell, J.A., Hunt, D.F., *et al.* (2000). Mitotic phosphorylation of histone H3 is governed by Ipl1/aurora kinase and Glc7/PP1 phosphatase in budding yeast and nematodes. Cell *102*, 279-291.

Hunter, A.P., and Games, D.E. (1994). Chromatographic and mass spectrometric methods for the identification of phosphorylation sites in phosphoproteins. Rapid Commun Mass Spectrom *8*, 559-570.

Ishihama, Y., Wei, F.Y., Aoshima, K., Sato, T., Kuromitsu, J., and Oda, Y. (2007). Enhancement of the efficiency of phosphoproteomic identification by removing phosphates after phosphopeptide enrichment. J Proteome Res *6*, 1139-1144.

Jeyaprakash, A.A., Klein, U.R., Lindner, D., Ebert, J., Nigg, E.A., and Conti, E. (2007). Structure of a Survivin-Borealin-INCENP core complex reveals how chromosomal passengers travel together. Cell *131*, 271-285.

Juang, Y.L., Huang, J., Peters, J.M., McLaughlin, M.E., Tai, C.Y., and Pellman, D. (1997). APC-mediated proteolysis of Ase1 and the morphogenesis of the mitotic spindle. Science *275*, 1311-1314.

Kang, S., Liao, P., Gage, D.A., and Esselman, W.J. (1997). Identification of in vivo phosphorylation sites of CD45 protein-tyrosine phosphatase in 70Z/3.12 cells. J Biol Chem *272*, 11588-11596.

Kelly, A.E., and Funabiki, H. (2009). Correcting aberrant kinetochore microtubule attachments: an Aurora B-centric view. Curr Opin Cell Biol *21*, 51-58.

Kelly, A.E., Sampath, S.C., Maniar, T.A., Woo, E.M., Chait, B.T., and Funabiki, H. (2007). Chromosomal enrichment and activation of the aurora B pathway are coupled to spatially regulate spindle assembly. Dev Cell *12*, 31-43.

Khodjakov, A., and Rieder, C.L. (1999). The sudden recruitment of gamma-tubulin to the centrosome at the onset of mitosis and its dynamic exchange throughout the cell cycle, do not require microtubules. J Cell Biol *146*, 585-596.

Kirschner, M.W., and Mitchison, T. (1986). Microtubule dynamics. Nature *324*, 621.

Kline-Smith, S.L., and Walczak, C.E. (2004). Mitotic spindle assembly and chromosome segregation: refocusing on microtubule dynamics. Mol Cell *15*, 317-327.

Knight, Z.A., Schilling, B., Row, R.H., Kenski, D.M., Gibson, B.W., and Shokat, K.M. (2003). Phosphospecific proteolysis for mapping sites of protein phosphorylation. Nat Biotechnol *21*, 1047-1054.

Knipscheer, P., Flotho, A., Klug, H., Olsen, J.V., van Dijk, W.J., Fish, A., Johnson, E.S., Mann, M., Sixma, T.K., and Pichler, A. (2008). Ubc9 sumoylation regulates SUMO target discrimination. Mol Cell *31*, 371-382.

Kondo, H., Rabouille, C., Newman, R., Levine, T.P., Pappin, D., Freemont, P., and Warren, G. (1997). p47 is a cofactor for p97-mediated membrane fusion. Nature *388*, 75-78.

Krutchinsky, A.N. (2007). A novel high-capacity ion trap-quadrupole tandem mass spectrometer. Int J Mass Spectrom.

Kuyama, H., Toda, C., Watanabe, M., Tanaka, K., and Nishimura, O. (2003). An efficient chemical method for dephosphorylation of phosphopeptides. Rapid Commun Mass Spectrom *17*, 1493-1496.

Lampson, M.A., Renduchitala, K., Khodjakov, A., and Kapoor, T.M. (2004). Correcting improper chromosome-spindle attachments during cell division. Nat Cell Biol *6*, 232-237.

Lan, W., Zhang, X., Kline-Smith, S.L., Rosasco, S.E., Barrett-Wilt, G.A., Shabanowitz, J., Hunt, D.F., Walczak, C.E., and Stukenberg, P.T. (2004). Aurora B phosphorylates centromeric MCAK and regulates its localization and microtubule depolymerization activity. Curr Biol *14*, 273-286.

Larsen, M.R., Sorensen, G.L., Fey, S.J., Larsen, P.M., and Roepstorff, P. (2001). Phospho-proteomics: evaluation of the use of enzymatic de-phosphorylation and differential mass spectrometric peptide mass mapping

for site specific phosphorylation assignment in proteins separated by gel electrophoresis. Proteomics *1*, 223-238.

Lee, K.K., Gruenbaum, Y., Spann, P., Liu, J., and Wilson, K.L. (2000). C. elegans nuclear envelope proteins emerin, MAN1, lamin, and nucleoporins reveal unique timing of nuclear envelope breakdown during mitosis. Mol Biol Cell *11*, 3089-3099.

Lenart, P., Bacher, C.P., Daigle, N., Hand, A.R., Eils, R., Terasaki, M., and Ellenberg, J. (2005). A contractile nuclear actin network drives chromosome congression in oocytes. Nature *436*, 812-818.

Li, J., Meyer, A.N., and Donoghue, D.J. (1997). Nuclear localization of cyclin B1 mediates its biological activity and is regulated by phosphorylation. Proc Natl Acad Sci U S A *94*, 502-507.

Li, X., Gerber, S.A., Rudner, A.D., Beausoleil, S.A., Haas, W., Villen, J., Elias, J.E., and Gygi, S.P. (2007). Large-scale phosphorylation analysis of alpha-factor-arrested Saccharomyces cerevisiae. J Proteome Res *6*, 1190-1197.

Liao, P.C., Leykam, J., Andrews, P.C., Gage, D.A., and Allison, J. (1994). An approach to locate phosphorylation sites in a phosphoprotein: mass mapping by combining specific enzymatic degradation with matrix-assisted laser desorption/ionization mass spectrometry. Anal Biochem *219*, 9-20.

Littlepage, L.E., and Ruderman, J.V. (2002). Identification of a new APC/C recognition domain, the A box, which is required for the Cdh1-dependent

destruction of the kinase Aurora-A during mitotic exit. Genes Dev *16*, 2274-2285.

Littlepage, L.E., Wu, H., Andresson, T., Deanehan, J.K., Amundadottir, L.T., and Ruderman, J.V. (2002). Identification of phosphorylated residues that affect the activity of the mitotic kinase Aurora-A. Proc Natl Acad Sci U S A *99*, 15440-15445.

Liu, D., Vader, G., Vromans, M.J., Lampson, M.A., and Lens, S.M. (2009). Sensing chromosome bi-orientation by spatial separation of aurora B kinase from kinetochore substrates. Science *323*, 1350-1353.

Lohka, M.J., and Maller, J.L. (1985). Induction of nuclear envelope breakdown, chromosome condensation, and spindle formation in cell-free extracts. J Cell Biol *101*, 518-523.

Lohka, M.J., and Masui, Y. (1983). Formation in vitro of sperm pronuclei and mitotic chromosomes induced by amphibian ooplasmic components. Science *220*, 719-721.

Makhnevych, T., Sydorskyy, Y., Xin, X., Srikumar, T., Vizeacoumar, F.J., Jeram, S.M., Li, Z., Bahr, S., Andrews, B.J., Boone, C., *et al.* (2009). Global map of SUMO function revealed by protein-protein interaction and genetic networks. Mol Cell *33*, 124-135.

Maldonado-Saldivia, J., van den Bergen, J., Krouskos, M., Gilchrist, M., Lee, C., Li, R., Sinclair, A.H., Surani, M.A., and Western, P.S. (2007). Dppa2 and

Dppa4 are closely linked SAP motif genes restricted to pluripotent cells and the germ line. Stem Cells *25*, 19-28.

Mann, M., Hendrickson, R.C., and Pandey, A. (2001). Analysis of proteins and proteomes by mass spectrometry. Annu Rev Biochem *70*, 437-473.

Marcantonio, M., Trost, M., Courcelles, M., Desjardins, M., and Thibault, P. (2007). Combined enzymatic and data mining approaches for comprehensive phosphoproteome analyses; application to cell signaling events of interferon- stimulated macrophages. Mol Cell Proteomics.

Matic, I., Macek, B., Hilger, M., Walther, T.C., and Mann, M. (2008). Phosphorylation of SUMO-1 occurs in vivo and is conserved through evolution. J Proteome Res *7*, 4050-4057.

Matunis, M.J., Coutavas, E., and Blobel, G. (1996). A novel ubiquitin-like modification modulates the partitioning of the Ran-GTPase-activating protein RanGAP1 between the cytosol and the nuclear pore complex. J Cell Biol *135*, 1457-1470.

McLachlin, D.T., and Chait, B.T. (2001). Analysis of phosphorylated proteins and peptides by mass spectrometry. Curr Opin Chem Biol *5*, 591-602.

Meyer, H.H. (2005). Golgi reassembly after mitosis: the AAA family meets the ubiquitin family. Biochim Biophys Acta *1744*, 108-119.

Mitchison, T.J., and Salmon, E.D. (2001). Mitosis: a history of division. Nat Cell Biol *3*, E17-21.

Moir, D., Stewart, S.E., Osmond, B.C., and Botstein, D. (1982). Cold-sensitive cell-division-cycle mutants of yeast: isolation, properties, and pseudoreversion studies. Genetics *100*, 547-563.

Montpetit, B., Hazbun, T.R., Fields, S., and Hieter, P. (2006). Sumoylation of the budding yeast kinetochore protein Ndc10 is required for Ndc10 spindle localization and regulation of anaphase spindle elongation. J Cell Biol *174*, 653-663.

Mora-Bermudez, F., Gerlich, D., and Ellenberg, J. (2007). Maximal chromosome compaction occurs by axial shortening in anaphase and depends on Aurora kinase. Nat Cell Biol *9*, 822-831.

Morgan, D.O. (1997). Cyclin-dependent kinases: engines, clocks, and microprocessors. Annu Rev Cell Dev Biol *13*, 261-291.

Mukhopadhyay, D., and Dasso, M. (2007). Modification in reverse: the SUMO proteases. Trends Biochem Sci *32*, 286-295.

Murray, A.W. (1991). Cell cycle extracts. Methods Cell Biol *36*, 581-605.

Murray, A.W., and Kirschner, M.W. (1989). Cyclin synthesis drives the early embryonic cell cycle. Nature *339*, 275-280.

Murray, A.W., Solomon, M.J., and Kirschner, M.W. (1989). The role of cyclin synthesis and degradation in the control of maturation promoting factor activity. Nature *339*, 280-286.

Nacerddine, K., Lehembre, F., Bhaumik, M., Artus, J., Cohen-Tannoudji, M., Babinet, C., Pandolfi, P.P., and Dejean, A. (2005). The SUMO pathway is essential for nuclear integrity and chromosome segregation in mice. Dev Cell *9*, 769-779.

Newmeyer, D.D., Lucocq, J.M., Burglin, T.R., and De Robertis, E.M. (1986). Assembly in vitro of nuclei active in nuclear protein transport: ATP is required for nucleoplasmin accumulation. EMBO J *5*, 501-510.

O'Brien, L.L., and Wiese, C. (2006). TPX2 is required for postmitotic nuclear assembly in cell-free Xenopus *laevis* egg extracts. J Cell Biol *173*, 685-694.

O'Connor, C., and Miko, I. (2008). Developing the chromosome theory. Nature Education *1*.

Oda, Y., Nagasu, T., and Chait, B.T. (2001). Enrichment analysis of phosphorylated proteins as a tool for probing the phosphoproteome. Nat Biotechnol *19*, 379-382.

Ohi, R., Coughlin, M.L., Lane, W.S., and Mitchison, T.J. (2003). An inner centromere protein that stimulates the microtubule depolymerizing activity of a KinI kinesin. Dev Cell *5*, 309-321.

Ohsugi, M., Adachi, K., Horai, R., Kakuta, S., Sudo, K., Kotaki, H., Tokai-Nishizumi, N., Sagara, H., Iwakura, Y., and Yamamoto, T. (2008). Kid-mediated chromosome compaction ensures proper nuclear envelope formation. Cell *132*, 771-782.

Olsen, J.V., Blagoev, B., Gnad, F., Macek, B., Kumar, C., Mortensen, P., and Mann, M. (2006). Global, in vivo, and site-specific phosphorylation dynamics in signaling networks. Cell *127*, 635-648.

Pandey, A., and Mann, M. (2000). Proteomics to study genes and genomes. Nature *405*, 837-846.

Pereira, G., and Schiebel, E. (2003). Separase regulates INCENP-Aurora B anaphase spindle function through Cdc14. Science *302*, 2120-2124.

Pinsky, B.A., Kung, C., Shokat, K.M., and Biggins, S. (2006). The Ipl1-Aurora protein kinase activates the spindle checkpoint by creating unattached kinetochores. Nat Cell Biol *8*, 78-83.

Postow, L., Ghenoiu, C., Woo, E.M., Krutchinsky, A.N., Chait, B.T., and Funabiki, H. (2008). Ku80 removal from DNA through double strand break-induced ubiquitylation. J Cell Biol *182*, 467-479.

Ptacek, J., and Snyder, M. (2006). Charging it up: global analysis of protein phosphorylation. Trends Genet *22*, 545-554.

Ramadan, K., Bruderer, R., Spiga, F.M., Popp, O., Baur, T., Gotta, M., and Meyer, H.H. (2007). Cdc48/p97 promotes reformation of the nucleus by extracting the kinase Aurora B from chromatin. Nature *450*, 1258-1262.

Reinders, J., and Sickmann, A. (2005). State-of-the-art in phosphoproteomics. Proteomics *5*, 4052-4061.

Roghi, C., Giet, R., Uzbekov, R., Morin, N., Chartrain, I., Le Guellec, R., Couturier, A., Doree, M., Philippe, M., and Prigent, C. (1998). The Xenopus protein kinase pEg2 associates with the centrosome in a cell cycle-dependent manner, binds to the spindle microtubules and is involved in bipolar mitotic spindle assembly. J Cell Sci *111 (Pt 5)*, 557-572.

Rout, M.P., and Aitchison, J.D. (2000). Pore relations: nuclear pore complexes and nucleocytoplasmic exchange. Essays Biochem *36*, 75-88.

Ruchaud, S., Carmena, M., and Earnshaw, W.C. (2007). Chromosomal passengers: conducting cell division. Nat Rev Mol Cell Biol *8*, 798-812.

Rusnak, F., Zhou, J., and Hathaway, G.M. (2004). Reaction of phosphorylated and O-glycosylated peptides by chemically targeted identification at ambient temperature. J Biomol Tech *15*, 296-304.

Saitoh, H., and Hinchey, J. (2000). Functional heterogeneity of small ubiquitin-related protein modifiers SUMO-1 versus SUMO-2/3. J Biol Chem *275*, 6252-6258.

Salina, D., Bodoor, K., Eckley, D.M., Schroer, T.A., Rattner, J.B., and Burke, B. (2002). Cytoplasmic dynein as a facilitator of nuclear envelope breakdown. Cell *108*, 97-107.

Sampath, S.C., Ohi, R., Leismann, O., Salic, A., Pozniakovski, A., and Funabiki, H. (2004). The chromosomal passenger complex is required for chromatin-induced microtubule stabilization and spindle assembly. Cell *118*, 187-202.

Sazer, S. (2005). Nuclear envelope: nuclear pore complexity. Curr Biol *15*, R23-26.

Schatten, G., Simerly, C., and Schatten, H. (1985). Microtubule configurations during fertilization, mitosis, and early development in the mouse and the requirement for egg microtubule-mediated motility during mammalian fertilization. Proc Natl Acad Sci U S A *82*, 4152-4156.

Schuh, M., and Ellenberg, J. (2007). Self-organization of MTOCs replaces centrosome function during acentrosomal spindle assembly in live mouse oocytes. Cell *130*, 484-498.

Sessa, F., Mapelli, M., Ciferri, C., Tarricone, C., Areces, L.B., Schneider, T.R., Stukenberg, P.T., and Musacchio, A. (2005). Mechanism of Aurora B activation by INCENP and inhibition by hesperadin. Mol Cell *18*, 379-391.

Seufert, W., Futcher, B., and Jentsch, S. (1995). Role of a ubiquitin-conjugating enzyme in degradation of S- and M-phase cyclins. Nature *373*, 78-81.

Shorter, J., and Warren, G. (1999). A role for the vesicle tethering protein, p115, in the post-mitotic stacking of reassembling Golgi cisternae in a cell-free system. J Cell Biol *146*, 57-70.

Shumaker, D.K., Solimando, L., Sengupta, K., Shimi, T., Adam, S.A., Grunwald, A., Strelkov, S.V., Aebi, U., Cardoso, M.C., and Goldman, R.D. (2008). The highly conserved nuclear lamin Ig-fold binds to PCNA: its role in DNA replication. J Cell Biol *181*, 269-280.

Sullivan, M., and Morgan, D.O. (2007). Finishing mitosis, one step at a time. Nat Rev Mol Cell Biol *8*, 894-903.

Suzuki, R., Shindo, H., Tase, A., Kikuchi, Y., Shimizu, M., and Yamazaki, T. (2009). Solution structures and DNA binding properties of the N-terminal SAP domains of SUMO E3 ligases from Saccharomyces cerevisiae and Oryza sativa. Proteins *75*, 336-347.

Tackett, A.J., Dilworth, D.J., Davey, M.J., O'Donnell, M., Aitchison, J.D., Rout, M.P., and Chait, B.T. (2005). Proteomic and genomic characterization of chromatin complexes at a boundary. J Cell Biol *169*, 35-47.

Takahashi, Y., Iwase, M., Konishi, M., Tanaka, M., Toh-e, A., and Kikuchi, Y. (1999). Smt3, a SUMO-1 homolog, is conjugated to Cdc3, a component of septin rings at the mother-bud neck in budding yeast. Biochem Biophys Res Commun *259*, 582-587.

Tanaka, T.U., Rachidi, N., Janke, C., Pereira, G., Galova, M., Schiebel, E., Stark, M.J., and Nasmyth, K. (2002). Evidence that the Ipl1-Sli15 (Aurora kinase-INCENP) complex promotes chromosome bi-orientation by altering kinetochore-spindle pole connections. Cell *108*, 317-329.

Torres, M.P., Thapar, R., Marzluff, W.F., and Borchers, C.H. (2005). Phosphatase-directed phosphorylation-site determination: a synthesis of methods for the detection and identification of phosphopeptides. J Proteome Res *4*, 1628-1635.

Uchiyama, K., and Kondo, H. (2005). p97/p47-Mediated biogenesis of Golgi and ER. J Biochem *137*, 115-119.

Vader, G., Kauw, J.J., Medema, R.H., and Lens, S.M. (2006). Survivin mediates targeting of the chromosomal passenger complex to the centromere and midbody. EMBO Rep *7*, 85-92.

Walczak, C.E., Gan, E.C., Desai, A., Mitchison, T.J., and Kline-Smith, S.L. (2002). The microtubule-destabilizing kinesin XKCM1 is required for chromosome positioning during spindle assembly. Curr Biol *12*, 1885-1889.

Walczak, C.E., Mitchison, T.J., and Desai, A. (1996). XKCM1: a Xenopus kinesin-related protein that regulates microtubule dynamics during mitotic spindle assembly. Cell *84*, 37-47.

Ward, G.E., and Kirschner, M.W. (1990). Identification of cell cycle-regulated phosphorylation sites on nuclear lamin C. Cell *61*, 561-577.

Wassarman, P.M., and Fujiwara, K. (1978). Immunofluorescent anti-tubulin staining of spindles during meiotic maturation of mouse oocytes in vitro. J Cell Sci *29*, 171-188.

Wei, Y., Yu, L., Bowen, J., Gorovsky, M.A., and Allis, C.D. (1999). Phosphorylation of histone H3 is required for proper chromosome condensation and segregation. Cell *97*, 99-109.

Wheatley, S.P., Henzing, A.J., Dodson, H., Khaled, W., and Earnshaw, W.C. (2004). Aurora-B phosphorylation in vitro identifies a residue of survivin

that is essential for its localization and binding to inner centromere protein (INCENP) in vivo. J Biol Chem *279*, 5655-5660.

Woo, E.M., Fenyo, D., Kwok, B.H., Funabiki, H., and Chait, B.T. (2008). Efficient identification of phosphorylation by mass spectrometric phosphopeptide fingerprinting. Anal Chem *80*, 2419-2425.

Wright, S.J. (1999). Sperm nuclear activation during fertilization. Curr Top Dev Biol *46*, 133-178.

Yasui, Y., Urano, T., Kawajiri, A., Nagata, K., Tatsuka, M., Saya, H., Furukawa, K., Takahashi, T., Izawa, I., and Inagaki, M. (2004). Autophosphorylation of a newly identified site of Aurora-B is indispensable for cytokinesis. J Biol Chem *279*, 12997-13003.

Ye, Y., Meyer, H.H., and Rapoport, T.A. (2003). Function of the p97-Ufd1-Npl4 complex in retrotranslocation from the ER to the cytosol: dual recognition of nonubiquitinated polypeptide segments and polyubiquitin chains. J Cell Biol *162*, 71-84.

Zeller, M., and Konig, S. (2004). The impact of chromatography and mass spectrometry on the analysis of protein phosphorylation sites. Anal Bioanal Chem *378*, 898-909.

Zhang, X., Herring, C.J., Romano, P.R., Szczepanowska, J., Brzeska, H., Hinnebusch, A.G., and Qin, J. (1998). Identification of phosphorylation sites in proteins separated by polyacrylamide gel electrophoresis. Anal Chem *70*, 2050-2059.

Zhang, X.D., Goeres, J., Zhang, H., Yen, T.J., Porter, A.C., and Matunis, M.J. (2008). SUMO-2/3 modification and binding regulate the association of CENP-E with kinetochores and progression through mitosis. Mol Cell *29*, 729-741.

Zhou, W., Merrick, B.A., Khaledi, M.G., and Tomer, K.B. (2000). Detection and sequencing of phosphopeptides affinity bound to immobilized metal ion beads by matrix-assisted laser desorption/ionization mass spectrometry. J Am Soc Mass Spectrom *11*, 273-282.

Zhu, J., Zhu, S., Guzzo, C.M., Ellis, N.A., Sung, K.S., Choi, C.Y., and Matunis, M.J. (2008). Small ubiquitin-related modifier (SUMO) binding determines substrate recognition and paralog-selective SUMO modification. J Biol Chem *283*, 29405-29415.

Zhu, S., Goeres, J., Sixt, K.M., Bekes, M., Zhang, X.D., Salvesen, G.S., and Matunis, M.J. (2009). Protection from isopeptidase-mediated deconjugation regulates paralog-selective sumoylation of RanGAP1. Mol Cell *33*, 570-580.